2012

Hyphenated Applications of Mass Spectrometry for the Analysis of Biological Compounds

Derrick Morast
Iowa State University

Hyphenated applications of mass spectrometry

for the analysis of biological compounds

by

Derrick L. Morast

A dissertation submitted to the graduate faculty

in partial fulfillment of the requirements for the degree of

DOCTOR OF PHILOSOPHY

Major: Analytical Chemistry

Program of Study Committee:

R. Sam Houk, Major Professor
Young Jin Lee
Emily Smith
Joseph Burnett
Jesudoss Kingston

Iowa State University

Ames, Iowa

2012

TABLE OF CONTENTS

CHAPTER 1. GENERAL INTRODUCTION

Biomolecular Mass Spectrometry 1

Ionization Methods 2

Electrospray Ionization 2

Laser Desorption/Ionization 3

Atmospheric Pressure Photoionization 4

Mass Spectrometry for Protein Analysis 5

High Resolution Mass Spectrometry 5

Bottom-up Approach for Proteomics 6

Top-down Approach for Proteomics 6

Ion/Ion Reactions 7

Ion Mobility Spectrometry Mass Spectrometry 8

Principles of Ion Mobility 9

Instrumentation for Ion Mobility Spectrometry Mass Spectrometry 11

Dissertation Overview 12

References 14

Figures 20

CHAPTER 2. PROTEIN CATIONS IN HIGHLY FOLDED CONFORMATIONS FROM MODERATELY ALKALINE (pH 8.0) SOLUTIONS BY ELECTROSPRAY IONIZATION ION MOBLITY MASS SPECTROMETRY

Abstract 22

Keywords 22

Introduction 23

Materials and Methods 24

Proteins and Chemicals 24

Ion Mobility and Mass Spectrometer 24

Collision Cross Sections 26

Results and Discussion 27

Ubiquitin 27

Cytochrome *c* 28

Lysozyme 30

Alpha-Lactalbumin 31

Conclusion 33

Acknowledgements 33

References 34

Figures 39

CHAPTER 3. COMPREHENSIVE IDENTIFICATION OF ALPHA-ZEIN PROTEINS BY HIGH-PERFORMANCE LIQUID CHROMATOGRAPHY ACCURATE-MASS TIME-OF-FLIGHT MASS SPECTROMETERY

Abstract 45

Keywords 45

Introduction 46

Materials and Methods 48

Alpha-Zein Protein Extraction 48

HPLC-TOF Mass Spectrometry 49

Results and Discussion 50

Previous Mass Spectrometry Studies of Zein Proteins 50

Measured Mass Spectra and M_r Values 51

Alpha-Zein Proteins with Database Entries 52

Alpha-Zein Proteins without Database Entries 55

Acknowledgements 58

References 59

Tables and Figures 62

CHAPTER 4. CHARACTERIZATION OF PHOSVITIN PHOSPHOPEPTIDES BY ELECTROSPRAY IONIZATION TANDEM MASS SPECTROMETRY

Abstract 69

Keywords 69

Introduction 70

Materials and Methods 72

Enzymatic Digestions of Phosvitin 73

Dephosphorylation of Phosvitin 73

LC-ESI-MS/MS Sample Preparation and Instrumentation 74

Results and Discussion 74

Optimization of Phosvitin Digestions 74

Previous Mass Spectrometry Analysis of Phosvitin Phosphopeptides 76

Tandem Mass Spectrometry Analysis of Digested Phosvitin Samples 77

Tandem Mass Spectrometry Results of Trypsin Digestion 78

Tandem Mass Spectrometry Results of Chymotrypsin Digestion 79

Tandem Mass Spectrometry of Multifect® P-3000 Digestion 81

Acknowledgements 81

References 82

Tables and Figures 85

Supporting Information 91

CHAPTER 5. ULTRAVIOLET LASER DESORPTION ATMOSPHERIC PRESSURE PHOTOIONIZATION MASS SPECTROMETRY

Abstract 95

Keywords 95

Introduction 96

Materials and Methods 97

Chemicals 97

Sample Preparation for LD APPI Experiments 98

Mass Spectrometer and Laser 98

LD APPI Ion Source 99

Results and Discussion 99

LD APPI Ion Source Configuration 99

Matrix-Free Desorption and Ionization of Chalcone 100

Desorption and Ionization of an Alkane 101

Desorption and Ionization of Fatty Acids 102

Conclusion 103

Acknowledgements 103

References 104

Figures 106

CHAPTER 6. GENERAL CONCLUSIONS 110

ACKNOWLEDGEMENTS 113

APPENDIX I. TIME-RESOLVED HEATING AND UNFOLDING OF PROTEIN IONS DUE TO ION INJECTION CONDITIONS IN AN ION TRAP – ION MOBILITY – TIME-OF-FLIGHT MASS SPECTROMETER 115

CHAPTER 1

GENERAL INTRODUCTION

Biomolecular mass spectrometry – Since its commercialization is the 1940's, mass spectrometry (MS) has evolved into a powerful analytical tool for the analysis of biomolecules. Along the way, hundreds of improvements have contributed to the diversity of biological applications in which MS is employed. These improvements include the development of novel ionization methods, mass analyzers, and ion detectors as well as MS combined with analytical separation techniques such as high-performance liquid chromatography (HPLC) (*1-7*), gas chromatography (GC) (*8-10*), capillary electrophoresis (CE) (*11*), and ion mobility spectrometry (IMS) (*12-14*), to name a few. The developments have led to a countless number of "hyphenated" MS techniques.

Early ionization techniques such as electron ionization (EI) and chemical ionization (CI) were suitable for the analysis of low mass volatile organic molecules but not larger, non-volatile biomolecules. The utility of MS for biological applications was enhanced by the development of novel desorption methods such as fast atom bombardment (FAB) (*15*), matrix-assisted secondary ion MS (SIMS) (*16*) and laser desorption ionization (LDI) and matrix-assisted laser desorption/ionization (MALDI) (*17-20*) along with novel continuous flow techniques like electrospray ionization (ESI) (*21*), nano-ESI or nanospray (nESI) (*22, 23*), thermospray (*24*), ion spray (*6*), and sonic spray (*25*). ESI and MALDI have become the two most widely used ionization techniques for the analysis of biomolecules; Fenn and Tanaka were jointly awarded the Nobel Prize in Chemistry in 2002 "for their development of soft desorption ionization methods for mass spectrometric analyses of biological

macromolecules" (*26*). MALDI and LDI are also useful ionization methods for mass spectrometric imaging of biological samples (*27*).

Ionization Methods

Electrospray ionization – ESI is a "soft" ionization technique commonly used for the analysis of peptides and proteins. In ESI, a solution of analyte is pumped through a capillary at a low flow rate (typically 0.1-1 mL/min). A voltage (2 to 5 kV) is applied to the capillary. This voltage creates an electric field gradient, which causes the electrically conductive analyte solution to form a Taylor cone at the capillary tip (*28*). Simultaneously, the solution picks up excess charges on its surface. Droplets are generated at the end of the Taylor cone. These droplets begin to desolvate until they reach the Rayleigh limit, which is the point at which the repulsion between positive (or negative) charges equals the surface tension of the solution. The droplets undergo a Columbic explosion. This results in the formation of smaller droplets, which repeat the process until all of the solution has been desolvated. Once desolvated, charged analyte molecules enter the mass spectrometer for detection. Large biomolecules, like peptides and proteins, are often multiply charged when ionized via ESI.

Nano-ESI, an analog of ESI, is a popular technique for the analysis of proteins for several reasons. The flow rate of nESI is ~10-40 nL/min, which results in less samples consumption. A stable spray is generated by nESI without the use of an auxiliary pump. The small inner diameter of the capillary in nESI results in the formation of smaller droplets from the Taylor cone compared to ESI (200 nm vs. 1 or 2 µm) (*23*). This allows for a stable spray to be generated from a wide variety of solvents, including 100% water.

Laser desorption/ionization – MALDI has become a popular method for the analysis of biomolecules. In MALDI, the analyte is co-crystalized with a matrix. The matrix is typically an organic acid such as 2,5-dihydroxy benzoic acid (DHB) or α-cyano-4-hydroxycinnamic acid (CHCA) (*29, 30*). The matrix absorbs energy during laser irradiation and assists the desorption and ionization of the analyte molecule in a mechanism that is still not completely understood (*31-33*). Ionization of the analyte is often accomplished by proton donation from the matrix, resulting in singly (or less often a doubly) charged ions (*18*).

Although traditional MALDI is commonly used for IMS, it has several disadvantages as well. The matrix is present at a much higher concentration than the analyte (more than a 1000:1 ratio), which can result in high background signal at m/z values < 500. In order for efficient desorption and ionization of the analyte molecule, co-crystallization with the MALDI matrix is essential. For this reason, many compounds, particularly small hydrophobic molecules, can be difficult to analyze. The matrices used in MALDI typically form crystals > 10 μm in size. This can lead to issues with sample homogeneity, shot-to-shot reproducibility, and unstable signal stability. Finally, MALDI analysis is typically performed at intermediate pressure (~1 mbar) within the mass spectrometer. Volatile compounds readily evaporate once the sample is placed in this environment.

Due to the disadvantages listed above, there has recently been great interest in the development of atmospheric pressure (AP) LDI, along with other AP ionization methods, for imaging mass spectrometry applications (*34-40*). AP LDI is not without its own challenges; one of the main areas of focus is the poor ionization and extraction efficiency. This issue has spurred interest in the development of post-ionization techniques. Several examples are

matrix-assisted laser desorption electrospray ionization (MALDESI) (*41*), laser ablation electrospray ionization (LAESI) (*42, 43*), electrospray-assisted laser desorption/ionization (ELDI) (*44*), and laser ablation atmospheric pressure photoionization (LA APPI) (*45*). Chapter 5 of this dissertation introduces a novel variation of LA APPI.

Atmospheric pressure photoionization – Although APPI is sometimes considered a relatively "young" ionization technique, photoionization (PI) has been used as a detector in gas chromatography since the 1970's (*46-48*) and in liquid chromatography about a decade later (*49, 50*). In APPI, the analyte is dissolved in a solvent. The solution is generally vaporized with the aid of a nebulizing gas, typically nitrogen. The vaporized solutions is then exposed ultraviolet (UV) light generated from a discharge lamp. The most common lamp uses krypton, which produces two photons with energy 10.0 eV and 10.6 eV. The analyte undergoes photoexcitation and ionization:

$$M + h\nu \rightarrow M^* \quad [1]$$

$$M^* \rightarrow M^{+\bullet} + e^- \quad [2]$$

where M^* is the excited analyte species. Ionization can also occur through a secondary reaction with excited background gas or additive molecules (e.g. toluene) since the process takes place at atmospheric pressure.

The APPI ionization process is different from the atmospheric pressure ionization (API) techniques of ESI and atmospheric pressure chemical ionization (APCI) (*51, 52*) in that is does not rely on the analyte's proton affinity. As such, APPI is well suited for the

ionization and detection of low polarity and nonpolar compounds, particularly for those with high UV absorption (e.g. polyaromatic hydrocarbons).

Mass Spectrometry for Protein Analysis

There are several analytical tools used for the analysis and characterization of proteins: nuclear magnetic resonance (NMR), x-ray crystallography, and circular dichroism (CD) are three examples. Since the development of ESI and MALDI, mass spectrometry has also become a powerful tool for the analysis of proteins and has a number of useful applications and advantages over other analytical instrumentation. MS can provide accurate molecular weights, amino acid sequences, and higher order folding structures (conformations) of proteins. These three aspects of protein analysis play an important role in proteomics (the large-scale study of the structure and function of proteins) and are discussed further below.

High resolution mass spectrometry – High resolution mass spectrometry (HRMS) can be used to provide an accurate molecular mass of intact proteins, peptides resulting from protein digestion, or MS/MS fragment ions for protein sequencing. Fourier transform-ion cyclotron resonance (FT-ICR) mass spectrometers were the first ultra-high resolution instruments capable of resolving the ^{13}C isotopic distribution of multiply charged protein ions (*53, 54*). The recently developed orbitrap mass spectrometer is another example of an ultra-high resolution instrument (*55*). Both FT-ICR and orbitrap instruments have greater than 100,000 mass resolution and sub-ppm mass accuracy. Accurate mass time-of-flight (TOF) instruments can also provide HRMS data, with mass resolution greater than 50,000. However, this resolution typically isn't enough to resolve the ^{13}C isotopic distribution of the

higher charge states of protein ions generated via ESI. It is suitable, though, for accurate mass information of tandem mass spectrometry (MS/MS) protein and peptide fragments. However, TOF instruments generally have much higher mass ranges than FT-ICR or orbitrap instruments. For this reason, they are ideally suited for intact protein analysis via MALDI.

Along with providing accurate molecular weight information of proteins and peptides, HRMS instruments are very useful for determining their primary sequence as well. Bottom-up and top-down protein analysis are two general methods which have been developed for this purpose (*56-62*).

Bottom-up approach for proteomics – The bottom-up approach to proteomics utilizes proteolytic digestion of proteins prior to analysis by mass spectrometry. Resulting peptide fragments are then characterized by MS, or more routinely, MS/MS (*63*). Collision induced dissociation (CID) is the most common method used to fragment the peptide. In CID, ions collide with an inert gas (He, N_2, or Ar) and fragment along the peptide backbone (between the carboxyl carbon and amino nitrogen) into a series of so-called b- and y-ions (*64*). The fragmentation pattern can be analyzed (usually through database searches) to deduce the sequence of the original peptide and protein. This approach is referred to as de novo sequencing (without database) or MS/MS protein matching (with database) (*65-67*). LC separation prior to MS analysis is also commonly used to separate isobaric peptides, i.e. peptides with the same amino acids and m/z ratio but different sequences.

Top-down approach for proteomics – A more recent approach for proteomics is the top-down method, which was advanced by McLafferty and co-workers (*58*). The intact protein (or mixture of proteins) is introduced into the high resolution mass spectrometer. MS

spectra are generated for each protein in the sample. Then, individual charge states of each protein are isolated and dissociated. The fragments, in combination with the accurate mass of the intact protein, can be used for sequencing information. One of the main benefits of the top down approach is that it requires much less sample preparation than the bottom up approach. However, it also requires costly specialized instrumentation, namely a high resolution mass spectrometer.

Another approach to top-down proteomics, which has all but replaced the above described method, uses gas-phase ion/ion reactions to fragment the intact protein. The fragmentation is accomplished by electron capture dissociation (ECD) (*68-70*) or electron transfer dissociation (ETD) (*71*). In ECD, low energy electrons are introduced into the mass spectrometer. These electrons are trapped with the gas phase protein ions and produce odd-electron, free-radical driven fragmentation along the protein backbone. The fragmentation process for ETD is the same as ECD; the difference is the source of the free electrons. In ETD, free electrons are transferred to the protein ion by a radical anion (e.g. azobenzene, $[(C_6H_5)_2N_2]^{-\bullet}$). Both ECD and ETD result in so-called c- and y-type fragment ions (*64*).

Although the top-down approach is not utilized in this dissertation, there is much interest in other gas-phase ion/ion reactions for the characterization of biomolecules. One type ion/ion reaction in particular, proton transfer charge reduction, is employed for the analysis of protein conformations in Chapter 2.

Ion/ion reactions – The development of gas-phase ion/ion reactions for the characterization of proteins and peptides has been an area of recent interest (*72-74*). For these reactions, positive and negative ions are simultaneously stored, usually in an ion trap.

The electrostatic attraction between these ions causes their ion clouds to overlap. Of interest for this work is the development of proton transfer reactions (*75-81*).

Proton transfer reactions involve the transfer of a proton, usually from a multiply charged protein cation, to a singly charged even-electron anion. The product of the reaction is a charge reduced cation and a neutral species:

$$[M + nH]^{n+} + B^{-} \rightarrow [M + (n-1)H]^{n-1+} + HB \quad [3]$$

where B is an electronegative anion such as perfluoromethyldecalin (PMD) or perfluoro-1,3-dimethylcylcohexane (PDCH).

Since ESI produces high charge state protein ions, proton transfer reactions can be used to reduce the charge of the protein to a more "native" value. This is important for the work presented herein as we are interested in measuring the three-dimensional gas-phase conformations of proteins. Proteins typically unfold as they gain more charge due to the Columbic repulsion of like charges. As a protein ion is charge reduced into a more "native-like" charge state, it will refold into more compact conformations (*82-85*). In this dissertation, these conformations are measured via ion mobility spectrometry-mass spectrometry (IMS-MS).

Ion Mobility Spectrometry Mass Spectrometry

Ion mobility spectrometry involves the measurement of the time required for an ion to travel through a buffer gas under an axial electric field (*86*). When coupled to a mass spectrometer, IMS provides valuable information about the gas-phase conformation of an ion

(*87*, *88*). The ion mobility and mass spectral information can be used to probe the tertiary and quaternary structure of proteins and other biomolecules (*82*, *89-96*).

Principles of ion mobility – In IMS, ions travel inside a drift tube. This drift tube has a uniform electric field which carries the ions through the tube. The drift tube also contains a buffer gas, typically He. As the ion moves through the drift tube, collisions with the background gas impede the forward motion. The consequent drift velocity can be written as (*97*):

$$v_d = KE = L/t_d \quad [4]$$

where K is the ion mobility coefficient and is an intrinsic property of the ion, v_d is the velocity of the ion, E is the applied electric field (V/cm), L is the length of the drift tube (cm), and t_d is the amount of time it takes the ion to travel through the drift tube, referred to as drift time (s). Given the same charge, an ion with a more compact conformation will have fewer collisions with the background gas and will therefore travel through the drift tube faster than an ion in a more elongated conformation. For this reason, ion mobility is said to separate ions based on their size-to-charge ratio whereas a mass spectrometer separates ions based on their mass-to-charge ratio.

In order to calculate the mobility of an ion through a drift tube, other experimental parameters have to be taken into consideration. Equation 4 does not take into account the physical properties of the buffer gas system (pressure and temperature). Therefore, ion mobility is measured and specific experimental parameters are used to report the reduced

mobility, K_0, of the ion at standard temperature and pressure. Adding these parameters and rearranging to solve for K_0, Equation 4 becomes:

$$K_0 = \frac{L^2}{t_d V} \times \frac{273.3}{T} \times \frac{p}{760} \quad [5]$$

where V is the voltage drop across the drift tube (V/cm), T is temperature of the buffer gas (K) and p is the pressure of the buffer gas (Torr).

The ratio of the electric field to the number density of the buffer gas (*E/N*) is another important parameter that defines the energy of the ion in the drift tube. The velocity of an ion through the drift tube is directly proportional to the applied electric field. As the electric field increases, the collisions between the buffer gas and the ion become more energetic. At some *E/N* ratio, the excess energy from these collisions is converted to thermal energy. This thermal energy can change the shape of the ion. In the low-field regime (low *E/N* ratio), the energy gained by the ion is dissipated by collisions with the buffer gas and the mobility coefficient is independent of the electric field. In the high-field regime (high *E/N* ratio), the energy the ion gains from the collisions with the buffer gas is greater than the energy dissipated by the collisions (*98-101*) and the mobility of the ion through the drift tube is dependent on the *E/N* ratio.

All experiments in this work were performed in the low-field region. Therefore, the mobility of the ion is dependent on the average collision cross section ($Å^2$), Ω_{ave}, of the ion and can be mathematically expressed by the following (*91, 102*):

$$K = \frac{(18\pi)^{1/2}}{16}\left[\frac{1}{m} + \frac{1}{m_b}\right]^{1/2} \frac{ze}{(k_B T)^{1/2}\Omega_{ave}^{(1,1)}}\frac{1}{N} \quad [6]$$

where m and m_b are the mass of the ion and buffer gas, respectively (kg), k_B is the Boltzmann constant, T is temperature (K), z is the charge of the ion, and N is the buffer gas number density. If we combine equations 5 and 6, simplify the terms, use the corrected nested drift time, t_d, and solve for the average collision cross section, Ω_{ave}, we get:

$$\Omega_{ave} = \frac{3}{16}\sqrt{\frac{2\pi}{\mu k_B T}}\frac{Q}{N}\frac{t_d U}{L^2} \quad [7]$$

where μ is the reduced mass, Q is the charge (coulombs), and U is the voltage drop across the drift tube (V). In a normal experiment, the reduced mass, temperature, charge, number density, voltage across the drift tube, and length of the drift tube are held constant. These parameters can be entered into equation 7, along with the measured drift time, to calculate the three-dimensional rotationally-averaged gas-phase collision cross section of a particular charge state of a protein ion.

Instrumentation for ion mobility spectrometry mass spectrometry – The instrument used in this dissertation to collect mobility information and perform the proton transfer reactions was a custom built 3-D ion trap – ion mobility – time-of-flight mass spectrometer (*103*). A schematic of this instrument can be seen in Figure 1. The instrument was designed with three ionization sources, two ESI and one atmospheric sampling glow discharge ionization (ASGDI). The ASGDI source is used to generate negative anions for ion/ion reactions. Ions enter the mass spectrometer through a series of lenses and are focused

onto the axis of the instrument by a turning quadrupole (TQ). After the TQ, the ions are stored in a 3-D ion trap. The voltages applied to the lenses and TQ can be alternated between positive and negative to allow ions of each polarity into be simultaneously stored and reacted. Once the ions have reacted for a set amount of time, the product ions are ejected from the trap and injected into the ion mobility drift tube. The drift tube is 44.45 cm long and has an ion funnel at the exit to focus the ion packet toward the drift tube exit. The drift tube is constructed with alternating 12.7 cm diameter 304 stainless steel lenses and Delrin insulating rings and is filled with ~ 1.5 Torr He to serve as the buffer gas. After the ions exit the drift tube they pass through a series of lenses and a quadrupole collision cell, which transmits the ion packet to the orthogonal W-reflectron TOF. For these experiments, the TOF was operated in V-reflectron mode. Ions are then detected by an eight-anode micro-channel plate. This design provides the user with both drift time and mass spectral information.

Dissertation Overview

This dissertation focuses on utilizing hyphenated mass spectrometry methods for the characterization of biomolecules. In Chapter 2, ion trap – ion mobility – time-of-flight mass spectrometry is used to investigate the conformations of positive protein ions generated directly from a solution at pH 8.0. These conformations are compared to conformations obtained via proton transfer reactions. Chapter 3 focuses on the application of HPLC accurate-mass time-of-flight mass spectrometry for the identification of α-zein proteins from maize. This study represents the first comprehensive accurate mass analysis of these proteins. Chapter 4 utilizes MS/MS on an accurate-mass time-of-flight mass spectrometer to

identify and sequence phosphopeptides from proteolytic digestions of phosvitin, a hen-egg yolk protein. And finally, Chapter 5 introduces a novel ionization technique for the application of atmospheric pressure imaging mass spectrometry. The ion source combines UV-laser ablation LDI with APPI for post-ionization. The purpose of the ion source is to improve the detection of nonpolar analytes.

REFERENCES

1. Talroze, V. L.; Karpov, G. V.; Gorodets.Ig; Skurat, V. E., Capillary system for the introduction of liquid mixtures into an analytical mass spectrometer. *Russ. J. Phys. Chem.* **1968,** *42*, 1658-1664.
2. Melera, A., Design, operation, and applications of a novel LCMS CI interface. *Adv. Mass Spectrom.* **1980,** *88*, 1597-1615.
3. Caprioli, R. M.; Fan, T.; Cottrell, J. S., Continuous flow sample probe for fast atom bombardment mass spectrometry. *Anal. Chem.* **1986,** *58*, 2949-2954.
4. Blakley, C. R.; McAdams, M. J.; Vestal, M. L., Crossed-beam liquid chromatograph-mass spectrometer combination. *J. Chromatogr.* **1978,** *158*, 261-276.
5. Vestal, M. L.; Fergusson, G. J., Thermospray liquid chromatograph-mass spectrometer interface with direct electrical heating of the capillary. *Anal. Chem.* **1985,** *57*, 2373-2378.
6. Bruins, A. P.; Covey, T. R.; Henion, J. D., Ion spray interface for combined liquid chromatography-atmospheric pressure ionization mass spectrometry. *Anal. Chem.* **1987,** *59*, 2642-2646.
7. Covey, T. R.; Lee, E. D.; Bruins, A. P.; Henion, J. D., Liquid chromatography mass spectrometry. *Anal. Chem.* **1986,** *58*, 1451-1461.
8. Gohlke, R. S.; McLafferty, F. W., Early gas-chromatography mass spectrometry. *J Am Soc. Mass Spectrom.* **1993,** *4*, 367-371.
9. Gohlke, R. S., Time-of-flight mass spectrometry and gas-liquid partition chromatography. *Anal. Chem.* **1959,** *31*, 535-541.
10. Holmes, J. C.; Morrell, F. A., Oscillographic mass spectrometric monitoring of gas chromatography *Appl. Spectrosc.* **1957,** *11*, 86-87.
11. Olivares, J. A.; Nguyen, N. T.; Yonker, C. R.; Smith, R. D., Online mass-spectrometric detection for capillary zone electrophoresis. *Anal. Chem.* **1987,** *59*, 1230-1232.
12. McAfee, K. B.; Edelson, D., Identification and mobility of ions in a Townsend discharge by time-resolved mass spectrometry. *Proc. Phys. Soc. London* **1963,** *81*, 382-384.
13. McKnight, L. G.; McAfee, K. B.; Sipler, D. P., Low-field drift velocities and reactions of nitrogen ions in nitrogen. *Phys. Rev.***1967,** *164*, 62-70.
14. Cohen, M. J.; Carroll, D. I.; Wernlund, R. F.; Kilpatrick, W. D. Apparatus and methods for detecting and identifying trace gases. U.S. Patent 3,621,240, May 27, 1969.
15. Barber, M.; Bordoli, R. S.; Sedgwick, R. D.; Tyler, A. N., Fast atom bombardment of solids (FAB) - A new ion-source for mass spectrometry. *J. Chem. Soc.-Chem. Commun.* **1981**, 325-327.
16. Liu, L. K.; Busch, K. L.; Cooks, R. G., Matrix-assisted secondary ion mass spectra of biological compounds. *Anal. Chem.* **1981,** *53*, 109-113.
17. Karas, M.; Bachmann, D.; Hillenkamp, F., Influence of the wavelength in high-irradiance ultraviolet laser desorption mass spectrometry of organic molecules. *Analytical Chemistry* **1985,** *57*, 2935-2939.
18. Karas, M.; Gluckmann, M.; Schafer, J., Ionization in matrix-assisted laser desorption/ionization: singly charged molecular ions are the lucky survivors. *J. Mass Spectrom.* **2000,** *35*, 1-12.

19. Tanaka, K.; Waki, H.; Ido, Y.; Akita, S.; Yoshida, Y.; Yohida, T., Protein and polymer analyses up to m/z 100,000 by laser ionization time-of-flight mass spectrometry. *Rapid Commun. Mass Spectrom.* **1988,** *2*, 151-153.
20. Hillenkamp, F.; Karas, M.; Beavis, R. C.; Chait, B. T., Matrix-assisted laser desorption ionization mass spectrometry of biopolymers. *Anal. Chem.* **1991,** *63*, A1193-A1202.
21. Fenn, J. B.; Mann, M.; Meng, C. K.; Wong, S. F.; Whitehouse, C. M., Electrospray ionization for mass spectrometry of large biomolecules. *Science* **1989,** *246*, 64-71.
22. Karas, M.; Bahr, U.; Dulcks, T., Nano-electrospray ionization mass spectrometry: Addressing analytical problems beyond routine. *Fresenius' J. Anal. Chem.* **2000,** *366*, 669-676.
23. Wilm, M.; Mann, M., Analytical properties of the nanoelectrospray ion source. *Anal. Chem.* **1996,** *68*, 1-8.
24. Blakley, C. R.; Vestal, M. L., Thermospray interface for liquid chromatography-mass spectrometry. *Anal. Chem.* **1983,** *55*, 750-754.
25. Hirabayashi, A.; Sakairi, M.; Koizumi, H., Sonic spray ionization method for atmospheric pressure ionization mass spectrometry. *Anal. Chem.* **1994,** *66*, 4557-4559.
26. The Nobel prize in chemistry 2002. http://www.nobelprize.org/nobel_prizes/chemistry/laureates/2002/ (July 1, 2012),
27. Spengler, B.; Hubert, M.; Kaufmann, R., MALDI ion imaging and biological ion imaging with a new scanning UV-laser microprobe. *Proc. of the 42nd Annual Conf. of Mass Spectrom. and Allied Topics* **1994**, 1041.
28. Taylor, G., Disintegration of water drops in an electric field. *Proc. of the Royal Soc. of London* **1964,** *280*, 383-397.
29. Beavis, R. C.; Chaudhary, T.; Chait, B. T., Alpha-cyano-4-hydroxycinnamic acid as a matrix for matrix-assisted laser desorption mass spectrometry. *Org. Mass Spectrom.* **1992,** *27*, 156-158.
30. Kampmeier, J.; Dreisewerd, K.; Schurenberg, M.; Strupat, K., Investigations of 2,5-DHB and succinic acid as matrices for IR and UV MALDI. Part I: UV and IR laser ablation in the MALDI process. *Int. J. Mass Spectrom.* **1997,** *169*, 31-41.
31. Karas, M.; Kruger, R., Ion formation in MALDI: The cluster ionization mechanism. *Chem. Rev.* **2003,** *103*, 427-439.
32. Gluckmann, M.; Pfenninger, A.; Kruger, R.; Thierolf, M.; Karas, M.; Horneffer, V.; Hillenkamp, F.; Strupat, K., Mechanisms in MALDI analysis: surface interaction or incorporation of analytes? *Int. J. Mass Spectrom.* **2001,** *210*, 121-132.
33. Knochenmuss, R., Ion formation mechanisms in UV-MALDI. *Analyst* **2006,** *131*, 966-986.
34. Weston, D. J., Ambient ionization mass spectrometry: current understanding of mechanistic theory; analytical performance and application areas. *Analyst* **2010,** *135*, 661-668.
35. Cooks, R. G.; Ouyang, Z.; Takats, Z.; Wiseman, J. M., Ambient mass spectrometry. *Science* **2006,** *311*, 1566-1570.
36. Wiseman, J. M.; Ifa, D. R.; Zhu, Y.; Kissinger, C. B.; Manicke, N. E.; Kissinger, P. T.; Cooks, R. G., Desorption electrospray ionization mass spectrometry: Imaging drugs and metabolites in tissues. *Proc. Natl. Acad. Sci. U. S. A.* **2008,** *105*, 18120-18125.

37. Esquenazi, E.; Yang, Y.-L.; Watrous, J.; Gerwick, W. H.; Dorrestein, P. C., Imaging mass spectrometry of natural products. *Nat. Prod. Rep.* **2009,** *26*, 1521-1534.
38. Zimmerman, T. A.; Monroe, E. B.; Tucker, K. R.; Rubakhin, S. S.; Sweedler, J. V., Imaging of cells and tissues with mass spectrometry: Adding chemical information to imaging. *Methods Cell Biol.* **2008,** *89*, 361-390.
39. Vickerman, J. C., Molecular imaging and depth profiling by mass spectrometry-SIMS, MALDI or DESI? *Analyst* **2011,** *136*, 2199-2217.
40. Wiseman, J. M.; Ifa, D. R.; Song, Q.; Cooks, R. G., Tissue imaging at atmospheric pressure using desorption electrospray ionization (DESI) mass spectrometry. *Angew. Chem.* **2006,** *45*, 7188-7192.
41. Sampson, J. S.; Hawkridge, A. M.; Muddiman, D. C., Generation and detection of multiply-charged peptides and proteins by matrix-assisted laser desorption electrospray ionization (MALDESI) Fourier transform ion cyclotron resonance mass spectrometry. *J. Am. Soc. Mass Spectrom.* **2006,** *17*, 1712-1716.
42. Shrestha, B.; Nemes, P.; Nazarian, J.; Hathout, Y.; Hoffman, E. P.; Vertes, A., Direct analysis of lipids and small metabolites in mouse brain tissue by AP IR-MALDI and reactive LAESI mass spectrometry. *Analyst* **2010,** *135*, 751-758.
43. Nemes, P.; Vertes, A., Laser ablation electrospray ionization for atmospheric pressure, in vivo, and imaging mass spectrometry. *Anal. Chem.* **2007,** *79*, 8098-8106.
44. Shiea, J.; Huang, M. Z.; Hsu, H. J.; Lee, C. Y.; Yuan, C. H.; Beech, I.; Sunner, J., Electrospray-assisted laser desorption/ionization mass spectrometry for direct ambient analysis of solids. *Rapid Commun. Mass Spectrom.* **2005,** *19*, 3701-3704.
45. Vaikkinen, A.; Shrestha, B.; Kauppila, T. J.; Vertes, A.; Kostiainen, R., Infrared laser ablation atmospheric pressure photoionization mass spectrometry. *Anal. Chem.* **2012,** *84*, 1630-1636.
46. Driscoll, J. N., Application of a photoionization detector in gas chromatography. *Am. Lab.* **1976,** *8*, 71-75.
47. Driscoll, J. N., Evaluation of a new photoionization detector for organic compounds. *J. Chromatog.* **1977,** *134*, 49-55.
48. Driscoll, J. N.; Clarici, J. B., A new photoionization detector for gas chromatography. *Chromatographia* **1976,** *9*, 567-570.
49. Locke, D. C.; Dhingra, B. S.; Baker, A. D., Liquid phase detector for liquid chromatography. *Analytical Chemistry* **1982,** *54*, 447-450.
50. Driscoll, J. N.; Conron, D. W.; Ferioli, P.; Krull, I. S.; Xie, K. H., Trace analysis of organic compounds by high-performance liquid chromatography with photoionization detection. *J. Chromatog.* **1984,** *302*, 43-50.
51. Carroll, D. I.; Dzidic, I.; Stillwell, R. N.; Haegele, K. D.; Horning, E. C., Atmospheric pressure ionization mass spectrometry - corona discharge ion source for use in liquid chromatograph-mass spectrometer-computer analytical system. *Anal. Chem.* **1975,** *47*, 2369-2373.
52. Horning, E. C.; Horning, M. G.; Carroll, D. I.; Dzidic, I.; Stillwel.Rn, New picogram detection system based on a mass spectrometer with an external ionization source at atmospheric pressure. *Anal. Chem.* **1973,** *45*, 936-943.
53. Comisaro.Mb; Marshall, A. G., Fourier-transform ion-cyclotron resonance spectroscopy. *Chem. Phys. Lett.* **1974,** *25*, 282-283.

54. Henry, K. D.; Williams, E. R.; Wang, B. H.; McLafferty, F. W.; Shabanowitz, J.; Hunt, D. F., Fourier-transform mass spectrometry of large molecules by electrospray ionization. *Proc. Natl. Acad. Sci. U. S. A.* **1989,** *86*, 9075-9078.
55. Hu, Q. Z.; Noll, R. J.; Li, H. Y.; Makarov, A.; Hardman, M.; Cooks, R. G., The Orbitrap: a new mass spectrometer. *J. Mass Spectrom.* **2005,** *40*, 430-443.
56. Chait, B. T., Mass spectrometry: Bottom-up or top-down? *Science* **2006,** *314*, 65-66.
57. Bogdanov, B.; Smith, R. D., Proteomics by FTICR mass spectrometry: Top down and bottom up. *Mass Spectrom. Rev.* **2005,** *24*, 168-200.
58. Kelleher, N. L.; Lin, H. Y.; Valaskovic, G. A.; Aaserud, D. J.; Fridriksson, E. K.; McLafferty, F. W., Top down versus bottom up protein characterization by tandem high-resolution mass spectrometry. *J. Am. Chem. Soc.* **1999,** *121*, 806-812.
59. Aebersold, R.; Goodlett, D. R., Mass spectrometry in proteomics. *Chem. Rev.* **2001,** *101*, 269-295.
60. Ong, S. E.; Mann, M., Mass spectrometry-based proteomics turns quantitative. *Nat. Chem. Bio.* **2005,** *1*, 252-262.
61. Aebersold, R.; Mann, M., Mass spectrometry-based proteomics. *Nature* **2003,** *422*, 198-207.
62. Bantscheff, M.; Schirle, M.; Sweetman, G.; Rick, J.; Kuster, B., Quantitative mass spectrometry in proteomics: a critical review. *Anal. Bioanal. Chem.* **2007,** *389*, 1017-1031.
63. Hunt, D. F.; Yates, J. R.; Shabanowitz, J.; Winston, S.; Hauer, C. R., Protein sequencing by tandem mass spectrometry. *Proc. Natl. Acad. Sci. U. S. A.* **1986,** *83*, 6233-6237.
64. Roepstorff, P.; Fohlman, J., Proposal for a common nomenclature for sequence ions in mass spectra of peptides. *Biomed. Mass Spectrom.* **1984,** *11*, 601-601.
65. Dancik, V.; Addona, T. A.; Clauser, K. R.; Vath, J. E.; Pevzner, P. A., De novo peptide sequencing via tandem mass spectrometry. *J. Comput. Biol.* **1999,** *6*, 327-342.
66. Dahiyat, B. I.; Mayo, S. L., De novo protein design: Fully automated sequence selection. *Science* **1997,** *278*, 82-87.
67. Shevchenko, A.; Chernushevich, I.; Ens, W.; Standing, K. G.; Thomson, B.; Wilm, M.; Mann, M., Rapid 'de novo' peptide sequencing by a combination of nanoelectrospray, isotopic labeling and a quadrupole/time-of-flight mass spectrometer. *Rapid Commun. Mass Spectrom.* **1997,** *11*, 1015-1024.
68. Zubarev, R. A.; Horn, D. M.; Fridriksson, E. K.; Kelleher, N. L.; Kruger, N. A.; Lewis, M. A.; Carpenter, B. K.; McLafferty, F. W., Electron capture dissociation for structural characterization of multiply charged protein cations. *Anal. Chem.* **2000,** *72*, 563-573.
69. Zubarev, R. A.; Kruger, N. A.; Fridriksson, E. K.; Lewis, M. A.; Horn, D. M.; Carpenter, B. K.; McLafferty, F. W., Electron capture dissociation of gaseous multiply-charged proteins is favored at disulfide bonds and other sites of high hydrogen atom affinity. *J. Am. Chem. Soc.* **1999,** *121*, 2857-2862.
70. Zubarev, R. A.; Kelleher, N. L.; McLafferty, F. W., Electron capture dissociation of multiply charged protein cations. A nonergodic process. *J. Am. Chem. Soc.* **1998,** *120*, 3265-3266.

71. Syka, J. E. P.; Coon, J. J.; Schroeder, M. J.; Shabanowitz, J.; Hunt, D. F., Peptide and protein sequence analysis by electron transfer dissociation mass spectrometry. *Proc. Natl. Acad. Sci. U. S. A.* **2004,** *101*, 9528-9533.
72. McLuckey, S. A.; Stephenson, J. L., Ion/ion chemistry of high-mass multiply charged ions. *Mass Spectrom. Rev.* **1999,** *18*, 83-86.
73. McLuckey, S. A. In *Recent developments in ion/ion chemistry for bioanalysis*, Federation of Analytical Chemistry and Spectroscopy Societies Conference, Memphis, TN, 2007; Memphis, TN, 2007.
74. Pitteri, S. J.; McLuckey, S. A., Recent developments in the ion/ion chemistry of high-mass multiply charged ions. *Mass Spectrom. Rev.* **2005,** *24*, 931-958.
75. Stephenson, J. L.; McLuckey, S. A., Ion/ion proton transfer reactions for protein mixture analysis. *Anal. Chem.* **1996,** *68*, 4026-4032.
76. Stephenson, J. L.; McLuckey, S. A., Ion/ion reactions in the gas phase: Proton transfer reactions involving multiply-charged proteins. *J. Am. Chem. Soc.* **1996,** *118*, 7390-7397.
77. Stephenson, J. L.; McLuckey, S. A., Adaptation of the Paul Trap for study of the reaction of multiply charged cations with singly charged anions. *Int. J. Mass Spectrom. Ion Processes* **1997,** *162*, 89-106.
78. Stephenson, J. L.; McLuckey, S. A., Charge manipulation for improved mass determination of high- mass species and mixture components by electrospray mass spectrometry. *J. Mass Spectrom.* **1998,** *33*, 664-672.
79. McLuckey, S. A.; Stephenson, J. L., Ion ion chemistry of high-mass multiply charged ions. *Mass Spectrom. Rev.* **1998,** *17*, 369-407.
80. McLuckey, S. A.; Stephenson, J. L.; Asano, K. G., Ion/ion proton-transfer kinetics: Implications for analysis of ions derived from electrospray of protein mixtures. *Anal. Chem.* **1998,** *70*, 1198-1202.
81. Stephenson, J. L.; McLuckey, S. A., Simplification of product ion spectra derived from multiply charged parent ions via ion/ion chemistry. *Anal. Chem.* **1998,** *70*, 3533-3544.
82. Shelimov, K. B.; Clemmer, D. E.; Hudgins, R. R.; Jarrold, M. F., Protein structure in vacuo: Gas-phase conformations of BPTI and cytochrome c. *J. Am. Chem. Soc.* **1997,** *119*, 2240-2248.
83. Valentine, S. J.; Anderson, J. G.; Ellington, A. D.; Clemmer, D. E., Disulfide-intact and -reduced lysozyme in the gas phase: Conformations and pathways of folding and unfolding. *J. Phys. Chem. B* **1997,** *101*, 3891-3900.
84. Badman, E. R.; Hoaglund-Hyzer, C. S.; Clemmer, D. E., Monitoring structural changes of proteins in an ion trap over similar to 10-200 ms: Unfolding transitions in cytochrome c ions. *Anal. Chem.* **2001,** *73*, 6000-6007.
85. Badman, E. R.; Myung, S.; Clemmer, D. E., Evidence for unfolding and refolding of gas-phase cytochrome c ions in a Paul trap. *J. Am. Soc. Mass Spectrom.* **2005,** *16*, 1493-1497.
86. Hill, H. H.; Siems, W. F.; Stlouis, R. H.; McMinn, D. G., Ion mobility spectrometry. *Anal. Chem.* **1990,** *62*, A1201-A1209.
87. Wu, C.; Siems, W. F.; Asbury, G. R.; Hill, H. H., Electrospray ionization high-resolution ion mobility spectrometry - mass spectrometry. *Anal. Chem.* **1998,** *70*, 4929-4938.

88. Henderson, S. C.; Valentine, S. J.; Counterman, A. E.; Clemmer, D. E., ESI/ion trap/ion mobility/time-of-flight mass spectrometry for rapid and sensitive analysis of biomolecular mixtures. *Anal. Chem.* **1999,** *71*, 291-301.
89. Mesleh, M. F.; Hunter, J. M.; Shvartsburg, A. A.; Schatz, G. C.; Jarrold, M. F., Structural information from ion mobility measurements: Effects of the long-range potential. *J. Phys. Chem.* **1996,** *100*, 16082-16086.
90. Chen, Y. L.; Collings, B. A.; Douglas, D. J., Collision cross sections of myoglobin and cytochrome c ions with Ne, Ar, and Kr. *J. Am. Soc. Mass Spectrom.* **1997,** *8*, 681-687.
91. Clemmer, D. E.; Jarrold, M. F., Ion mobility measurements and their applications to clusters and biomolecules. *J. Mass Spectrom.* **1997,** *32*, 577-592.
92. Hudgins, R. R.; Woenckhaus, J.; Jarrold, M. F., High resolution ion mobility measurements for gas phase proteins: correlation between solution phase and gas phase conformations. *Int. J. Mass Spectrom.* **1997,** *165*, 497-507.
93. Liu, Y. S.; Clemmer, D. E., Characterizing oligosaccharides using injected-ion mobility mass spectrometry. *Anal. Chem.* **1997,** *69*, 2504-2509.
94. Liu, Y. S.; Valentine, S. J.; Counterman, A. E.; Hoaglund, C. S.; Clemmer, D. E., Injected-ion mobility analysis of biomolecules. *Anal. Chem.* **1997,** *69*, A728-A735.
95. Shelimov, K. B.; Jarrold, M. F., Conformations, unfolding, and refolding of apomyoglobin in vacuum: An activation barrier for gas-phase protein folding. *J. Am. Chem. Soc.* **1997,** *119*, 2987-2994.
96. Hoaglund, C. S.; Valentine, S. J.; Sporleder, C. R.; Reilly, J. P.; Clemmer, D. E., Three-dimensional ion mobility TOFMS analysis of electrosprayed biomolecules. *Anal. Chem.* **1998,** *70*, 2236-2242.
97. Mason, E. A.; McDaniel, E. W., *Transport properties of ions in gases*. Wiley: New York, 1988.
98. Buryakov, I. A.; Krylov, E. V.; Nazarov, E. G.; Rasulev, U. K., A new method of separation of multi-atomic ions by mobility at atmospheric-pressure using a high-frequency amplitude-asymmetric strong electric-field. *Int. J. Mass Spectrom. Ion Processes* **1993,** *128*, 143-148.
99. Purves, R. W.; Guevremont, R.; Day, S.; Pipich, C. W.; Matyjaszczyk, M. S., Mass spectrometric characterization of a high-field asymmetric waveform ion mobility spectrometer. *Review of Scientific Instruments* **1998,** *69*, 4094-4105.
100. Guevremont, R.; Purves, R. W., Atmospheric pressure ion focusing in a high-field asymmetric waveform ion mobility spectrometer. *Rev. Sci. Instrum.* **1999,** *70*, 1370-1383.
101. Guevremont, R., High-field asymmetric waveform ion mobility spectrometry: A new tool for mass spectrometry. *J. Chromatog. A* **2004,** *1058*, 3-19.
102. Revercomb, H. E.; Mason, E. A., Theory of plasma chromatography gaseous electrophoresis - review. *Anal. Chem.* **1975,** *47*, 970-983.
103. Zhao, Q.; Soyk, M. W.; Schieffer, G. M.; Fuhrer, K.; Gonin, M. M.; Houk, R. S.; Badman, E. R., An ion trap-ion mobility-time-of-flight mass spectrometer with three ion sources for ion/ion reactions. *J. Am. Soc. Mass Spectrom.* **2009,** *20*, 1549-1561.

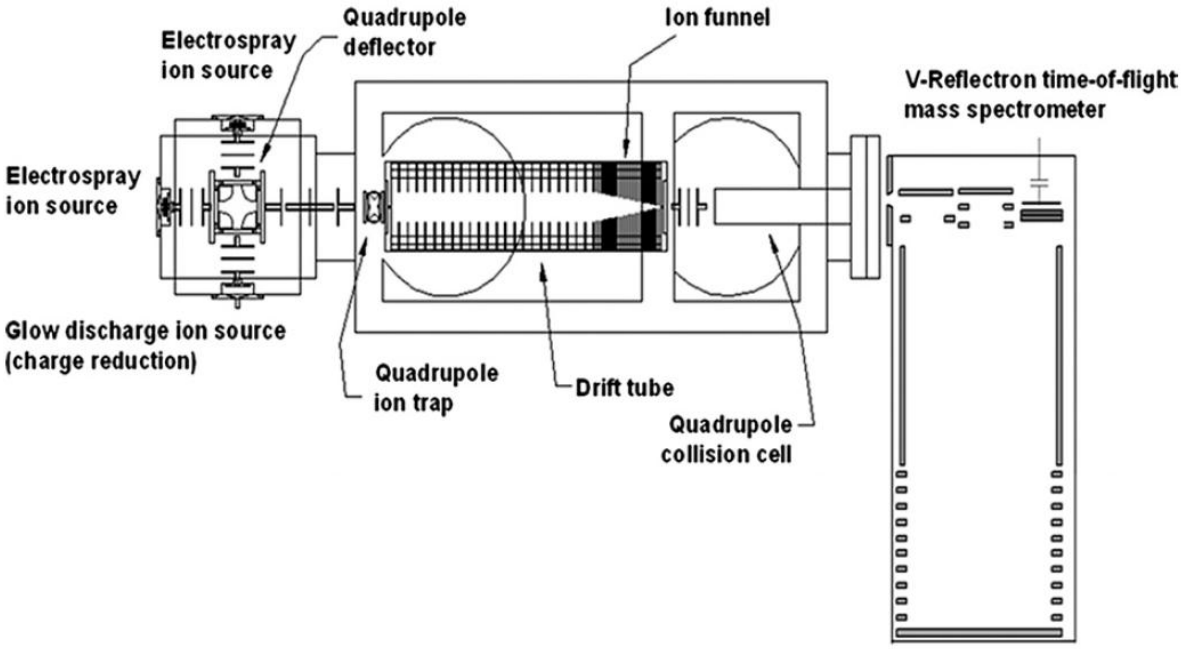

Figure 1. Scale diagram showing overall instrument, including two ESI and one ASGDI sources, ion optics, quadrupole deflector, IT, IM drift tube with ion funnel, and q-TOP. The ion source cube is 20 cm wide (*103*).

CHAPTER 2

PROTEIN CATIONS IN HIGHLY FOLDED CONFORMATIONS FROM MODERATELY ALKALINE (pH 8.0) SOLUTIONS BY ELECTROSPRAY IONIZATION ION MOBILITY MASS SPECTROMETRY

Derrick L. Morast[a,b], Timothy J. Anderson[a,b], James K. Anderson[a], Royce W. Blackledge[b], Michael T. Zimmermann[c], Ethan R. Badman[d], R. S. Houk[*a,b]

[a]Ames Laboratory U. S. Department of Energy, Ames, IA 50011 USA

[b]Department of Chemistry, Iowa State University, Ames, IA 50011 USA

[c]Bioinformatics and Computational Biology, Iowa State University, Ames, IA 50011 USA

[d]Hoffman-La Roche, Nutley, NJ 07110 USA

*Corresponding Author. Tel (515) 294-9462 Fax-0050 rshouk@iastate.edu

A manuscript for submission to The Journal of the American Society for Mass Spectrometry

ABSTRACT

Ion mobility spectrometry mass spectrometry (IMS-MS) is used to measure gas-phase conformations of ubiquitin, cytochrome *c*, lysozyme, and α-lactalbumin sprayed from an ammonium acetate solution titrated to pH 8.0. Ion mobility drift time measurements are converted to collision cross section values, in $Å^2$, and compared to corresponding charge state conformations generated via proton transfer charge reduction ion/ion reactions. Ions made directly from the alkaline solution in low charge states have conformations which are found to be 14 to 36% more compact than ions generated from proton transfer reactions.

KEYWORDS

Ion mobility spectrometry, mass spectrometry, ubiquitin, cytochrome *c*, lysozyme, α-lactalbumin

INTRODUCTION

Ion mobility spectrometry coupled to mass spectrometry (IMS-MS) is a useful analytical tool which can measure gas-phase conformations of biomolecules (*1-7*). Typically, electrospray ionization (ESI) is used to transport the analyte from solution to the gas-phase of the mass spectrometer. Biomolecules are dissolved in solvents ranging from pure water to 50/50 water/methanol. As most analysis utilizes positive-mode ESI, the analyte solution is generally acidified with a low percentage (0.1 to 1%) of either formic or acetic acid. The development of nano-electrospray (nESI) (*8*) has advanced the use of native mass spectrometry in which biomolecules are analyzed using "native" solution conditions, i.e. no organic solvent and biological pH (~7.4).

ESI produces highly charged protein ions, especially from acidic solutions. The protein ions generated via ESI generally contain more protons than expected from the solution charge of the protein. Mass spectra of proteins from native solution ESI usually have fewer charges compared to their acidic counterparts; however, the resulting protein ions are still routinely more protonated than they were in the solution phase. One method of analyzing more "native" charge states is through the use of proton transfer reactions (*9-15*). These ion/ion reactions can be used to charge reduce highly protonated protein ions through a gas-phase reaction between the positively charged protein and an electronegative anion.

With the rapid expansion of IMS-MS (including the commercialization of the technique) there has been much discussion/debate about whether gas-phase ions adapt conformations resembling those in solution phase (*16-22*). An aspect of this question that is widely accepted is that solution conditions can influence protein tertiary structure. If the goal

of the experiment is to measure biologically relevant conformations, it is important to know the solution conditions in which the particular protein retains native structure.

The present work examines gas-phase collision cross sections (CCS) of ubiquitin, cytochrome *c*, lysozyme, and α-lactalbumin from a slightly alkaline solution (pH = 8.0) using positive-mode IMS-MS. These samples are obtained by partially titrating the ammonium acetate solution (originally pH 7.2) commonly used for native ESI (*23, 24*). The measured cross sections are compared with data obtained from acidic and native solutions via proton transfer reactions. Many mass spectrometry studies have been performed on proteins from alkaline solutions in negative ion mode (*22, 25-32*), often at much more basic pH values than the 8.0 used here. Bowers, et al. have recently shown that positive and negative 6+, 7+, and 8+ ions of ubiquitin from pure water and 50/50 water/methanol solutions have similar cross sections (*22*). However these solutions would have pH values closer to 7.0 than 8.0. Ions in low charge states with minimal intramolecular electrostatic repulsion are emphasized.

MATERIALS AND METHODS

Proteins and Chemicals - Ammonium acetate (certified ACS), glacial acetic acid (certified ACS Plus), and methanol (HPLC grade) were purchased from Fisher Scientific (Waltham, MA, USA). Perfluoro(methyldecalin) (PMD, $C_{11}F_{20}$) was purchased from Sigma-Aldrich (St. Louis, MO, USA). Bovine ubiquitin, bovine heart cytochrome *c*, chicken egg white lysozyme, and bovine milk α-lactalbumin were purchased from Sigma-Aldrich (St. Louis, MO, USA) and used without further purification.

Ion Mobility and Mass Spectrometer - Nano-ESI spray tips were made from borosilicate glass capillaries (1.5 mm o.d., 0.86 mm i.d.) using a micropipette puller (P-97; Sutter Instruments, Novato, CA). The spray tips were loaded with ~ 10 µL of protein solution at 20 to 30 µM. Proteins were prepared in one of three ESI solutions: 0.5 mM ammonium acetate in water (native solution), 1% acetic acid in water (acidic solution), and 0.5 mM ammonium acetate in water adjusted to pH 8.0 with ammonium hydroxide (alkaline solution). The observed signal was ~ 2 to 3 times lower for each protein from the alkaline solution compared to the native solution and ~ 8 to 10 times lower than the acidic solution.

Nano-ESI was done in air at atmospheric pressure and room temperature by applying between +1.0 and +1.2 kV to the protein solution via a stainless steel wire inserted into the back of the sample capillary.

All IMS-MS data was collected using a home-built three source ion trap-ion mobility-time-of-flight mass spectrometer. The design and general operating conditions of the instrument have been described previously (*33*). Briefly, ESI-generated protein ions enter an interface region, which is kept at ~ 1 mbar with a mechanical pump. Ions are guided to a turning quadrupole (TQ) where they were deflected 90° onto the axis of the instrument. From the TQ, the ions are focused and stored in a 3D quadrupole ion trap (IT).

For charge reduction gas-phase ion/ion reactions, negative ions were generated via atmospheric sampling glow discharge ionization (ASGDI). PMD was used as the proton transfer reagent. Positive protein ions were stored in the 3D ion trap first. Negative ions were then introduced into the trap by switching the ion lens voltages. Positive protein ions and negative PMD ions were allowed to react between 50 and 80 ms. Reaction time varied

depending on the desired charge state, with longer reaction times resulting in lower charge states. Previous studies have indicated, at least for this time regime, cytochrome *c* conformers are not strongly dependent on trapping time (*18, 34, 35*). This was also verified for the proteins used in this study (data not shown).

After the ions had been allowed to react, the negative ions were ejected from the IT. The remaining protein ions were cooled for 30 ms and then injected into the drift tube for IM separation. The drift tube was 44.45 cm long and filled with helium at ~ 2 mbar. The voltage drop across the drift tube was 450 V (-50 V applied to the drift tube entrance plate and -500 V applied to the drift tube exit plate). The ion trap ejection pulse was -100 V. The ion trap ejection pulse length was optimized for each protein to minimize heating and unfolding during injection. Following IM separation of the product ions, *m/z* analysis and detection was performed by TOF-MS.

Collision Cross Sections - Collision cross sections (Ω), reported in $Å^2$, were calculated from the mass resolved mobility spectra and instrument parameters as described previously (*33, 36*). The drift time for each ion was calculated by measuring the total elapsed time between the ion trap exit pulse and TOF detection, with the flight time between the drift tube exit and TOF source region subtracted from the total time.

Cross sections were calculated from X-ray diffraction or NMR structures with MOBCAL, a Fortran program for calculating mobilities of ions, using the exact hard sphere scattering (EHSS) method (*37-39*). This gave results very close to those generated by the more rigorous but computationally intensive trajectory method (TM). The projection

approximation method generally underestimates the cross section value of proteins and was not used here.

RESULTS AND DISCUSSION

Ubiquitin - Ubiquitin is a small protein with 76 amino acids and a molecular weight of 8.5 kDa. Its structure has been well characterized by x-ray crystallography and nuclear magnetic resonance (NMR) (*40-42*). The gas-phase conformations of ubiquitin have also been vigorously explored by IMS-MS (*22, 33, 43-47*). The structure of ubiquitin is very stable at neutral pH, with a denaturation temperature >100 °C (*48, 49*). NMR studies have established that ubiquitin is stable in solution up to pH 8.5 (*50*).

MOBCAL simulations from x-ray crystallography measurements have estimated the collision cross section of native ubiquitin using the RSCB Protein Data Bank (PDB) (*51*) entry 1UBQ (*40*); EHSS and TM simulations were reported as 1088 and 1055 $Å^2$, respectively (*21*). These two values are usually chosen to be characteristic of the "native" conformation (*22, 43, 45, 52*).

On our instrument, typical charge states of ubiquitin from native or acidic aqueous solutions are between 6+ and 8+. Collision cross sections of gas-phase ubiquitin ions from nESI of a 1% acetic acid in water solution have been previously reported for this instrument (*33*). These ions were generated via proton transfer charge reduction of 7+ and 8+ ubiquitin. For 3+, 4+, and 5+ ions, the most compact conformation had cross sections between 800 and 900 $Å^2$. Collision cross sections of ubiquitin analyzed via matrix-assisted laser

desorption/ionization (MALDI)-IMS-MS have also been reported (*47*). MALDI primarily produces singly charged ions. Cross section values for the 1+ ion of ubiquitin were reported as 821 Å^2.

Figure 1 shows ion mobility spectra, converted to collision cross sections in Å^2, obtained from ubiquitin ions directly from the alkaline solution. The apex of the 3+ peak is centered on 585 Å^2. This value is about 28% more compact than the corresponding cross section obtained for the same 3+ ion via proton transfer reactions. The 4+ ion has a calculated collision cross section of 740 Å^2, which is 14% more compact than the 4+ ion made by proton transfer. The 5+ ion has two distinct conformations. The more compact conformation (leftmost peak) has a collision cross section of 743 Å^2 while the less compact conformation (rightmost peak) has a collision cross section of 852 Å^2. Conventional nomenclature would refer to the two peaks as compact and partially folded; however, conformations with cross sections below 1120 Å^2 are thought to be fully folded ubiquitin (*43*). The conformation with a cross section of 743 Å^2 is about 15% more compact the than the most compact value generated from proton transfer reactions (872 Å^2) (*33*).

Cytochrome *c* - Cytochrome *c* (104 amino acids plus Fe-heme group, 12.3 kDa) is another protein whose structure has been well characterized and studied by x-ray crystallography (*53*), NMR (*54*), and IMS-MS (*18, 35, 47, 55-57*). In 1941, oxidized cytochrome c (ferricytochrome c) was found to have five resolvable, pH dependent states (named states I to V) using absorption spectrophotometry (*58*). The native state, III, undergoes an alkaline transition, with an apparent pK_a of 8.4 to 8.9 (*59*).

MOBCAL simulations from x-ray crystallography measurements, PDB entry 1HRC (*53*), yielded collision cross section estimations of 1056, 1317, and 1310 Å^2 for PA, EHSS, and TM, respectively (*21*). Simulations from NMR solution coordinates, PBD entry 1LC1 (*60*), estimated the cytochrome *c* collision cross section to be 1324 and 1314 Å^2 for EHSS and TM, respectively (*61*).

MS analysis of cytochrome *c* from native or acidic aqueous solutions typically results in ions from 7+ to 9+. Collision cross sections of ions in lower charge states generated directly from native solutions and via proton transfer reactions from charge states 8+ and 9+ have been previously reported for this instrument (*35*). Ions in compact conformation(s) from 4+ to 6+ had measured collision cross sections between 970 and 1179 Å^2. Shelimov et al. (*56*) and Badman et al. (*18*) reported collision cross section values for cytochrome *c* down to the 3+ charge state. However, their experiments did not measure any cytochrome *c* ion having a calculated cross section lower than 1100 Å^2. Bowers and coworkers (*57*) used a modified Waters Ultima Q-TOF with a stacked ring drift cell to investigate gas-phase conformations of cytochrome *c*. They measured similar cross section values as the two previously cited studies; however they also report a 5+ cytochrome *c* ion with a calculated collision cross section between 850 and 900 Å^2 (*57*). Solution conditions were not reported for this analysis; however this value is the most compact conformation we found reported in the literature. Cross sections for 1+ ion of cytochrome *c* obtained via MALDI-IMS-MS have been reported as 983 Å^2 (*47*).

Figure 2 displays the collision cross sections of cytochrome *c* 4+ to 6+ ions measured directly from the alkaline solution. The 4+, 5+, and 6+ ions have measured collision cross

sections of 870, 997, and 1160 Å^2, respectively. The measured cross section values for the 5+ and 6+ ions have similar cross sections to the most abundant conformation of the 5+ and 6+ ions previously reported from acidic solutions for this instrument (*35*). The 4+ ion, however, is about 14% more compact than the value measured for the same ions made via proton transfer reactions (1015 Å^2). The measured cross section of 870 Å^2 is very similar in size to the smaller value reported for the 5+ cytochrome *c* ion by Bowers. To our knowledge, Bowers' paper and ours are the only ion mobility experiments that report such a compact conformation for cytochrome *c*.

Lysozyme - Lysozyme (128 amino acids, 14.3 kDa) was the first enzyme whose three-dimensional structure was characterized by x-ray crystallography (*62*). Its solution and gas phase structures have also been explored via NMR (*63*) and IMS-MS (*19, 47*). Lysozyme contains four disulfide bonds, which help stabilize the tertiary structure. These bonds also prevent the protein from completely unfolding. As such, similar ESI charge states are observed from aqueous and aqueous/organic solutions (typically 8+ to 10+ ions). Lysozyme is biologically active over a pH range of 6.0 to 9.0. The enzyme undergoes an alkaline conformational transition near its isoelectric point of 11.2, a pH value well above the 8.0 used in the present work (*64*). The native and alkaline solutions used in these experiments should, therefore, have similar solution phase conformations.

MOBCAL simulations from x-ray crystallography coordinates, PDB entry 1DPX (*65*), estimate the collision cross section of lysozyme at 1461 and 1468 Å^2 for EHSS and TM, respectively (*21*). In this PBD entry, lysozyme was precipitated from a pH 8.0 solution.

Simulations from solution NMR data, PDB entry 1GXX (*66*), yielded collision cross section values of 1451 and 1445 Å^2 for EHSS and TM, respectively (*61*).

Clemmer et al. reported collision cross sections of the lysozyme 5+ ion around 1300 Å^2 (*19*). Mao et al. also investigated and reported cross sections for lysozyme using ESI and H/D exchange (*67*). Their reported value for the lysozyme 6+ ion was around 1000 Å^2. Analysis via MALDI-IMS-MS measured a collision cross section for the 1+ ion of lysozyme of 1017 Å^2 (*47*).

Figure 3 shows ion mobility spectra of lysozyme 4+ to 6+ ions from the native solution (top panel) and the alkaline solution (bottom panel). The ions from the native solution were generated from gas-phase lysozyme 8+ to 10+ ions via proton transfer reactions in the ion trap. All ions in the bottom panel were generated directly from the alkaline solution. Charge reduction of native solution ions resulted in a smallest lysozyme conformer of ~1280 Å^2 for all three charge states shown. The alkaline solution lacked this conformer completely and yielded ions with smaller cross sections: 815, 910, and 1007 Å^2 for the 4+, 5+, and 6+ ions respectively. These values represent conformations which are 36, 29, and 21% more compact than the corresponding ions generated via proton transfer charge reduction reactions. To our knowledge, ions of this size have not been reported previously.

Alpha-Lactalbumin - Alpha-lactalbumin, which has a molecular weight of 14.1 kDa and four disulfide bonds, is structurally similar to lysozyme. The tertiary structure of α-lactalbumin has also been characterized by x-ray crystallography (*68-70*), NMR (*71, 72*), and IMS-MS (*57*). The alkaline conformational transition of α-lactalbumin occurs at pH 9.5 (*73, 74*). Therefore, the native and alkaline solutions used herein should have similar α-

lactalbumin solution structures, although this "transitional" pH is closer to the value used than was the case for lysozyme.

MOBCAL simulations for α-lactalbumin x-ray crystallography coordinates, PDB entry 1HFX (*69*), found collision cross section values of 1511 and 1523 Å^2 for EHSS and TM, respectively (*21*).

Figure 4A is a mass spectrum of α-lactalbumin from the native solution. Charge states > 8+ were generated directly from the solution. These ions were charge reduced to produce the lower charge states. Figure 4B is a mass spectrum of α-lactalbumin from the alkaline solution with all ions generated directly from the solution. In general, the peaks from the alkaline solution were not as well resolved as the peaks from proton transfer reactions. This is most likely due to salt adducts. However, the instrument software allowed selection of only a restricted m/z window (i.e., the m/z of the protein ion of interest plus 10 m/z units) for generation of the IM spectra and the resulting cross sections.

Figure 5 shows ion mobility spectra of α-lactalbumin 4+ to 6+ ions generated via proton transfer charge reduction vs. those directly from the alkaline solution. The 4+ to 6+ ions from proton transfer reactions had collision cross sections between 1200 and 1220 Å^2. These ions were charge reduced from 8+ to 11+ ions. Identical results were observed for both the native and the acidic solution. The 4+ ion directly from the alkaline solution had a calculated collision cross section of 884 Å^2 while the 5+ ion had a collision cross section of 996 Å^2. The measured collision cross section of the 4+ ion is about 26% more compact than the 4+ ion from proton transfer reactions. The measured value for the 5+ ion is about 17% more compact than the corresponding charge reduction ion. Virtually all the 4+ and 5+

lactalbumin ions from the alkaline solution are in the "overfolded" conformations. The 6+ ion, with a collision cross section of 1195 Å^2, was nearly identical in size to the charge reduced 6+ ion.

CONCLUSION

There has been ongoing interest in mass spectrometric analysis of proteins in their native state. The debate over whether or not IMS-MS collision cross section values represent solution phase structures also continues. The results presented herein demonstrate the significant impact solution conditions can have on observed protein conformations. We have shown that a small change in pH, from the commonly used "native" 7.4 to an alkaline 8.0, results in conformations much smaller than those usually seen. The biological significance of these observations remains unclear.

ACKNOWLEDGEMENTS

The authors would like to thank the U.S. Department of Energy Science Undergraduate Laboratory Internship Program for providing the internship and funding for James Anderson. Derrick Morast would like to acknowledge the Velmer A. and Mary K. Fassel Fellowship (Iowa State University, 2010) and GAANN Fellowship (Iowa State University, 2010) for financial support.

REFERENCES

1. Collins, D. C.; Lee, M. L., Developments in ion mobility spectrometry-mass spectrometry. *Anal. Bioanal. Chem.* **2002,** *372*, 66-73.
2. Wyttenbach, T.; Bowers, M. T., Gas-phase conformations: The ion mobility/ion chromatography method. *Top. Curr. Chem.* **2003,** *225*, 207-232.
3. Bohrer, B. C.; Merenbloom, S. I.; Koeniger, S. L.; Hilderbrand, A. E.; Clemmer, D. E., Biomolecule analysis by ion mobility spectrometry. *Annu. Rev. Anal. Chem.* **2008,** *1*, 293-327.
4. Borsdorf, H.; Mayer, T.; Zarejousheghani, M.; Eiceman, G. A., Recent developments in ion mobility spectrometry. *Appl. Spectrosc. Rev.* **2011,** *46*, 472-521.
5. Harvey, S. R.; MacPhee, C. E.; Barran, P. E., Ion mobility mass spectrometry for peptide analysis. *Methods* **2011,** *54*, 454-461.
6. Zhong, Y. Y.; Hyung, S. J.; Ruotolo, B. T., Ion mobility-mass spectrometry for structural proteomics. *Expert Rev. Proteomics* **2012,** *9*, 47-58.
7. Goodwin, C. R.; Fenn, L. S.; Derewacz, D. K.; Bachmann, B. O.; McLean, J. A., Structural mass spectrometry: Rapid methods for separation and analysis of peptide natural products. *J. Nat. Prod.* **2012,** *75*, 48-53.
8. Wilm, M.; Mann, M., Analytical properties of the nanoelectrospray ion source. *Anal. Chem.* **1996,** *68*, 1-8.
9. Stephenson, J. L.; McLuckey, S. A., Ion/ion proton transfer reactions for protein mixture analysis. *Anal. Chem.* **1996,** *68*, 4026-4032.
10. Stephenson, J. L.; McLuckey, S. A., Ion/ion reactions in the gas phase: Proton transfer reactions involving multiply-charged proteins. *J. Am. Chem. Soc.* **1996,** *118*, 7390-7397.
11. Stephenson, J. L.; McLuckey, S. A., Adaptation of the Paul Trap for study of the reaction of multiply charged cations with singly charged anions. *Int. J. Mass Spectrom. Ion Processes* **1997,** *162*, 89-106.
12. Stephenson, J. L.; McLuckey, S. A., Charge manipulation for improved mass determination of high- mass species and mixture components by electrospray mass spectrometry. *J. Mass Spectrom.* **1998,** *33*, 664-672.
13. McLuckey, S. A.; Stephenson, J. L., Ion ion chemistry of high-mass multiply charged ions. *Mass Spectrom. Rev.* **1998,** *17*, 369-407.
14. McLuckey, S. A.; Stephenson, J. L.; Asano, K. G., Ion/ion proton-transfer kinetics: Implications for analysis of ions derived from electrospray of protein mixtures. *Anal. Chem.* **1998,** *70*, 1198-1202.
15. Stephenson, J. L.; McLuckey, S. A., Simplification of product ion spectra derived from multiply charged parent ions via ion/ion chemistry. *Anal. Chem.* **1998,** *70*, 3533-3544.
16. Scarff, C. A.; Patel, V. J.; Thalassinos, K.; Scrivens, J. H., Probing hemoglobin structure by means of traveling-wave ion mobility mass spectrometry. *J. Am. Soc. Mass Spectrom.* **2009,** *20*, 625-631.
17. Breuker, K.; McLafferty, F. W., Stepwise evolution of protein native structure with electrospray into the gas phase, 10(-12) to 10(2) S. *Proc. Natl. Acad. Sci. U. S. A.* **2008,** *105*, 18145-18152.

18. Badman, E. R.; Hoaglund-Hyzer, C. S.; Clemmer, D. E., Monitoring structural changes of proteins in an ion trap over similar to 10-200 ms: Unfolding transitions in cytochrome *c* ions. *Anal. Chem.* **2001,** *73*, 6000-6007.
19. Valentine, S. J.; Anderson, J. G.; Ellington, A. D.; Clemmer, D. E., Disulfide-intact and -reduced lysozyme in the gas phase: Conformations and pathways of folding and unfolding. *J. Phys. Chem. B* **1997,** *101*, 3891-3900.
20. Clemmer, D. E.; Hudgins, R. R.; Jarrold, M. F., Naked protein conformations - cytochrome *c* in the gas-phase. *J. Am. Chem. Soc.* **1995,** *117*, 10141-10142.
21. Jurneczko, E.; Barran, P. E., How useful is ion mobility mass spectrometry for structural biology? The relationship between protein crystal structures and their collision cross sections in the gas phase. *Analyst* **2011,** *136*, 20-28.
22. Wyttenbach, T.; Bowers, M. T., Structural stability from solution to the gas phase: Native solution structure of ubiquitin survives analysis in a solvent-free ion mobility-mass spectrometry environment. *J. Phys. Chem. B* **2011,** *115*, 12266-12275.
23. Heck, A. J. R., Native mass spectrometry: A bridge between interactomics and structural biology. *Nat. Methods* **2008,** *5*, 927-933.
24. van den Heuvel, R. H.; Heck, A. J. R., Native protein mass spectrometry: From intact oligomers to functional machineries. *Curr. Opin. Chem. Biol.* **2004,** *8*, 519-526.
25. Konermann, L.; Douglas, D. J., Unfolding of proteins monitored by electrospray ionization mass spectrometry: A comparison of positive and negative ion modes. *J. Am. Soc. Mass Spectrom.* **1998,** *9*, 1248-1254.
26. Pan, P.; Gunawardena, H. P.; Xia, Y.; McLuckey, S. A., Nanoelectrospray ionization of protein mixtures: Solution pH and protein pI. *Anal. Chem.* **2004,** *76*, 1165-1174.
27. Gao, J.; Cassady, C. J., Negative ion production from peptides and proteins by matrix-assisted laser desorption/ionization time-of-flight mass spectrometry. *Rapid Commun. Mass Spectrom.* **2008,** *22*, 4066-4072.
28. Sogbein, O. O.; Simmons, D. A.; Konermann, L., Effects of pH on the kinetic reaction mechanism of myoglobin unfolding studied by time-resolved electrospray ionization mass spectrometry. *J. Am. Soc. Mass Spectrom.* **2000,** *11*, 312-319.
29. Prakash, H.; Mazumdar, S., Direct correlation of the crystal structure of proteins with the maximum positive and negative charge states of gaseous protein ions produced by electrospray ionization. *J. Am. Soc. Mass Spectrom.* **2005,** *16*, 1409-1421.
30. Watt, S. J.; Oakley, A.; Sheil, M. M.; Beck, J. L., Comparison of negative and positive ion electrospray ionization mass spectra of calmodulin and its complex with trifluoperazine. *Rapid Commun. Mass Spectrom.* **2005,** *19*, 2123-2130.
31. Leblanc, J. C. Y.; Guevremont, R.; Siu, K. W. M., Electrospray mass spectrometry of some proteins and the aqueous solution acid-base equilibrium model in the negative-ion detection mode. *Int. J. Mass Spectrom. Ion Processes* **1993,** *125*, 145-153.
32. Kelly, M. A.; Vestling, M. M.; Fenselau, C. C.; Smith, P. B., Electrospray analysis of proteins: A comparison of positive-ion and negative-ion mass spectra at high and low pH. *Org. Mass Spectrom.* **1992,** *27*, 1143-1147.
33. Zhao, Q.; Soyk, M. W.; Schieffer, G. M.; Fuhrer, K.; Gonin, M. M.; Houk, R. S.; Badman, E. R., An ion trap-ion mobility-time-of-flight mass spectrometer with three ion sources for ion/ion reactions. *J. Am. Soc. Mass Spectrom.* **2009,** *20*, 1549-1561.

34. Badman, E. R.; Myung, S.; Clemmer, D. E., Evidence for unfolding and refolding of gas-phase cytochrome c ions in a Paul trap. *J. Am. Soc. Mass Spectrom.* **2005,** *16,* 1493-1497.
35. Zhao, Q.; Schieffer, G. M.; Soyk, M. W.; Anderson, T. J.; Houk, R. S.; Badman, E. R., Effects of ion/ion proton transfer reactions on conformation of gas-phase cytochrome *c* ions. *J. Am. Soc. Mass Spectrom.* **2010,** *21,* 1208-1217.
36. Clemmer, D. E.; Jarrold, M. F., Ion mobility measurements and their applications to clusters and biomolecules. *J. Mass Spectrom.* **1997,** *32,* 577-592.
37. Shvartsburg, A. A.; Jarrold, M. F., An exact hard-spheres scattering model for the mobilities of polyatomic ions. *Chem. Phys. Lett.* **1996,** *261,* 86-91.
38. Mesleh, M. F.; Hunter, J. M.; Shvartsburg, A. A.; Schatz, G. C.; Jarrold, M. F., Structural information from ion mobility measurements: Effects of the long-range potential. *J. Phys. Chem.* **1996,** *100,* 16082-16086.
39. Shvartsburg, A. A.; Schatz, G. C.; Jarrold, M. F., Mobilities of carbon cluster ions: Critical importance of the molecular attractive potential. *J. Chem. Phys.* **1998,** *108,* 2416-2423.
40. Vijay-Kumar, S.; Bugg, C. E.; Cook, W. J., Structure of ubiquitin refined at 1.8 A resolution. *J. Mol. Biol.* **1987,** *194,* 531-544.
41. Di Stefano, D. L.; Wand, A. J., Two dimensional H NMR study of human ubiquitin - A main chain directed assignment and structure analysis. *Biochemistry* **1987,** *26,* 7272-7281.
42. Weber, P. L.; Brown, S. C.; Mueller, L., Sequential H NMR assignments and secondary structure identification of human ubiquitin. *Biochemistry* **1987,** *26,* 7282-7290.
43. Valentine, S. J.; Counterman, A. E.; Clemmer, D. E., Conformer-dependent proton-transfer reactions of ubiquitin ions. *J. Am. Soc. Mass Spectrom.* **1997,** *8,* 954-961.
44. Badman, E. R.; Hoaglund-Hyzer, C. S.; Clemmer, D. E., Dissociation of different conformations of ubiquitin ions. *J. Am. Soc. Mass Spectrom.* **2002,** *13,* 719-723.
45. Myung, S.; Badman, E. R.; Lee, Y. J.; Clemmer, D. E., Structural transitions of electrosprayed ubiquitin ions stored in an ion trap over similar to 10 ms to 30 s. *J. Phys. Chem. A* **2002,** *106,* 9976-9982.
46. Koeniger, S. L.; Clemmer, D. E., Resolution and structural transitions of elongated states of ubiquitin. *J. Am. Soc. Mass Spectrom.* **2007,** *18,* 322-331.
47. Fernandez-Lima, F. A.; Blase, R. C.; Russell, D. H., A study of ion-neutral collision cross-section values for low charge states of peptides, proteins, and peptide/protein complexes. *Int. J. Mass Spectrom.* **2010,** *298,* 111-118.
48. Makhatadze, G. I.; Lopez, M. M.; Richardson, J. M.; Thomas, S. T., Anion binding to the ubiquitin molecule. *Protein Sci.* **1998,** *7,* 689-697.
49. Ibarra-Molero, B.; Loladze, V. V.; Makhatadze, G. I.; Sanchez-Ruiz, J. M., Thermal versus guanidine-induced unfolding of ubiquitin. An analysis in terms of the contributions from charge-charge interactions to protein stability. *Biochemistry* **1999,** *38,* 8138-8149.
50. Lenkinski, R. E.; Chen, D. M.; Glickson, J. D.; Goldstein, G., Nuclear magnetic resonance studies of denaturation of ubiquitin. *Biochim. Biophys. Acta* **1977,** *494,* 126-130.
51. Bernstein, F. C.; Koetzle, T. F.; Williams, G. J. B.; Meyer, E. F.; Brice, M. D.; Rodgers, J. R.; Kennard, O.; Shimanouchi, T.; Tasumi, M., Protein data bank: Computer based archival file for macromolecular structures. *J. Mol. Biol.* **1977,** *112,* 535-542.

52. Koeniger, S. L.; Merenbloom, S. I.; Sevugarajan, S.; Clemmer, D. E., Transfer of structural elements from compact to extended states in unsolvated ubiquitin. *J. Am. Chem. Soc.* **2006,** *128*, 11713-11719.
53. Bushnell, G. W.; Louie, G. V.; Brayer, G. D., High resolution 3-dimensional structure of horse heart cytochrome *c*. *J. Mol. Biol.* **1990,** *214*, 585-595.
54. Qi, P. X.; Distefano, D. L.; Wand, A. J., Solution structure of horse heart ferrocytochrome c determined by high-resolution NMR and restrained simulated annealing. *Biochemistry* **1994,** *33*, 6408-6417.
55. Valentine, S. J.; Clemmer, D. E., H/D exchange levels of shape-resolved cytochrome c conformers in the gas phase. *J. Am. Chem. Soc.* **1997,** *119*, 3558-3566.
56. Shelimov, K. B.; Clemmer, D. E.; Hudgins, R. R.; Jarrold, M. F., Protein structure in vacuo: Gas-phase conformations of BPTI and cytochrome c. *J. Am. Chem. Soc.* **1997,** *119*, 2240-2248.
57. Thalassinos, K.; Slade, S. E.; Jennings, K. R.; Scrivens, J. H.; Giles, K.; Wildgoose, J.; Hoyes, J.; Bateman, R. H.; Bowers, M. T., Ion mobility mass spectrometry of proteins in a modified commercial mass spectrometer. *Int. J. Mass Spectrom.* **2004,** *236*, 55-63.
58. Theorell, H.; Akesson, A., Studies on cytochrome c. II. The optical properties of pure cytochrome c and some of its derivatives. *J. Am. Chem. Soc.* **1941,** *63*, 1812-1818.
59. Silkstone, G. G.; Cooper, C. E.; Svistunenko, D.; Wilson, M. T., EPR and optical spectroscopic studies of Met80X mutants of yeast ferricytochrome c. models for intermediates in the alkaline transition. *J. Am. Chem. Soc.* **2005,** *127*, 92-99.
60. Sivakolundu, S. G.; Mabrouk, P. A., Structure-function relationship of reduced cytochrome c probed by complete solution structure determination in 30% acetonitrile/water solution. *J. Biol. Inorg. Chem.* **2003,** *8*, 527-539.
61. Scarff, C. A.; Thalassinos, K.; Hilton, G. R.; Scrivens, J. H., Travelling wave ion mobility mass spectrometry studies of protein structure: biological significance and comparison with X-ray crystallography and nuclear magnetic resonance spectroscopy measurements. *Rapid Commun. Mass Spectrom.* **2008,** *22*, 3297-3304.
62. Blake, C. C. F.; Koenig, D. F.; Mair, G. A.; North, A. C. T.; Phillips, D. C.; Sarma, V. R., Structure of hen egg-white lysozyme - A 3-dimensional Fourier synthesis at 2 angstrom resolution. *Nature* **1965,** *206*, 757-&.
63. Redfield, C.; Dobson, C. M., Sequential 1H NMR assignments and secondary structure of hen egg-white lysozyme in solution. *Biochemistry* **1988,** *27*, 122-136.
64. Aboderin, A. A.; Boedefel.E; Luisi, P. L., Alkaline conformational transition of chicken egg-white lysozyme. *Biochim. Biophys. Acta* **1973,** *328*, 31-34.
65. Weiss, M. S.; Palm, G. J.; Hilgenfeld, R., Crystallization, structure solution and refinement of hen egg-white lysozyme at pH 8.0 in the presence of MPD. *Acta Crystallogr., Sect. D: Biol. Crystallogr.* **2000,** *56*, 952-958.
66. Refaee, M.; Tezuka, T.; Akasaka, K.; Williamson, M. P., Pressure-dependent changes in the solution structure of hen egg-white lysozyme. *J. Mol. Biol.* **2003,** *327*, 857-865.
67. Mao, D. M.; Babu, K. R.; Chen, Y. L.; Douglas, D. J., Conformations of gas-phase lysozyme ions produced from two different solution conformations. *Anal. Chem.* **2003,** *75*, 1325-1330.

68. Chrysina, E. D.; Brew, K.; Acharya, K. R., Crystal structures of apo- and holo-bovine alpha-lactalbumin at 2.2-A resolution reveal an effect of calcium on inter-lobe interactions. *J. Biol. Chem.* **2000,** *275*, 37021-37029.
69. Pike, A. C. W.; Brew, K.; Acharya, K. R., Crystal structures of guinea-pig, goat and bovine alpha-lactalbumin highlight the enhanced conformational flexibility of regions that are significant for its action in lactose synthase. *Structure* **1996,** *4*, 691-703.
70. Acharya, K. R.; Stuart, D. I.; Walker, N. P. C.; Lewis, M.; Phillips, D. C., Refined structure of baboon alpha-lactalbumin at 1.7 angstrom resolution: Comparison with c-type lysozyme. *J. Mol. Biol.* **1989,** *208*, 99-127.
71. Baum, J.; Dobson, C. M.; Evans, P. A.; Hanley, C., Characterization of a partly folded protein by NMR methods: Studies on the molten globule state of guinea pig alpha-lactalbumin. *Biochemistry* **1989,** *28*, 7-13.
72. Wijesinha-Bettoni, R.; Dobson, C. M.; Redfield, C., Comparison of the structural and dynamical properties of holo and apo bovine alpha-lactalbumin by NMR spectroscopy. *J. Mol. Biol.* **2001,** *307*, 885-898.
73. Kronman, M. J.; Holmes, L. G.; Robbins, F. M., Inter- and intramolecular interactions of alpha-lactalbumin. VIII. Alkaline conformational change. *Biochim. Biophys. Acta* **1967,** *133*, 46-55.
74. Kuwajima, K., The molten globule state as a clue for understanding the folding and cooperativity of globular protein structure. *Proteins* **1989,** *6*, 87-103.

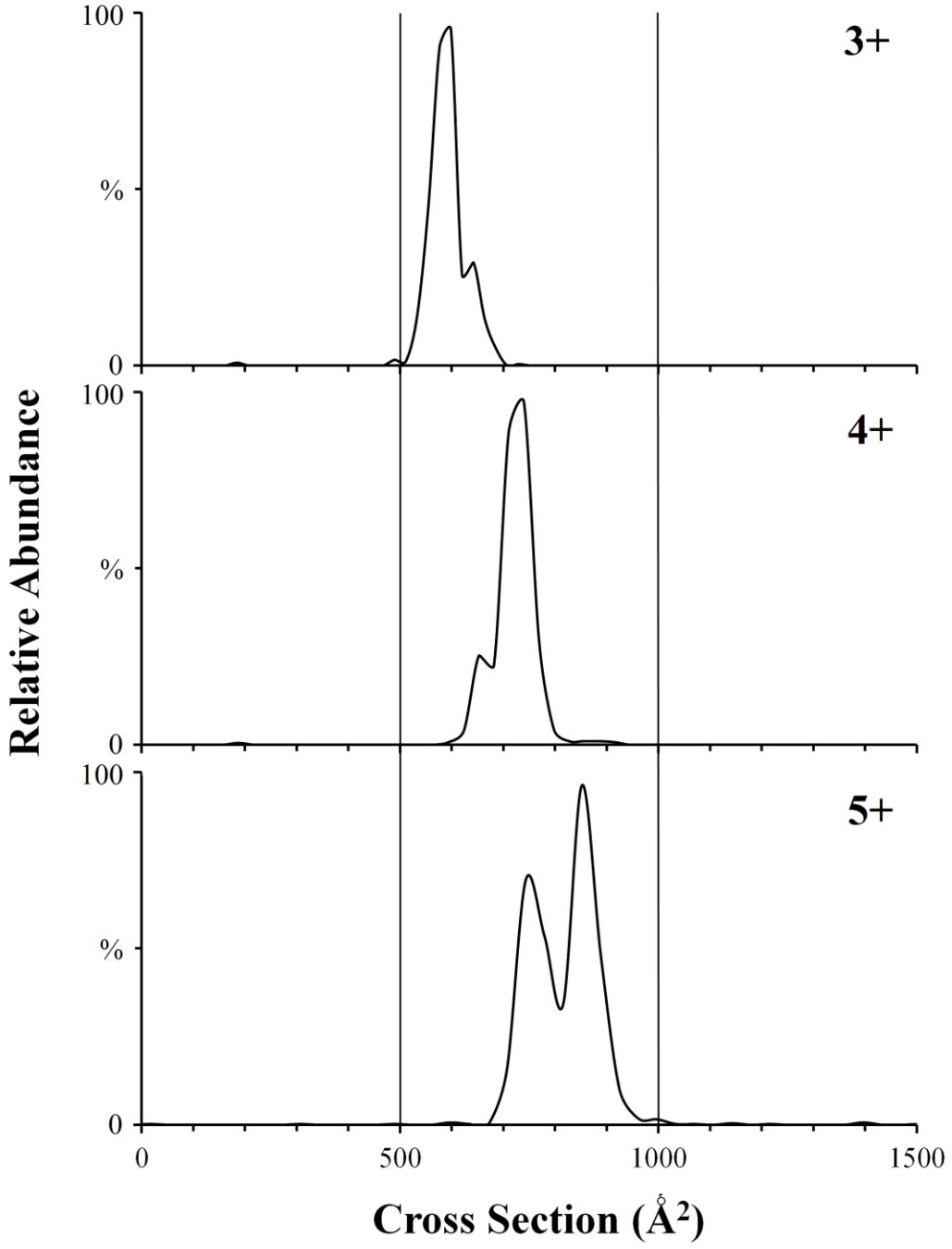

Figure 1. Ion mobility spectra, converted to collision cross section in Å^2, of ubiquitin from a pH 8.0 aqueous solution. The 3+ ion has a calculated collision cross section of 585 Å^2. The 4+ ion has a calculated collision cross section of 740 Å^2. The apex of the more compact conformation of the 5+ ion (leftmost peak) is centered on 743 Å^2 while the less compact conformation (rightmost peak) is centered on 852 Å^2.

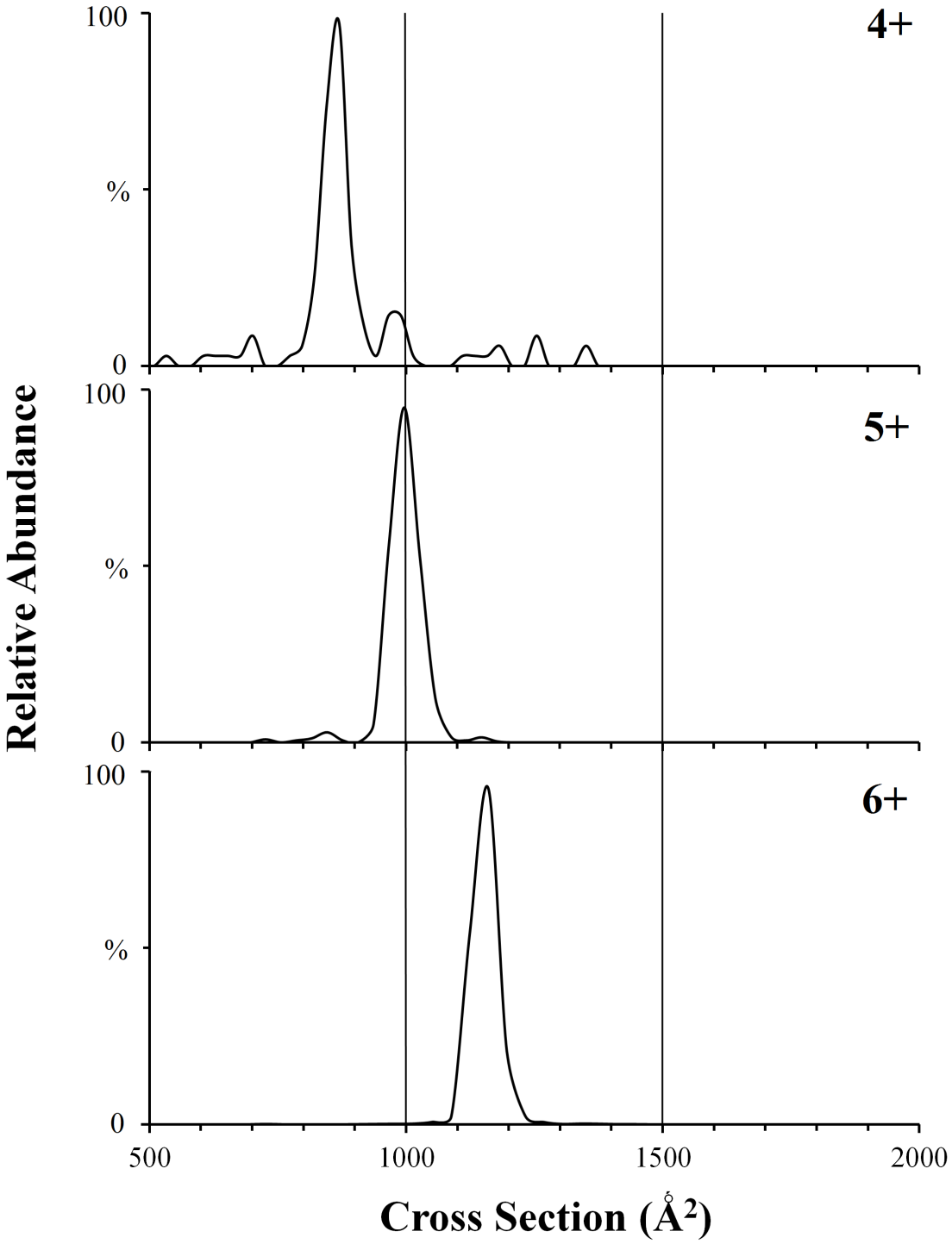

Figure 2. Ion mobility spectra, converted to collision cross section in Å^2, of cytochrome *c* from a pH 8.0 aqueous solution. The calculated collision cross section of the 3+ ion is 870 Å^2. The 4+ ion has a conformation with a collision cross section of 997 Å^2. The 6+ ion has a calculated collision cross section of 1160 Å^2.

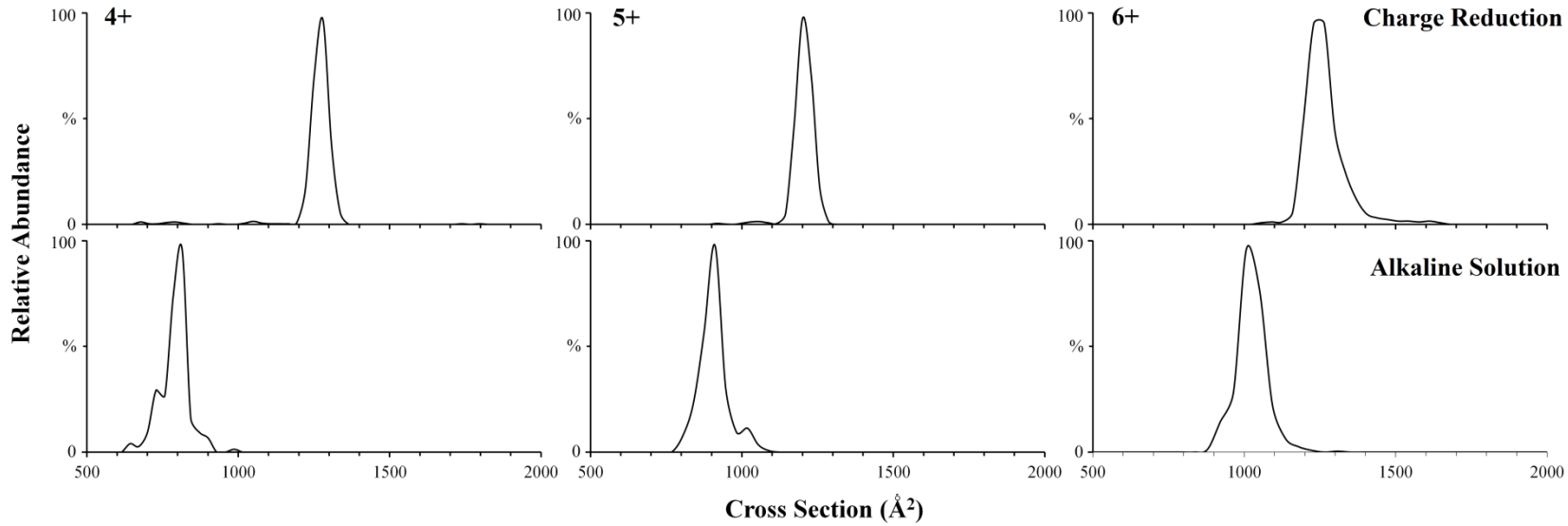

Figure 3. Ion mobility spectra, converted to collision cross section in $Å^2$, of lysozyme. The charge states in the top spectra were obtained via proton transfer ion/ion reactions from the native solution. The ions in the bottom spectra were measured directly from the pH 8.0 aqueous solution.

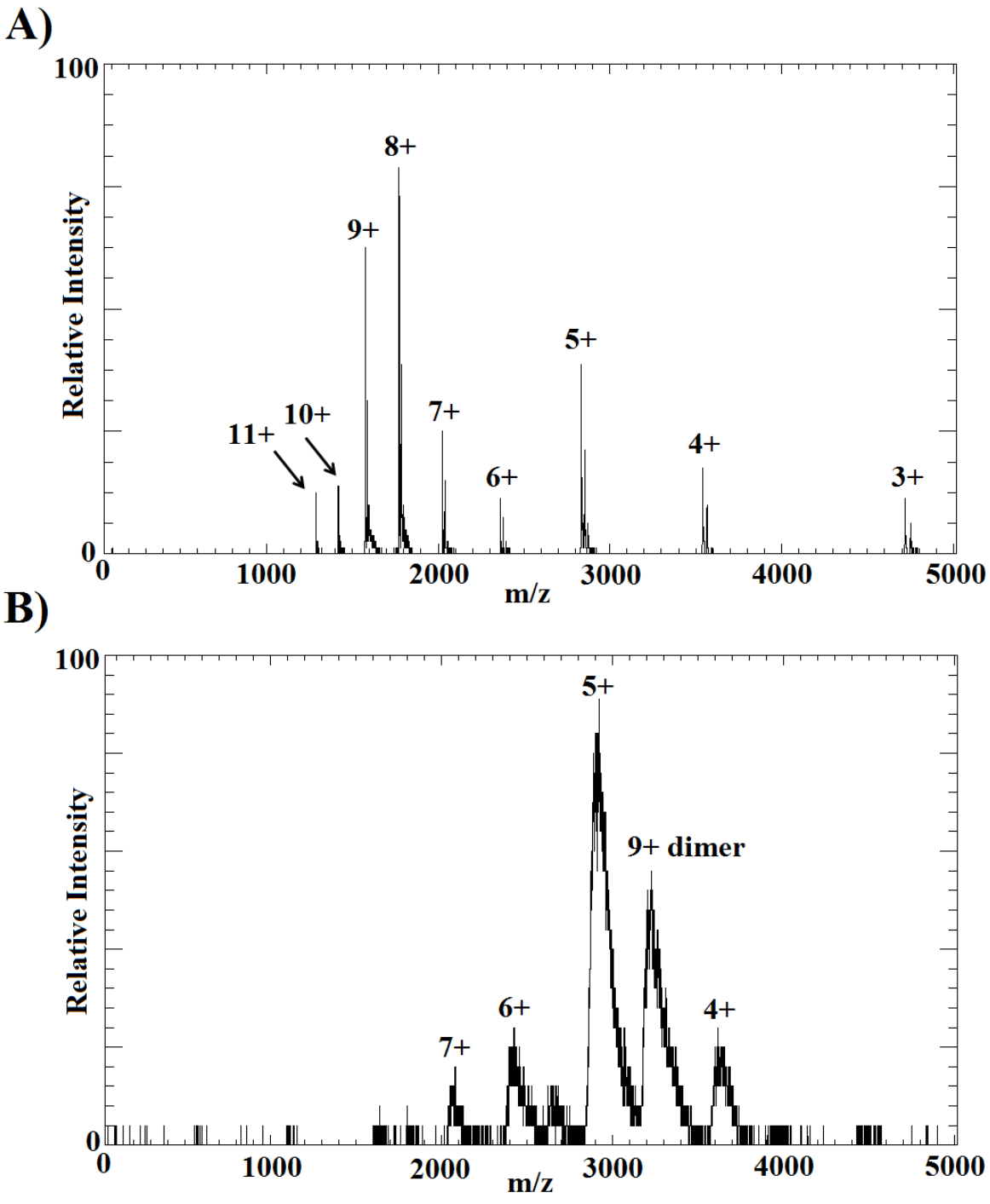

Figure 4. Mass spectra of α-lactalbumin from proton transfer of native solution (A) and directly from alkaline solution (B). A restricted m/z window (calculated m/z of the protein ion plus 10 m/z units) was selected to generate IM spectra. Therefore, the adducts peaks seen in the native solution spectra for the 4+, 5+, and 6+ ions, which were about + 96 Da, were not selected.

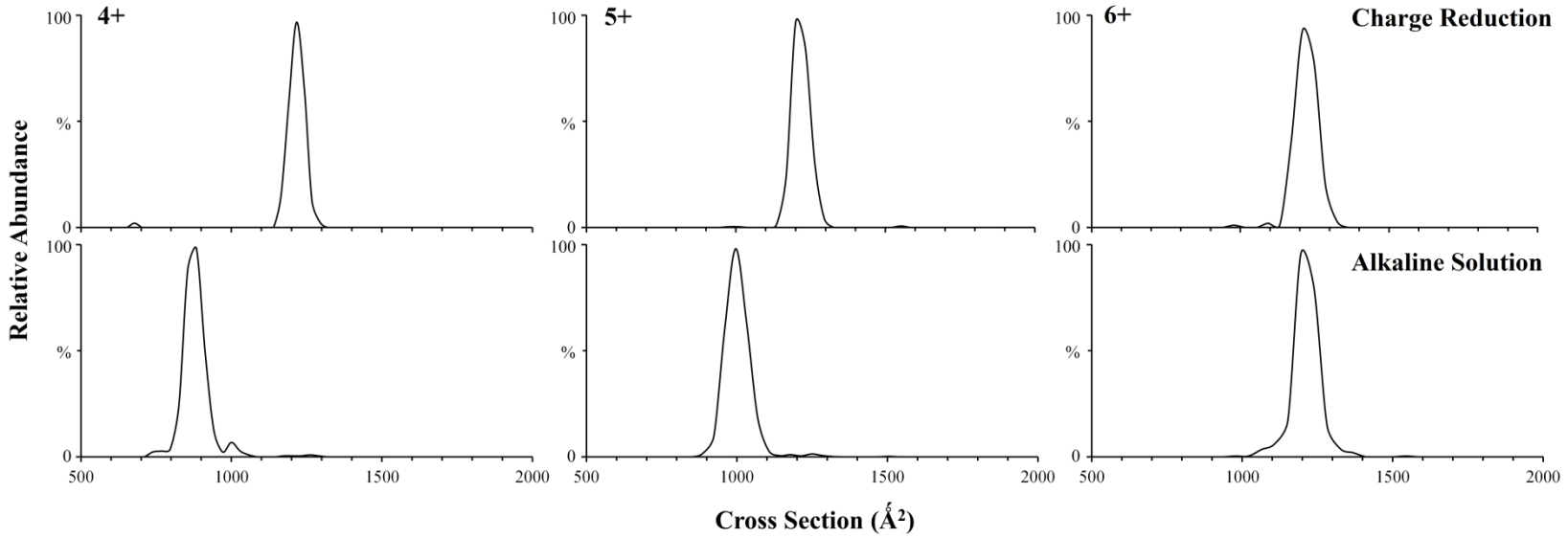

Figure 5. Ion mobility spectra, converted to collision cross section in Å^2, of α-lactalbumin. The ions in the top spectra were generated via proton transfer ion/ion reactions from the native solution. Ions in the bottom spectra were measured directly from the pH 8.0 aqueous solution.

CHAPTER 3

COMPREHENSIVE IDENTIFICATION OF ALPHA-ZEIN PROTEINS BY HIGH-PERFORMANCE LIQUID CHROMATOGRAPHY ACCURATE-MASS TIME-OF-FLIGHT MASS SPECTROMETRY

Derrick L. Morast, Timothy J. Anderson, R. S. Houk*

Ames Laboratory, U.S. Department of Energy

Department of Chemistry

Iowa State University, Ames, IA 50011

*Corresponding Author. Tel: (515) 294-9462 Fax-0050 rshouk@iastate.edu

A manuscript for submission to The Journal of Agricultural and Food Chemistry

ABSTRACT

High-resolution mass spectrometry (HRMS) was used for a comprehensive analysis of α-zein proteins extracted from corn gluten meal (CGM) and distillers' dried grains with solubles (DDGS). High-performance liquid chromatography (HPLC) was utilized for the separation of the complex protein mixture. Proteins were introduced from the HPLC column into the mass spectrometer via electrospray ionization (ESI). Results were searched against protein database entries and previous mass spectrometric α-zein analyses. Overall, ninety-five α-zein proteins were identified, forty-eight of which were similar in molecular weight (M_r) to previously reported proteins. The remaining forty-seven proteins are identified for the first time.

KEYWORDS

Zein, corn gluten meal, distillers' dried grains with solubles, high-resolution mass spectrometry, high-performance liquid chromatography

INTRODUCTION

Corn prolamines, also known as zeins, are alcohol-soluble storage proteins. Their main function is to provide nitrogen during germination. Zeins have a high content of glutamine and proline and are insoluble in water. There are currently many commercial applications for zeins, including use in the adhesive and plastics industries. There is considerable interest in utilizing zein as a polymeric material for films, coatings, and plastics since it is both biodegradable and renewable (*1-4*).

Several methods, and corresponding nomenclature systems, have been reported for the extraction of zeins from maize endosperm (*5-8*). The most widely used nomenclature, described by Esen and used herein, classifies zein fractions as α-, β-, γ-, and δ-zeins based on differences in solubility and amino acid sequence (*9, 10*). Of the four, α-zein is the most abundant, containing 75 to 85% of total zein proteins. They range in size from 210 to 245 amino acids and are commonly divided into two groups, M_r 22 kDa and M_r 19 kDa, based on relative SDS-PAGE migration. Within each group, the protein sequences are ~ 90% homologous and ~ 60% homologous between the two groups (*11*). The α-zein proteins contain about 25% glutamine, 20% leucine, 15% alanine, and 11% proline (*12*).

Zein is produced from corn using four different methods, two of which will be discussed further. Corn wet-milling and the dry-grind ethanol process both generate coproducts which contain α-zein proteins. CGM, a coproduct of the corn wet-milling process, can contain between 62 to 74% protein (*13*). Many commercially useful applications have been found for CGM and most commercial zein extraction methods extract

mainly α-zein proteins from CGM (*14*, *15*). For this reason, CGM is fairly valuable and currently sells for around $550/ton.

The dry-grind ethanol process is used for the production of ethanol from corn. DDGS is a coproduct of the dry-grind ethanol process. Protein content in DDGS is about 28 to 30% (*16*). During the ethanol process, a high-temperature cooking step (90-105 °C for 1 to 3 hrs) is used. This process may cause α-zein proteins to become adulterated. Only small scale extractions of α-zein proteins from DDGS have been reported (*17*). DDGS has found little commercial application outside of use as livestock feed and currently sells for less than $100/ton.

These zein extraction procedures yield complex mixtures of many proteins. Mass spectrometry (MS) is a powerful tool for the analysis of such protein mixtures. When ionized by electrospray ionization (ESI), proteins are highly charged and are observed in a wide variety of charge states. This charge state distribution allows for the molecular weight of the protein to be calculated from many measured mass-to-charge (m/z) values. A high-resolution mass spectrometer (HRMS) gives a more accurate mass than lower resolution instruments. In fact, compounds can often be identified reliably by HRMS alone, especially if isotope peaks within individual charge states can be resolved.

High-performance liquid chromatography (HPLC) has the ability to separate complex mixtures of proteins. However, the complexity of the sample and the sequence homology of the α-zein proteins make it difficult to get complete separation with HPLC. A previous 2-dimensional electrophoresis study identified 41 α-zein proteins and it was noted that this number was well below the estimated number of α-zein genes in the genome (*18*). One

benefit of using HRMS is that baseline LC separation of the proteins is often not necessary. Also, deconvolution software can identify most co-eluting proteins.

To our knowledge, all previous maize protein separations by HPLC used UV absorbance detection instead of MS. Although HPLC/UV has many useful applications, the lack of mass information limits its ability to identify proteins in such complex mixtures. In particular, proteins cannot be identified from retention time alone unless the analytes are baseline resolved and retention time is compared against a purified reference standard of each protein of interest. Given the inability of HPLC to baseline separate each α-zein protein and the lack of standards, identification of coeluting compounds in very complex mixtures is difficult solely by UV absorbance detection.

Capillary electrophoresis (CE) has also been coupled to a mass spectrometer via electrospray ionization (ESI) for the analysis of maize proteins (*19, 20*). CE generally provides a faster separation with higher resolution than HPLC, however coupling CE to a mass spectrometer is not as straightforward. For that reason, HPLC is a more widely used technique.

MATERIALS AND METHODS

Alpha-Zein Protein Extraction - CGM was obtained from Cargill, Inc. (Eddyville, IA) and DDGS was obtained from Lincolnway Energy (Nevada, IA). The CGM and DDGS extractions were previously reported (*21, 22*). A variety of solvent systems were employed. For CGM, a total of ten samples were extracted using five different solvent systems: 88% aqueous 2-propanol (IPA), 70% aqueous IPA, 55% aqueous IPA, 70% aqueous IPA with

22.5% glycerol, and 70% aqueous ethanol (EtOH). Each extraction was done with or without sodium hydroxide (NaOH) and a reductant (sodium bisulfate). For DDGS, a total of 6 samples were extracted using three different solvent systems: 88% aqueous IPA, 70% aqueous IPA, and 70% aqueous EtOH. These solvents were chosen based on performance results from previous CGM extractions (*21*). Half of the 6 samples were pretreated with a mixture of 0.4% Multifect GX GC and 0.1% Multifect pectinase FE (Genencor International, New York, NY) while the other half had no enzyme pretreatment.

After extraction with the solvent of interest, the solution was centrifuged for 15 min at room temperature and 8,000 x g (Beckman, Palo Alto, CA). The supernatant was cold precipitated at -20 °C overnight. The suspended precipitate was centrifuged at -20 °C and 8,000 x g to remove excess solvent and impurities, leaving a purified zein protein pellet. This pellet was dissolved in 88% IPA in water and dried in a vacuum oven at 50 °C at 0.6 bar. Dried samples were kept at 4 °C until use.

Figure 1 shows two representative SDS-PAGE gels of CGM and DDGS extraction products. The two bands observed for each sample correspond to the 19 and 22kDa α-zein protein fractions. All five samples for CGM were extracted without sodium hydroxide or a reducing agent. A similar band pattern was observed for the five corresponding extractions with sodium hydroxide and the reducing agent. For DDGS, samples 1-3 had no enzyme pretreatment prior to extraction while samples 4-6 were pretreated.

HPLC-TOF MS - Fifty milligrams of α-zein protein extract were dissolved in 55% aqueous IPA with 5% (v/v) 2-mercaptoethanol. A 5 µL sample was injected onto a 3.0 x 150 mm, 3.5 µm Agilent Zorbax 300 Å Stable Bond-C_3 column. Proteins were eluted using a 60

minute linear gradient from 50% to 60% acetonitrile, with 0.1% trifluoroacetic acid (TFA), on an Agilent 1260 Infinity LC system (Agilent Technologies). The accurate-mass Agilent 6224 time-of-flight mass spectrometer was operated at a data acquisition rate of 4 GHz. Mass spectra were deconvoluted using Agilent MassHunter BioConfirm software. Protein molecular weights were identified using a minimum of ten consecutive charge states, a signal-to-noise (S/N) of thirty or more, and a protein fit score of at least 9 (out of 10).

RESULTS AND DISCUSSION

Previous MS Studies of Zein Proteins - Previous zein protein studies utilizing mass spectrometry involved low resolution instruments and relied on either matrix-assisted laser desorption/ionization (MALDI) or capillary electrophoresis (CE) coupled to electrospray ionization (ESI) (*19, 20, 23, 24*). There are several potential issues with each of these techniques, especially when coupled to a low resolution mass spectrometer. First, some α-zein proteins differ in molecular weight by only 2 Da. When using MALDI, each laser shot has the potential to ionize all proteins present in the sample. Without the separating power of a high resolution mass spectrometer, the direct analysis of every protein in the complex zein fraction would be very difficult. This is evident when referring to mass spectra generated via MALDI-MS by Wang et al. and Adams et al (*23, 24*). They saw broad mass spectral peaks spanning ~100 Da that are probably the sum of peaks from 10 or more α-zein proteins instead of individual proteins. A second concern when using MALDI is the ability to detect low concentration proteins within the complex mixture of α-zein proteins. Since no analytical separation is performed prior to ionization, most of the signal generated will be from proteins at higher concentrations.

Third, there could be issues with the proteins co-crystallizing with the matrix when using MALDI. Alpha-zein proteins are known to have peculiar properties, most notably their solubility characteristics. As solvent is removed, they tend to aggregate. These aggregates often form films. It is possible that during solvent evaporation, some α-zein proteins aggregate and therefore do not co-crystallize with the matrix. These proteins would not be ionized or detected efficiently by MALDI.

CE-ESI is a better alternative than MALDI when using a low resolution mass spectrometer. One advantage of CE over MALDI is the ability to separate proteins in the complex mixture prior to analysis. However, CE-ESI-MS has lower sensitivity (generally) than LC-ESI-MS. The number of charge states generated for each α-zein protein via CE-ESI appears to be lower as well, although it is probably a function of which background electrolyte is used during analysis. Erny et al. had to use as few as three charge states for protein identification whereas with LC-ESI we had criterion of at least ten observable peaks from consecutive charge states (*19*). In many cases, over 20 charge states were observed. Signal-to-noise ratio appears to be much lower for the previous CE studies than our current LC study as well.

Measured Mass Spectra and M_r Values - As an example of our results, Figure 2 shows a typical mass spectrum and the resulting deconvoluted spectra for protein M_r 24,137.61. At least three other proteins co-eluted during this timeframe. However, the deconvolution software is able to recognize the peaks corresponding to the protein of interest (bottom panel). The inset displays a zoomed in view of the 17+ peak showing that surrounding peaks are almost baseline resolved.

Using M_r data from the LC-ESI-MS measurements, GenBank and UniProt were searched for zein proteins from *zea mays*. Molecular weights of each protein, without the signal peptide, were calculated. The signal peptide for α-zein proteins is typically 21 amino acids in length. This peptide is cleaved off and therefore absent from the mature protein.

Alpha-Zein Proteins with Database Entries - Table 1 lists the observed molecular weights of those α-zein proteins, measured via high-resolution mass spectrometry, which closely matched database search results. In several cases, the amino acid sequence of different database entries only varied for the signal peptide. This resulted in multiple "matches" for the mature protein. For that reason, the literature column lists the reference cited for each entry (*19, 20, 23-41*). The CGM and DDGS columns list the number of samples (out of 10 and 6, respectively) in which each protein was identified. For only the proteins listed in Table 1, 70% (23 of 33) were in at least one CGM and DDGS sample. However, of those 23 proteins, 17 of them were in at least half of all CGM and DDGS samples. Four of the proteins were found only in CGM while five were only found in DDGS. Most of the proteins (85%) have observed molecular weights which are less than 2 Da from the calculated molecular weight. Fourteen of the proteins listed in Table 1 were identified in a previous mass spectrometry analysis of zein (*19, 20, 23, 24*). The remaining 19 proteins are being identified and reported via mass spectrometry for the first time.

The results in Table 1 lead to the following key points. First, absolute sequence confirmation of a protein cannot be established via mass spectrometry without either digesting the protein and sequencing the resulting peptides via collision induced dissociation (CID) (bottom-up proteomics) or fragmenting the intact protein using electron-capture

dissociation/electron-transfer dissociation (top-down proteomics). Neither of these techniques was utilized for the present study. Digestion and CID of LC α-zein protein fractions would provide more definitive assignments; however typical enzyme digestions occur in aqueous solutions and α-zein proteins are not soluble in water, The mass spectrometry studies cited above definitively match many specific database entries, namely those from Woo et al (*25*). In some cases, experimental molecular mass varied by 10s to 100s of Daltons from supposedly matched or identified protein. We, on the other hand, are acknowledging the limitations of our results and are only offering a "best guess". It is worth repeating our strict criteria used for protein identification, however. Each protein listed contained at least ten consecutive charge states with a minimum protein fit score of nine and a signal-to-noise ratio of at least thirty.

While we cannot definitively say each protein listed is the exact protein cited from the database, we are confident that each protein identified represents an actual protein in a CGM sample, a DDGS sample, or both. One special case is the two possible assignments for the 26,752.24 Da protein, noted in italics in Table 1. It fell 1.26 Da from 26,750.98 and 0.65 Da from 26,752.89. Although these two α-zein proteins share ~85% of their sequence, they also have 37 different amino acids. It was the only situation in which an observed protein closely matched two database proteins. Without a full digestion and sequence analysis, we cannot definitively know which sequence is correct, so both are listed.

Second, there are a few cases in which a protein was identified in only one sample. That is not to say the protein was not present in other samples. These proteins tended to be lower abundance components of the total sample. As such, they only met deconvolution

criteria in one (or a few) sample(s). When the criteria was lowered to a S/N of 10 and only 5 consecutive charge states, many of the low-abundance proteins were observed in multiple samples (data not shown).

For those proteins which were not identified in all CGM or DDGS samples, the various extraction procedures appeared to perform about the same. In other words, one protein might not be observed in CGM sample 2 (NaOH and sodium bisulfite treatment) while another protein was not observed in CGM sample 1 (same solvent extraction without NaOH or sodium bisulfite treatment). The same observation was found for the DDGS samples with or without enzyme treatment. A more detailed analysis of each sample extraction procedure, including protein purity, yield, and recovery assessments, can be found in previous publications (*21, 22*).

There were 15 proteins from Table 1 which were also identified in one of the previous mass spectrometry publications. Those proteins are listed in Table 2. All but two of the proteins listed in Table 2 were identified in over half of the CGM and DDGS samples. In addition, 12 of the 15 proteins were identified in 8 or more CGM samples while 13 of the 15 proteins were found in 4 or more of the DDGS samples.

Some proteins had been reported in multiple publications. For those proteins, both of the observed molecular weights and analysis methods are listed. In some cases the original publication may not have directly cited the specific database entry shown in Table 1. In other cases, the original publication did cite the database entry listed in Table 1, even though their observed molecular weights may deviate from the calculated value by a large margin. For these entries, we simply report the previous data and do not imply that both research

groups were actually identifying the same protein. As an extreme example, Adams et al. reported identifying GenBank accession number AF371268, with a calculated M_r of 24,705.60 Da (*23*). Their observed M_r was 24,515 Da. Our data, taken on an instrument with much higher resolution and accuracy, measured an α-zein protein with a M_r of 24,706.84 Da. We did not observe a protein fitting our acceptance criteria with a M_r of 24,515 Da (see Table 4).

For the data listed in Table 2, analysis via CE-ESI-MS generated data with observed molecular weights much closer to calculated values than previous MALDI-MS experiments (1.4 Da vs. 43.6 Da) (*19*, *20*). Of course the deviation from the calculated value for MALDI analysis is skewed by the small sample size and the 191 Da deviation listed above. If that value is removed, the deviation drops to 14.2 Da. Although this value is better, it is still much larger than that for the data generated via HRMS (1.2 Da, present work) and CE-MS (*19*, *20*). We believe this point illustrates the previous stated concerns regarding the analyses of a complex mixture of very similar proteins, such as α-zein proteins, via MALDI.

Alpha-Zein Proteins without Database Entries - Table 3 compares molecular weights of α-zein proteins measured via HRMS in which a database entry was not found but the protein molecular weight was similar to that of a protein previously reported using mass spectrometry. Nine of the 15 proteins listed in Table 3 were found in over half of the CGM and DDGS samples. Moreover, 10 of the 15 were found in 9 or more of the CGM samples and 11 of 15 were found in 4 or more of the DDGS samples. One protein, M_r 23,217.76, was found in all 10 of the CGM samples but none of the DDGS samples. Of the α-zein proteins which were compared to database entries or previous mass spectrometry studies (Tables 1

and 3), 28 of the 48 (58%) were found in over half of the CGM and DDGS samples. Twenty-nine proteins were identified in 8 or more of the CGM samples and thirty-six were found in 4 or more of the DDGS samples.

There are a few interesting notes to point out regarding our list of proteins from Tables 1 to 3 along with previously cited data. There are a number of instances in previous studies in which a protein was assigned to a specific GenBank accession number, implying that the protein observed has the same sequence as that given in the database. For example, Adams et al. (*23*) observed, via MALDI, an α-zein protein with M_r 24,069 Da. They assigned it to GenBank accession number AF371271 with a calculated M_r 24,087 Da. However, our study shows a protein having a mass of 24,071.90 Da and 24,087.90 Da, both of which were present in every CGM and DDGS sample. Wang et al. (*24*) report an α-zein protein of mass 24,097 Da, also via MALDI, and assign this protein to the same 24,087 Da protein. Our study found an α-zein protein having a mass of 24,096.55 Da. Erny et al. (*19*) report an α-zein protein of mass 24,695 Da, observed via CE-ESI-MS. This protein is compared to GenBank accession number AF371268 from Woo et al. (*25*) having a calculated M_r 24,706 Da. It is also compared to a protein found in Adams et al. (*23*) of mass 24,644 Da. Adams, however, actually compared their observed 24,644 Da protein to GenBank accession number AF371267, with a calculated mass of 24,818 Da. Our study found α-zein proteins having a mass of 24,694.62 Da and 24,096.55 Da. We did not observe an α-zein protein having a mass of 24,818 Da.

Table 4 contains a list of the other 47 proteins that fit the deconvolution criteria. These proteins could not be assigned to any database search or previous mass spectrometry

study. It is possible that some of these proteins are salt adducts of "known" proteins (*42*). Overall, only 10 of the 47 proteins were found in over half of the CGM and DDGS samples. Fifteen of the 47 proteins were found in 7 or more of the CGM samples and 18 of the 47 were found in 4 or more of the DDGS samples. Twelve of the 47 proteins were found only in a single CGM or DDGS sample; two of these, M_r 26,375 and 26,419.76, were identified in one CGM and one DDGS sample. Three of the proteins were identified in every DDGS sample but none of the CGM samples. Only one protein was found in every CGM sample but none of the DDGS samples.

One goal of the present work was to compare the individual α-zein proteins extracted from both CGM and DDGS. Most commercial zein is produced from CGM and as such, CGM commands a higher market price. Due to heating during the fermentation process, α-zein proteins in DDGS may be adulterated. However, previous studies have shown the ability to extract a high purity zein protein fraction from the much cheaper DDGS although no molecular weight information has been described other than that provided by SDS-PAGE (*22*, *43*, *44*). Of the α-zein proteins previously reported (Tables 1-3), about 71% (34 of 48) were found in both CGM and DDGS. Overall, 56 of the 95 (59%) α-zein proteins fitting our deconvolution criteria were found in both CGM and DDGS. As well, 22 proteins were found only in DDGS samples and 17 proteins were found only in CGM samples.

It is not possible to comment on the level of adulteration of the DDGS α-zein proteins based solely on these results. However, we believe our findings, in support with the information from previous publications, suggest DDGS contains viable α-zein proteins.

ACKNOWLEDGEMENTS

The authors would like to thank Professor Buddhi Lamsal (Iowa State University) for his guidance in the alpha zein protein extractions. Derrick Morast would like to acknowledge the GAANN Fellowship (Iowa State University, 2009) for financial support.

REFERENCES

1. Lawton, J. W., Zein: A history of processing and use. *Cereal Chem.* **2002**, *79*, 1-18.
2. Wu, Q. X.; Sakabe, H.; Isobe, S., Studies on the toughness and water resistance of zein-based polymers by modification. *Polymer* **2003**, *44*, 3901-3908.
3. Wang, Y.; Padua, G. W., Tensile properties of extruded Zein sheets and extrusion blown films. *Macromol. Mater. Eng.* **2003**, *288*, 886-893.
4. Lawton, J. W., Plasticizers for zein: Their effect on tensile properties and water absorption of zein films. *Cereal Chem.* **2004**, *81*, 1-5.
5. Wilson, C. M., A nomenclature for zein polypeptides based on isoelectric focusing and sodium dodecyl sulfate polyacrylamide gel electrophoresis. *Cereal Chem.* **1985**, *62*, 361-365.
6. Wilson, C. M., Serial analysis of zein by isoelectric focusing and sodium dodecyl sulfate gel electrophoresis. *Plant Physiol.* **1986**, *82*, 196-202.
7. Hastings, H.; Bonanomi, S.; Soave, C.; Di Fonzo, N.; Salamini, F., Mapping of genes for minor zein sodium dodecylsulfate subunits and revision of zein gene nomenclature. *Genet. Agrar.* **1984**, *38*, 447-464.
8. Esen, A., Separation of alcohol-soluble proteins (zeins) from maize into three fractions by differential solubility. *Plant Physiol.* **1986**, *80*, 623-627.
9. Thompson, G. A.; Larkins, B. A., Structural elements regulating zein gene expression. *Bioessays* **1989**, *10*, 108-113.
10. Esen, A., A proposed nomenclature for the alcohol-soluble proteins (zeins) of maize (Zea mays L.). *J. Cereal Sci.* **1987**, *5*, 117-128.
11. Coleman, C. E.; Larkins, B. A., The prolamins of maize. In *Seed Proteins*, Shewry, P. R.; Casey, R., Eds. Kluwer: Dordrecht, Netherlands, **1999**; pp 109-139.
12. Thompson, G. A.; Larkins, B. A., Characterization of zein genes and their regulation in maize endosperm. In *The Maize Handbook*, Freeling, M.; Walbot, V., Eds. Springer-Verlag: New York, **1994**; pp 639-647.
13. Wu, S. W.; Myers, D. J.; Johnson, L. A., Factors affecting yield and composition of zein extracted from commercial corn gluten meal. *Cereal Chem.* **1997**, *74*, 258-263.
14. Carter, R. a. R., D. R. Low temperature solvent extraction process for producing high purity zein. U.S. Patent 3,535,305, Oct. 20, 1970.
15. Takahashi, H. a. Y., N. Process for refining zein. U.S. Patent 5,342,923, Aug. 30, 1994.
16. Singh, V.; Moreau, R. A.; Hicks, K. B.; Belyea, R. L.; Staff, C. H., Removal of fiber from distillers dried grains with solubles (DDGS) to increase value. *Trans. ASAE* **2002**, *45*, 389-392.
17. Anderson, T. J.; Lamsal, B. P., Zein extraction from corn, corn products, and coproducts and modifications for various applications: A review. *Cereal Chem.* **2011**, *88*, 159-173.
18. Consoli, L.; Damerval, C., Quantification of individual zein isoforms resolved by two-dimensional electrophoresis: Genetic variability in 45 maize inbred lines. *Electrophoresis* **2001**, *22*, 2983-2989.

19. Erny, G. L.; Marina, M. L.; Cifuentes, A., Capillary-electrophoresis mass spectrometry of zein proteins from conventional and transgenic maize. *Electrophoresis* **2007**, *28*, 4192-4201.
20. Erny, G. L.; Leon, C.; Marina, M. L.; Cifuentes, A., Time of flight versus ion trap mass spectrometry coupled to capillary electrophoresis to analyse intact proteins. *J. Sep. Sci.* **2008**, *31*, 1810-1818.
21. Anderson, T. J.; Lamsal, B. P., Development of new method for extraction of α-zein from corn gluten meal using different solvents. *Cereal Chem.* **2011**, *88*, 356-362.
22. Anderson, T. J.; Ilankovan, P.; Lamsal, B. P., Two fraction extraction of alpha-zein from DDGS and its characterization. *Ind. Crops Prod.* **2012**, *37*, 466-472.
23. Adams, W. R.; Huang, S. S.; Kriz, A. L.; Luethy, M. H., Matrix-assisted laser desorption ionization time-of-flight mass spectrometry analysis of zeins in mature maize kernels. *J. Agric. Food Chem.* **2004**, *52*, 1842-1849.
24. Wang, J. F.; Geil, P. H.; Kolling, D. R. J.; Padua, G. W., Analysis of zein by matrix-assisted laser desorption/ionization mass spectrometry. *J. Agric. Food Chem.* **2003**, *51*, 5849-5854.
25. Woo, Y. M.; Hu, D. W. N.; Larkins, B. A.; Jung, R., Genomics analysis of genes expressed in maize endosperm identifies novel seed proteins and clarifies patterns of zein gene expression. *Plant Cell* **2001**, *13*, 2297-2317.
26. Alexandrov, N. N.; Brover, V. V.; Freidin, S.; Troukhan, M. E.; Tatarinova, T. V.; Zhang, H.; Swaller, T. J.; Lu, Y.-P.; Bouck, J.; Flavell, R. B.; Feldmann, K. A., Insights into corn genes derived from large-scale cDNA sequencing. *Plant Mol. Biol.* **2009**, *69*, 179-194.
27. Soderlund, C.; Descour, A.; Kudrna, D.; Bomhoff, M.; Boyd, L.; Currie, J.; Angelova, A.; Collura, K.; Wissotski, M.; Ashley, E.; Morrow, D.; Fernandes, J.; Walbot, V.; Yu, Y., Sequencing, mapping, and analysis of 27,455 maize full-length cDNAs. *Plos Genetics* **2009**, *5*.
28. Geraghty, D.; Peifer, M. A.; Rubenstein, I.; Messing, J., The primary structure of a plant storage protein: Zein. *Nucleic Acids Res.* **1981**, *9*, 5163-5174.
29. Marks, M. D.; Lindell, J. S.; Larkins, B. A., Nucleotide sequence analysis of zein messenger RNAs from maize endosperm. *J. Biol. Chem.* **1985**, *260*, 6451-6459.
30. Kriz, A. L.; Boston, R. S.; Larkins, B. A., Structural and transcriptional analysis of DNA sequences flanking genes that encode 19 kDa zeins. *Mol. Gen. Genet.* **1987**, *207*, 90-98.
31. Pedersen, K.; Devereux, J.; Wilson, D. R.; Sheldon, E.; Larkins, B. A., Cloning and sequence analysis reveal structural variation among related zein genes in maize. *Cell* **1982**, *29*, 1015-1026.
32. Marks, M. D.; Larkins, B. A., Analysis of sequence microheterogeneity among zein messenger RNAs. *Journal of Biological Chemistry* **1982**, *257*, 9976-9983.
33. Kim, C. S.; Hunter, B. G.; Kraft, J.; Boston, R. S.; Yans, S.; Jung, R.; Larkins, B. A., A defective signal peptide in a 19-kD alpha-zein protein causes the unfolded protein response and an opaque endosperm phenotype in the maize De*-B30 mutant. *Plant Physiol.* **2004**, *134*, 380-387.
34. Viotti, A.; Cairo, G.; Vitale, A.; Sala, E., Each zein gene class can produce polypeptides of different sizes. *EMBO J.* **1985**, *4*, 1103-1110.

35. Geraghty, D. E.; Messing, J.; Rubenstein, I., Sequence analysis and comparison of CDNAs of the zein multigene family. *EMBO J.* **1982**, *1*, 1329-1335.
36. Song, R. T.; Llaca, V.; Linton, E.; Messing, J., Sequence, regulation, and evolution of the maize 22-kD alpha zein in gene family. *Genome Res.* **2001**, *11*, 1817-1825.
37. Thompson, G. A.; Siemieniak, D. R.; Sieu, L. C.; Slightom, J. L.; Larkins, B. A., Sequence analysis of linked maize 22 kDa alpha-zein genes. *Plant Mol. Biol.* **1992**, *18*, 827-833.
38. Liu, C. N.; Rubenstein, I., Molecular characterization of two types of 22-kDa alpha-zein genes in a gene cluster in maize. *Mol. Gen. Genet.* **1992**, *234*, 244-253.
39. Spena, A.; Viotti, A.; Pirrotta, V., A homologous repetitive block structure underlies the heterogeneity of heavy and light chain zein genes. *EMBO J.* **1982**, *1*, 1589-1594.
40. Hu, N. T.; Peifer, M. A.; Heidecker, G.; Messing, J.; Rubenstein, I., Primary structure of a genomic zein sequence of maize. *EMBO J.* **1982**, *1*, 1337-1342.
41. Coleman, C. E.; Lopes, M. A.; Gillikin, J. W.; Boston, R. S.; Larkins, B. A., A defective signal peptide in the maize high lysine mutant Floury-2. *Proc. Natl. Acad. Sci. U. S. A.* **1995**, *92*, 6828-6831.
42. Tong, H.; Bell, D.; Tabei, K.; Siegel, M. M., Automated data massaging, interpretation, and E-mailing modules for high throughput open access mass spectrometry. *J. Am. Soc. Mass Spectrom.* **1999**, *10*, 1174-1187.
43. Xu, W.; Reddy, N.; Yang, Y., An acidic method of zein extraction from DDGS. *J. Agric. Food Chem.* **2007**, *55*, 6279-6284.
44. Lawton, J. W., Isolation of zein using 100% ethanol. *Cereal Chem.* **2006**, *83*, 565-568.

Table 1. A Comparison of Molecular Weights of α-Zein Proteins Measured via High-Resolution Mass Spectrometry to Protein Database Search Results

Molecular weight (obs., HRMS)	Molecular weight (from GenBank)	Difference	CGM samples	DDGS samples	Literature
23231.84	23230.87	0.97	8/10	6/6	(*20*, *26*, *27*)
23327.99	23324.99	3.00	0	6	(*28*)
23344.93	23346.09	-1.17	9	6	(*19*, *26*, *29*)
23358.33	23358.96	-0.63	9	6	(*20*, *23*, *25*, *26*)
23361.24	23360.04	1.20	9	6	(*19*, *20*, *24*, *26*, *30*)
23366.54	23367.03	-0.49	3	2	(*20*, *26*, *30*)
23420.76	23419.06	1.70	9	6	(*40*)
23493.78	23496.30	-2.52	0	6	(*31*, *32*)
23527.20	23527.33	-0.12	0	6	(*36*)
23568.96	23567.33	1.64	0	1	direct submission
24020.97	24019.79	1.18	10	6	(*33*)
24032.98	24036.82	-3.84	10	5	(*34*)
24077.73	24076.84	0.89	0	4	(*35*)
24087.90	24086.86	1.04	10	6	(*19*, *20*, *23*, *25*, *26*)
24137.61	24135.91	1.70	10	6	(*20*, *26*)
24326.40	24325.13	1.27	1	0	direct submission
24375.20	24377.15	-1.95	1	0	direct submission
24424.43	24423.12	1.31	10	6	(*19*, *20*, *26*)
24706.84	24705.60	1.24	1	2	(*23*, *25*)
26334.03	26336.59	-2.55	7	1	(*41*)
26359.84	26358.52	1.32	6	4	(*20*, *23*, *25*, *26*)
26590.24	26586.87	3.37	10	1	direct submission
26708.58	26709.86	-1.28	8	0	(*25*)
26752.24	26750.98	1.26	10	6	(*23*, *25*, *36*)
26752.24	26752.89	-0.65	10	6	(*37*)
26761.12	26760.01	1.11	10	6	(*19*, *20*, *36*)
26779.45	26779.04	0.42	2	5	(*26*, *38*)
26820.73	26819.12	1.61	10	6	(*20*, *26*, *32*, *36*)
26837.16	26838.17	-1.01	10	6	(*24*, *27*)
26859.75	26860.00	-0.25	4	0	(*34*, *39*)
26891.66	26891.06	0.60	6	2	(*36*)
26906.45	26905.08	1.37	0	2	(*36*, *38*)
26924.46	26923.17	1.30	10	5	(*19*, *20*, *25*)
27129.02	27127.53	1.49	9	5	(*19*, *20*, *40*)

Table 2. A Comparison of Molecular Weights of α-Zein Proteins Measured via High-Resolution Mass Spectrometry to Database Proteins Previously Identified via Mass Spectrometry

Molecular weight (obs., HRMS)	Molecular weight (from GenBank)	Molecular weight (reported)	Analysis type	CGM samples	DDGS samples	Literature
23231.84	23230.87	23232	CE-MS	8/10	6/6	(*20*)
23358.33	23358.96	23318/23358.5	MALDI-MS/CE-MS	9	6	(*20*, *23*)
23361.24	23360.04	23362/23361	MADLI-MS/CE-MS	9	6	(*20*, *24*)
23366.54	23367.03	23365.3	CE-MS	3	2	(*20*)
24087.90	24086.86	24069/24085.7	MALDI-MS/CE-MS	10	6	(*20*, *23*)
24137.61	24135.91	24137.3	CE-MS	10	6	(*20*)
24424.43	24423.12	24425/24426 (±4)	CE-MS/CE-MS	10	6	(*19*, *20*)
24706.84	24705.60	24515	MALDI-MS	1	2	(*23*)
26359.84	26358.52	26308	MALDI-MS	6	4	(*23*)
26752.24	26750.98	26741	MALDI-MS	10	6	(*23*)
26761.12	26760.01	26758.8	CE-MS	10	6	(*20*)
26820.73	26819.12	26817	CE-MS	10	6	(*20*)
26837.16	26838.17	26838	MALDI-MS	10	6	(*24*)
26924.46	26923.17	26922.8/26925 (±1)	CE-MS/CE-MS	10	5	(*19*, *20*)
27129.02	27127.53	27128.6	CE-MS	9	5	(*19*, *20*)

Table 3. A Comparison of Molecular Weights of α-Zein Proteins Measured via High-Resolution Mass Spectrometry to Proteins Not in Database Previously Identified via Mass Spectrometry

Molecular weight (obs., HRMS)	Molecular weight (reported)	Analysis type	CGM samples	DDGS samples	Literature
23217.76	23216.3	CE-MS	10/10	0/6	(*20*)
23141.98	23140.2	CE-MS	10	6	(*20*)
23379.00	23377	MALDI-MS	10	6	(*24*)
23404.27	23401 (±1)	CE-MS	2	5	(*19*)
23437.09	23436.4	CE-MS	9	6	(*20*)
23995.94	23993.6	CE-MS	10	6	(*20*)
24071.90	24069	MALDI-MS	10	6	(*23*)
24096.55	24097	MALDI-MS	1	4	(*24*)
24559.48	24558.8	CE-MS	9	6	(*20*)
24694.62	24695 (±1)	CE-MS	0	4	(*19*)
26386.02	26383.2	CE-MS	0	2	(*20*)
26632.19	26630.6	CE-MS	9	4	(*20*)
26811.46	26813 (±4)	CE-MS	9	5	(*19*)
26828.15	26831.1	CE-MS	9	3	(*20*)
27186.14	27185.5	CE-MS	1	0	(*20*)

Table 4. Molecular Weight of α-Zein Proteins Which Met Deconvolution Criteria, Not Previously Reported via Mass Spectrometric Analysis and No Database Entry

Molecular weight (obs., HRMS)	CGM samples	DDGS samples	Molecular weight (obs., HRMS)	CGM samples	DDGS samples
23241.83	1/10	0/6	24447.34	10/10	6/6
23308.89	9	4	24455.85	10	2
23331.97	0	2	24500.48	8	2
23394.45	0	2	24523.26	0	2
23407.36	0	5	24531.5	7	0
23442.62	6	6	24635.5	1	0
23455.25	2	6	26257.69	8	5
23458.20	10	6	26375.94	1	1
23470.26	1	0	26419.76	1	1
23476.11	0	6	26435.98	7	2
23510.95	0	6	26514.26	10	3
23519.50	10	0	26529.8	3	0
23523.17	0	6	26655.09	4	4
23554.11	0	3	26734.28	0	3
23599.38	2	4	26776.27	2	4
24010.05	10	4	26796.51	0	1
24108.57	8	6	26855.12	0	1
24148.26	2	0	26878.48	0	1
24155.42	5	6	26915.7	3	0
24164.22	10	6	26942.24	1	2
24195.96	0	2	26973.8	1	0
24213.00	10	6	27016.8	1	0
24240.38	1	0	27205.19	8	1
24441.77	0	1			

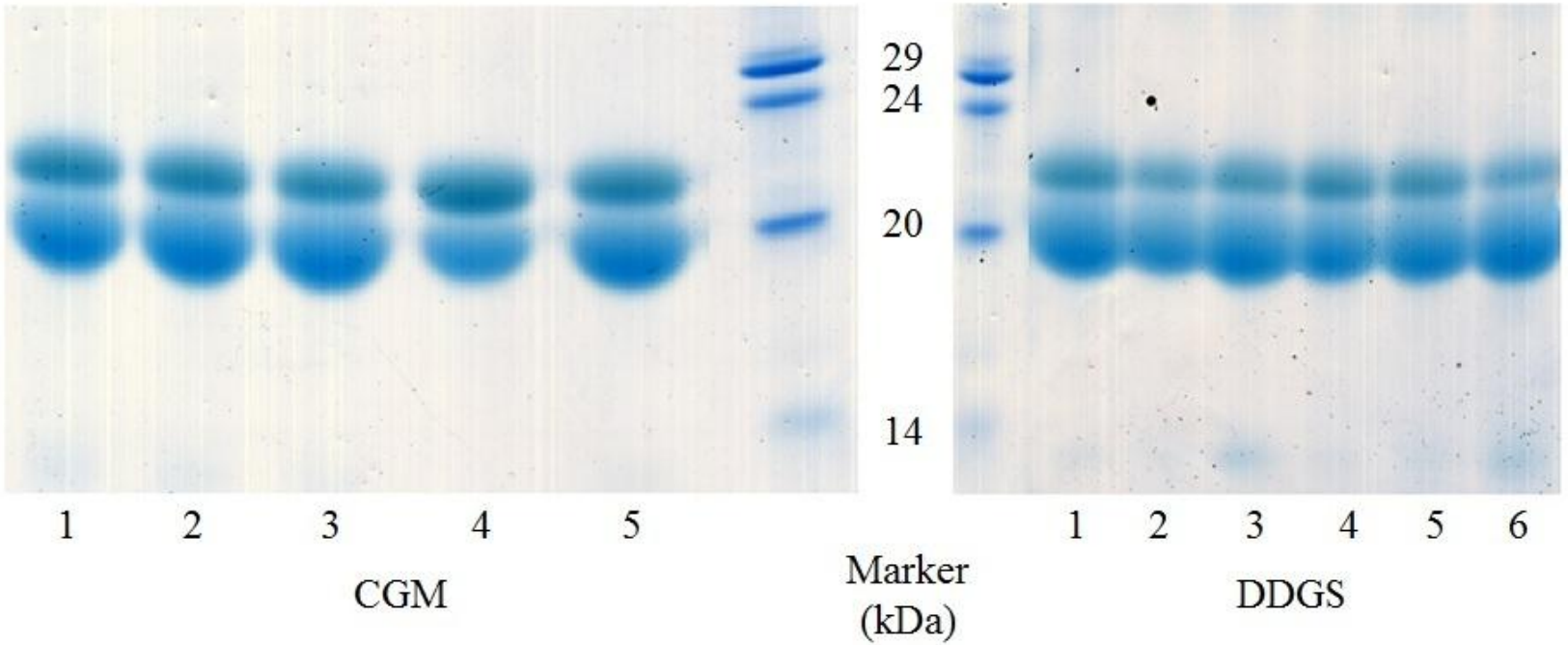

Figure 1. SDS-PAGE of α-zein protein extracts from CGM and DDGS. For the five CGM samples, all were extracted without sodium hydroxide and sodium bisulfate. A similar gel was observed for the five identical extractions which used sodium hydroxide and sodium bisulfate. CGM lane 1 was extracted with 88% aqueous 2-propanol, lane 2 with 70% aqueous 2-propanol, lane 3 with 55% aqueous 2-propanol, lane 4 with 70% 2-propanol,22.5% glycerol, and 7.5% water, and lane 5 with 70% aqueous ethanol. For the six DDGS samples, lanes 1-3 were not pretreated with enzyme while lanes 4-6 were pretreated. Lanes 1 and 4 were extracted with 88% aqueous 2-propanol, lanes 2 and 5 were extracted with 70% aqueous 2-propanol, and lanes 3 and 6 were extracted with 70% aqueous ethanol.

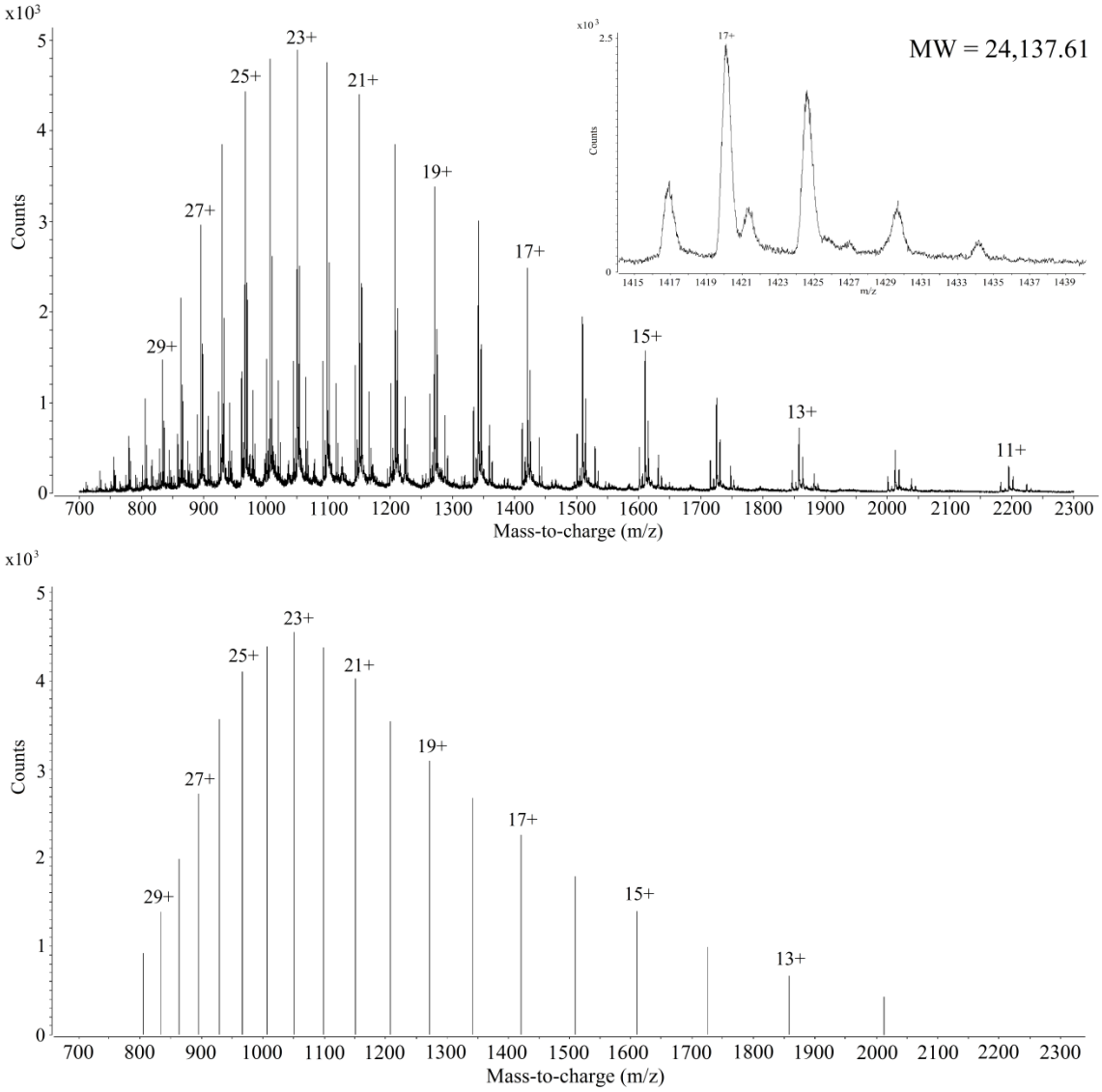

Figure 2. Mass spectrum of a mixture of α-zein proteins. Peaks for the protein with M_r = 24,137.61 Da are labeled. Top spectrum is raw data integration of total ion chromatograph from 41.6 to 42.7 minutes. A zoomed in view of the 17+ peak is displayed in the inset. The peak labeled 17+ belongs to the charge state progression for the protein shown in the bottom deconvoluted spectrum. The other peaks in the inset belong to charge state progressions from other proteins.

CHAPTER 4

CHARACTERIZATION OF PHOSVITIN PHOSPHOPEPTIDES BY ELECTROSPRAY IONIZATION TANDEM MASS SPECTROMETRY

Derrick L. Morast[a,b], Himali Samaraweera[c], Dong U. Ahn[c], R. S. Houk*[a,b]

[a]Department of Chemistry, Iowa State University, Ames, IA 50011 USA

[b]Ames Laboratory U. S. Department of Energy, Ames, IA 50011 USA

[c]Department of Animal Science, Iowa State University, Ames, IA 50011 USA

*Corresponding Author. Tel (515) 294-9462 Fax-0050 rshouk@iastate.edu

A manuscript for submission to Analytical and Bioanalytical Chemistry

ABSTRACT

Electrospray ionization (ESI) and tandem mass spectrometry (MS/MS) are used to characterize phosphopeptides from various digestions of phosvitin (PV) proteins from egg yolk. Phosvitin was digested with one of three enzymes: trypsin, chymotrypsin, or Multifect® P-3000 (MFP). The effect of partial dephosphorylation prior to enzymatic digestion and MS/MS analysis was also investigated. Partial dephosphorylation was accomplished by incubating phosvitin with either alkaline phosphatase or sodium hydroxide. Overall, twenty-seven total peptides and thirteen phosphopeptides were identified. Partial dephosphorylation improved the digestibility of PV as well as the ability to measure phosphopeptides via mass spectrometry.

KEYWORDS

Phosvitin, phosphopeptides, enzymatic digestion, electrospray ionization, tandem mass spectrometry

INTRODUCTION

Phosvitin, the major egg yolk glycophosphoprotein, accounts for 60% of the total egg yolk phosphoproteins and contains 80% of the total egg yolk phosphorous (*1, 2*). Phosvitin is a heterogeneous protein and consists mainly of a major (α) and minor (β) component with molecular weights of about 36,000 and 40,000 Da, respectively (*1, 3*). The α and β components make up nearly 95% of the total protein although phosvitin has been reported to consist of seven components (*3*). Phosvitin has an unusual amino acid composition in which serine accounts for greater than 55% of the total amino acids (*4*). Many of the serines are arranged in clusters of up to 15 consecutive residues (*5*). Moreover, nearly all of the serines are phosphorylated, making phosvitin one of the most highly phosphorylated proteins known (*6*). As such, phosvitin is a strong metal chelating agent. Ninety-five percent of egg yolk iron is bound to phosvitin (*7*). Manganese, cobalt, magnesium, and calcium also bind with PV over a range of pH and temperature (*8, 9*).

Its high abundance and many phosphate groups make PV an attractive source of phosphopeptides for various nutraceutical applications. Specifically, antioxidant and mineral binding peptides have garnished attention because they are especially useful in the food and pharmaceutical industries (*10, 11*). However, previous experiments have shown that phosvitin greatly resists protease activity (*12-14*). One explanation is that the consecutive phosphoserines interfere with the formation of the proper enzyme-substrate complex needed for hydrolysis. Even so, Jiang and Mine have demonstrated the calcium-binding capacity of phosphopeptides derived from partial dephosphorylation of phosvitin (*15*). Tryptic digestion was performed following treatment with alkaline phosphatase. The resulting

phosphopeptides had molecular weights between 1000 to 3000 Da. Also, Choi et al. investigated the effects of phosvitin phosphopeptides on calcium absorption and accumulation in rat bones (*16*). In their study, phosvitin was subjected to tryptic digestion for 24 hours. Calcium bioavailability increased in rats fed a diet containing these phosphopeptides.

Tandem mass spectrometry has played an increasingly important role in proteomics (*17-22*). De novo peptide sequencing is a key aspect of proteomics and is made possible through the use of collision-induced dissociation (CID) (*23*), electron capture dissociation (ECD) (*24*), or electron transfer dissociation (ETD) (*25*). The two most widely used ionization techniques are ESI (*26*) and matrix-assisted laser desorption/ionization (MALDI) (*27*).

A posttranslational modification (PTM), such as phosphorylation, results in the chemical modification of an amino acid. This modification changes the mass of the amino acid. With the use of a mass spectrometer, measuring the change in mass is generally adequate for identifying the modification (*28*). The phosphate group of a phosphopeptide is relatively labile and CID generally results in the neutral loss of H_3PO_4 (98 Da) or HPO_3 (80 Da) (*29*).

Analysis of phosphopeptides by MS/MS often presents several problems. Generally, phosphopeptide signal is substantially lower than that for equimolar amounts of the analogous unmodified peptide. Phosphopeptides tend to be present at lower concentrations as well. The phosphopeptide signal is greatly reduced if nonphosphorylated peptides are also being sprayed. These problems are compounded because the extent of phosphorylation is

variable, even for different molecules of a given protein (*29*, *30*). Also, phosphopeptides are hydrophilic and usually do not bind well to commonly used high-performance liquid chromatography (HPLC) columns which utilize a hydrophobic stationary phase. Successful use of MS/MS for proteomics requires detailed mass spectra to be generated from the peptide fragments (*31*). Therefore, the identification and characterization of phosphopeptides relies heavily upon the characteristics of the parent ion being dissociated, as well as the employed activation method (*32*).

Our previous work has evaluated both enzymatically and chemically derived digestions of phosvitin for antioxidant and mineral binding properties (*33*). However, sequence identification of the resulting peptides is needed for further investigation of their functional characteristics. Therefore, the current study has the objective of identifying peptides and phosphopeptides derived from a range of phosvitin hydrolysates using high-resolution MS/MS.

MATERIALS AND METHODS

Phosvitin was extracted from egg yolk following the method of Ko et al (*34*). Type I trypsin from bovine pancreas, type II α-chymotrypsin (chymotrypsin) from bovine pancreas, and alkaline phosphatase from bovine intestinal mucosa were purchased from Sigma-Aldrich (St. Louis, MO, USA). Multifect® P-3000 enzyme was a gift from Genencor International Inc. (New York, NY, USA). HPLC-grade water, acetonitrile (ACN), sodium hydroxide (NaOH), and formic acid were also purchased from Sigma.

Enzymatic Digestions of Phosvitin - Native and/or dephosphorylated phosvitin was digested using trypsin, chymotrypsin, or MFP. Phosvitin (10 mg/mL) was dissolved in distilled water and the pH was adjusted using 0.1 M HCl or NaOH prior to addition of the enzyme. Temperature and pH conditions for each enzyme were as follows: Trypsin and chymotrypsin, 37 °C and pH 8.0; MFP, 50 °C and pH 7.0. The enzyme/substrate ratio was 1:100 (w/w) in all cases. Digestions were carried out for 24 hr in a shaker water bath (C7 – New Brunswick Scientific, Edison, NJ, USA). The enzymatic digestions were stopped by keeping the samples in a boiling water bath for 10 min. The samples were lyophilized and stored at -20 °C until used.

Dephosphorylation of Phosvitin - Partially dephosphorylated samples of phosvitin were prepared using either alkaline phosphatase or 0.3 M NaOH. For alkaline phosphatase, phosvitin (10 mg/mL) was dissolved in 100 mM sodium phosphate buffer (pH 10) at an enzyme/substrate ratio of 1:25 (w/w) and incubated at 37 °C for 24 hr in a shaker water bath. Alkaline phosphatase was deactivated by placing the sample in a boiling water bath for 10 min. The sample was dialyzed for 24 hr at 4 °C and then lyophilized. Lyophilized samples were then subjected to enzymatic digestion following the above procedure.

For sodium hydroxide dephosphorylation, phosvitin (25 mg/mL) was dissolved in 0.3 M NaOH and incubated for 3 hr in a shaker water bath at room temperature. Samples were dialyzed for 24 hr at 4 °C and then lyophilized. Lyophilized samples were enzymatically digested following the above procedure, with one modification. Enzyme digestion time was 6 hours instead of 24 hours, for the reasons discussed below.

LC-ESI-MS/MS Sample Preparation and Instrumentation - Digested samples were dissolved at 10 mg/mL in HPLC grade water and centrifuged at 3,000 x g for 10 min. To facilitate the LC separation, the supernatant was filtered through a Millipore Millex-FH 0.45 µm filter (Billerica, MA, USA). Samples of the filtrate(5 µL) were injected onto a Waters Atlantis® dC_{18} 4.6 x 150 mm, 3.0 µm HPLC column (Milford, MA, USA). Mobile phase A was 100% H_2O with 0.1% formic acid. Mobile phase B was 100% ACN with 0.1% formic acid. An isocratic flow (5% mobile phase B at 0.5 mL/min) was used for 5 minutes to remove salts. A linear gradient from 5% to 95% mobile phase B over 45 min followed. ESI-MS/MS analysis was done using a high-resolution Agilent 6540 quadrupole time-of-flight mass spectrometer (TOF-MS) (Santa Clara, CA, USA). Fragmentation was accomplished using CID at a collision energy setting of 25 eV with N_2 as the collision gas.

RESULTS AND DISCUSSION

Optimization of Phosvitin Digestions - Phosvitin digestions were tested over a range of enzyme digestion times (6 to 48 hours), alkaline phosphatase reaction times (3 to 24 hours), NaOH concentrations (0.1 to 0.3 M), and NaOH reaction times (1 to 3 hours). All sample digestion products were initially separated using sodium dodecyl sulfate polyacrylamide gel electrophoresis (SDS-PAGE) to estimate the approximate extent of digestion (*33*).

Phosvitin was digested for up to 48 hours with each enzyme. Across all the enzymes tested, the SDS-PAGE band corresponding to native phosvitin became fainter and the amounts of lower molecular weight peptide fragments increased as digestion time increased

up to 24 hours (data not shown). Band patterns were similar for 24 and 48 hour digestions, therefore only 24 hour samples were analyzed by MS/MS.

Figure 1 shows a SDS-PAGE of five replicates of 24 hour trypsin digestion (lanes 4-8), along with two replicates of native phosvitin (lanes 1 and 2). Only one band corresponding to lower molecular weight fragments, those smaller than 10 kDa, is observed (boxed in region). This is due to the poor resolution of SDS-PAGE, which cannot distinguish between the molecular weights of these peptides. A larger molecular weight fragment, about 28 kDa, was also observed, particularly in replicates 7 and 8.

Phosvitin incubated with alkaline phosphatase for 24 hours followed by enzymatic digestion for 24 hours showed the most promising initial results using SDS-PAGE. Therefore, only those samples were used for subsequent MS/MS analysis.

Jiang and Mine demonstrated that phosvitin dephosphorylation reaches a plateau in which very little more phosphate is released if incubation time with 0.3 M NaOH is longer than three hours (*35*). Figure 2 shows the resulting SDS-PAGE band pattern after incubation of phosvitin with 0.3 M NaOH for up to three hours. The dark band in lane 1 corresponds to native phosvitin. This band is absent in all the digested samples. In fact, the only definite band observed in Figure 2 corresponds to small peptide fragments. This suggests that some alkaline hydrolysis has occurred along with the alkaline dephosphorylation. As a result, enzyme digestion times following NaOH pre-treatment were reduced from 24 hours to 6 hours.

Utilizing the most promising results from initial SDS-PAGE tests, the following phosvitin treatment protocols were chosen for LC-MS/MS analysis: 24 hour trypsin digestion, 24 hour chymotrypsin digestion, 24 hour MFP digestion, 24 hour alkaline phosphatase followed by 24 hour enzymatic digestion with either trypsin, chymotrypsin, or MFP, and 3 hour incubation with 0.3 M NaOH followed by 6 hour digestion with either trypsin, chymotrypsin, or MFP.

Previous MS Analysis of Phosvitin Phosphopeptides - As stated above, it has been well documented that phosvitin resists enzymatic digestion. The core of the protein (residues 56-154) contains 80 serine residues and is extensively phosphorylated. As such, it is difficult to predict which peptide fragments will be present in a given digestion. For instance, trypsin generally induces cleavage on the C-terminal side of lysine or arginine. Phosvitin contains 26 such sites. Ignoring locations where lysine and arginine residues are close together, a theoretical tryptic digestion should result in 12 to 15 peptides. However, gel filtration analysis revealed only two major fractions (*14*). It should be noted, though, that the second fraction was thought to be a heterogeneous mixture of fragments, mostly derived from the N-terminal chain (Ala 1 to Arg 35). Also, detection was by UV absorbance, not MS.

Young et al. used MALDI- and nano-ESI-TOF-MS to study PPP3, a phosvitin phosphopeptide (PPP) fraction derived from tryptic digestion (*36*). In their work, PPP3 was isolated using anion-exchange HPLC and dephosphorylated prior to analysis. Three main peptides were identified: GTEPDAKTSSSSSASSTATSSSSSSASSPNRKKPMDE (PV residues 4-41), NSKSSSSSSKSSSSSSRSRSSSKSSSSSSSSSSSSSSKSSSSR (+3 PO_4) (reported as PV residues 155-197, actually PV residues 105-147), and

EDDSSSSSSSSVLSKIWGRHEIYQ (reported as PV residues 244-257, actually PV residues 194-217). Ten additional fragments of those three main peptides were also identified, with nine of the ten coming from EDDSSSSSSSSVLSKIWGREIYQ. Although we did not observe exactly the same "main" peptides, many of our smaller fragments come from the same phosvitin region (see Table 1). These findings are not surprising, however. Phosphorylation is a heterogeneous process; each individual serine residue within a collection of phosvitin molecules is likely phosphorylated to different extents (*29*). This also plays into the difficulty of predicting enzymatic specificity for phosvitin digestion.

MS/MS Analysis of Digested Phosvitin Samples - Figure 3 shows representative MS/MS data. Panel A is the MS spectrum generated via ESI for the peptide AEFGTEPDAK (position 1-10). This peptide originated in the 24 hour MFP digestion of phosvitin, although it was identified in other samples as well (see Tables 1-3). A large signal for the doubly charged ion, *m/z* = 532.746, can be seen. Figure 3B is the resulting MS/MS spectrum of the above ion. Collision-induced dissociation of a peptide ion results in a series of so called b- and y-fragment ions (*37*). These ions are the result of backbone fragmentation between the carbonyl carbon and the amino nitrogen. The b-ions extend from the N-terminus and the y-ions from the C-terminus. Ions are labeled b_1, b_2, $b_3 \ldots b_n$ and y_1, y_2, $y_3 \ldots y_n$ corresponding to fragmentation after each subsequent amino acid. Identified b- and y-ions generated from CID of the peptide AEFGTEPDAK are labeled in Fig. 3B.

Figure 3C is the MS spectrum observed for a different peptide KKPMDEEENDQV (position 36-47). This peptide originated from a 24 hour trypsin digestion of phosvitin; it was identified in multiple samples from other treatment protocols (see Tables 1-3). Figure

3D is the MS/MS spectrum of the doubly charged ion, *m/z* = 731.390, with identified b- and y-ions labeled.

Table S1 in the supporting information has a comprehensive list of all peptides that were identified for all samples tested. In general, enzymatic digestion of partially dephosphorylated phosvitin resulted in greater sequence coverage. Also, potentially bioactive phosphopeptides were only identified in partially dephosphorylated samples. A total of 27 peptides were observed between the nine samples tested and many peptides were found in multiple samples. These peptides originated from the N- and C- terminus, with several phosphopeptides from the core region. One peptide, shown in italics in Table S1 and Table 3, could have originated from two neighboring locations within the phosvitin sequence. As we are unable to confirm the exact origin, both positions are listed.

MS/MS Results of Trypsin Digestion - Table 1 contains a list of all peptides identified from phosvitin digestions which used trypsin. Trypsin cleaves preferentially on the C-terminal side of lysine and arginine. Cleavage is suppressed if the adjacent amino acid is proline or is negatively charged (*38*). An adjacent basic residue also has a negative influence on trypsin cleavage. Trypsin has also been shown to have atypical cleavages, which have been described as "chymotrypsin-like" since they generally occur at aromatic or hydrophobic residues (*39*).

The exact effect of the high phosphorylation extent of PV on the specificity of tryptic digestion is unknown. The results in Table 1 show that sequence coverage improved dramatically for the partially dephosphorylated samples that were partially dephosphorylated prior to trypsin digestion (middle and bottom frames of Table 1). These results indicate that

the steric hindrance and anionic property of the phosphate group played a role in the low reactivity of native phosvitin.

The 24 hour trypsin digestion yielded five peptides, none of which were phosphopeptides. Three of the five peptides were from an overlapping region of phosvitin, namely position 36-51. The other two peptides were N- and C- terminus fragments.

Partial dephosphorylation of phosvitin with alkaline phosphatase showed much more promising results (middle frame of Table 1). Eight peptide fragments were observed, with five phosphopeptides. All but one of the peptides came from the first half of the amino acid sequence, although two of them did originate from the core region. The final phosphopeptide ended near the C-terminus.

The NaOH partially dephosphorylated sample (Table 1 bottom frame) also contained at least one phosphopeptide, although only four total peptides were observed. Three of these latter peptides were N-terminus cleavage products while the fourth peptide was the C-terminal fragment.

MS/MS Results of Chymotrypsin Digestion - Table 2 displays a list of peptides identified from phosvitin digestions with chymotrypsin. Carboxyl-terminus side cleavage after tryptophan (W), tyrosine (Y), phenylalanine (F), leucine (L), methionine (M), histidine (H), glutamine (Q), and asparagine (N) make up ninety percent of all cleavage sites for chymotrypsin (*38*). The specificity and cleavage rate, however, can be greatly affected by the adjacent amino acid on the C-terminal side. For instance, an adjacent proline residue inhibits cleavage nearly completely. Chymotrypsin cleavage rate is also greatly diminished

if the adjoining amino acid is aromatic (W, Y, or F) or negatively charged (aspartic acid, D; glutamic acid, E).

Conversely, an adjoining positively charged amino acid (lysine, K; arginine, R) enhances chymotrypsin cleavage (*38*). The phosphate group is negatively charged. This fact could explain why only two peptide fragments observed for the 24 hour chymotrypsin digestion without pretreatment (Table 2 top frame).

Many more peptide fragments are seen for our partially dephosphorylated samples, which provides further evidence that the phosphate group inhibits chymotrypsin digestion. Partial dephosphorylation with alkaline phosphatase increased the number of observed peptides to five, two of which were phosphorylated (Table 2 middle frame). Unlike the identical trypsin sample, both PPPs were from an overlapping region near the C-terminus with no peptides originating from the core region. This is not surprising, however, given that the core region does not contain any aromatic amino acids and has few other favorable sites for chymotrypsin digestion.

Interestingly, though, when phosvitin was treated with NaOH prior to chymotrypsin digestion, four peptides originating near the N-terminus were observed, including one PPP. Figure 2 shows the SDS-PAGE pattern results of phosvitin treated with 0.3 M NaOH for 1, 2, or 3 hours. After only one hour the band corresponding to native phosvitin has disappeared, indicating both alkaline dephosphorylation and alkaline hydrolysis occurred. It is likely because of this alkaline hydrolysis that we are able to observe N-terminal peptides in the sample digested with chymotrypsin only if the PV is pre-treated, with 0.3 M NaOH being the best reagent in this case.

MS/MS Results of Multifect® P-3000 Digestion - Table 3 contains a list of peptides identified from phosvitin digestions with Multifect® P-3000. Multifect® P-3000 is a bacterial alkaline serine endopeptidase. The effect of the excess negative charge from the phosphate group on the specificity of MFP is unknown. Phosvitin digested with MFP alone for 24 hours resulted in the identification of 4 peptides, none of them being PPPs. All of the peptides came from the N- or C-terminus. Again, pretreatment to induce partial dephosphorylation resulted in a more efficient digestion (Table 3). In fact, of all the pretreatments tested, 24 hour alkaline phosphatase followed by 24 hour MFP digestion produced the best sequence coverage (46%) and largest total number of observed peptides (13). The same sample also had at least 5 phosphopeptides which may have the potential for nutraceutical application. Pre-treatment with 0.3 M NaOH also improved the digestibility of PV compared to the native sample, although not to a large extent. Even so, this latter sample did contain one PPP.

ACKNOWLEDGEMENTS

The Agilent QTOF 6540 mass spectrometer was obtained with funds from the National Science Foundation under MRI Grant No. CHE 0840434. Any opinions, findings, and conclusions or recommendations expresses in this material are those of the author(s) and do not necessarily reflect the views of the National Science Foundation. The authors would like to thank Kamel Harrata for assistance with the mass spectrometer. Derrick Morast would also like to acknowledge the Velmer A. and Mary K. Fassel Fellowship (Iowa State University, 2010) and the GAANN Fellowship (Iowa State University, 2010) for financial support.

REFERENCES

1. Taborsky, G.; Mok, C. C., Phosvitin - Homogeneity and Molecular Weight. *J. Biol. Chem.* **1967,** *242*, 1495-1501.
2. Joubert, F. J.; Cook, W. H., Separation and Characterization of Lipovitellin From Hen Egg Yolk. *Can. J. Biochem. Physiol.* **1958,** *36*, 389-398.
3. Culbert, J.; McIndoe, W. M., Comparison of Heterogeneity of Phosvitin of Egg-Yolk and Blood-Plasma of Domestic Fowl (*Gallus domesticus*). *Int. J. Biochem.* **1971,** *2*, 617-622.
4. Taborsky, G., Phosvitin. *Adv. Inorg. Biochem.* **1983,** *5*, 235-279.
5. Byrne, B. M.; Schip, A. D. V.; Vandeklundert, J. A. M.; Arnberg, A. C.; Gruber, M.; Ab, G., Amino Acid Sequence of Phosvitin Derived From the Nucleotide Sequence of Part of the Chicken Vitellogenin Gene. *Biochemistry* **1984,** *23*, 4275-4279.
6. Clark, R. C., The Primary Structure of Avian Phosvitins - Contributions Through the Edman Degradation of Methylmercaptovitins Prepared From the Constituent Phosphoproteins. *Int. J. Biochem.* **1985,** *17*, 983-988.
7. Albright, K. J.; Gordon, D. T.; Cotterill, O. J., Release of Iron From Phosvitin by Heat and Food Additives. *J. Food Sci.* **1984,** *49*, 78-81.
8. Grizzuti, K.; Perlmann, G. E., Binding of Divalent Ions to Phosphoglycoprotein Phosvitin. *Abstr. Pap. Am. Chem. Soc.* **1973**, 1-1.
9. Grizzuti, K.; Perlmann, G. E., Further Studies on Binding of Divalent Cations to Phosphoglycoprotein Phosvitin. *Biochemistry* **1975,** *14*, 2171-2175.
10. Kitts, D. D., Bioactive Substances in Food - Identification and Potential Uses. *Can. J. Physiol. Pharm.* **1994,** *72*, 423-434.
11. Kitts, D. D.; Weiler, K., Bioactive proteins and peptides from food sources. Applications of bioprocesses used in isolation and recovery. *Curr. Pharm. Des.* **2003,** *9*, 1309-1323.
12. Mecham, D. K.; Olcott, H. S., Phosvitin, the Principal Phosphoprotein of Egg Yolk. *J. Am. Chem. Soc.* **1949,** *71*, 3670-3679.
13. Gray, H. B., Structural Models for Iron and Copper Proteins Based on Spectroscopic and Magnetic Properties. *Adv. Chem. Ser.* **1971**, 365-389.
14. Goulas, A.; Triplett, E. L.; Taborsky, G., Oligophosphopeptides of Varied Structural Complexity Derived From the Egg Phosphoprotein, Phosvitin. *J. Protein Chem.* **1996,** *15*, 1-9.
15. Jiang, B.; Mine, Y., Phosphopeptides derived from hen egg yolk phosvitin: Effect of molecular size on the calcium-binding properties. *Biosci., Biotechnol., Biochem.* **2001,** *65*, 1187-1190.
16. Choi, I.; Jung, C.; Choi, H.; Kim, C.; Ha, H., Effectiveness of phosvitin peptides on enhancing bioavailability of calcium and its accumulation in bones. *Food Chem.* **2005,** *93*, 577-583.
17. Yates, J. R., Mass spectrometry - from genomics to proteomics. *Trends Genet.* **2000,** *16*, 5-8.
18. Aebersold, R.; Mann, M., Mass spectrometry-based proteomics. *Nature* **2003,** *422*, 198-207.

19. van den Berg, B. H. J.; Tholey, A., Mass spectrometry-based proteomics strategies for protease cleavage site identification. *Proteomics* **2012,** *12*, 516-529.
20. Angel, T. E.; Aryal, U. K.; Hengel, S. M.; Baker, E. S.; Kelly, R. T.; Robinson, E. W.; Smith, R. D., Mass spectrometry-based proteomics: existing capabilities and future directions. *Chem. Soc. Rev.* **2012,** *41*, 3912-3928.
21. Xie, F.; Liu, T.; Qian, W.-J.; Petyuk, V. A.; Smith, R. D., Liquid Chromatography-Mass Spectrometry-based Quantitative Proteomics. *J. Biol. Chem.* **2011,** *286*, 25443-25449.
22. Bantscheff, M.; Schirle, M.; Sweetman, G.; Rick, J.; Kuster, B., Quantitative mass spectrometry in proteomics: a critical review. *Anal. Bioanal. Chem.* **2007,** *389*, 1017-1031.
23. Hunt, D. F.; Buko, A. M.; Ballard, J. M.; Shabanowitz, J.; Giordani, A. B., Sequence Analysis of Polypeptides by Collision Activated Dissociation on a Triple Quadrupole Mass Spectrometer. *Biom. Mass Spectrom.* **1981,** *8*, 397-408.
24. Kruger, N. A.; Zubarev, R. A.; Horn, D. M.; McLafferty, F. W., Electron capture dissociation of multiply charged peptide cations. *Int. J. Mass Spectrom.* **1999,** *185*, 787-793.
25. Syka, J. E. P.; Coon, J. J.; Schroeder, M. J.; Shabanowitz, J.; Hunt, D. F., Peptide and protein sequence analysis by electron transfer dissociation mass spectrometry. *Proc. Natl. Acad. Sci. U. S. A.* **2004,** *101*, 9528-9533.
26. Fenn, J. B.; Mann, M.; Meng, C. K.; Wong, S. F.; Whitehouse, C. M., Electrospray Ionization for Mass-Spectrometry of Large Biomolecules. *Science* **1989,** *246*, 64-71.
27. Tanaka, K.; Waki, H.; Ido, Y.; Akita, S.; Yoshida, Y.; Yohida, T., Protein and Polymer Analyses up to m/z 100,000 by Laser Ionization Time-of-Flight Mass Spectrometry. *Rapid Commun. Mass Spectrom.* **1988,** *2*, 151-153.
28. Yates, J. R.; Eng, J. K.; McCormack, A. L.; Schieltz, D., Method to Correlate Tandem Mass Spectra of Modified Peptides to Amino Acid Sequences in the Protein Database. *Anal. Chem.* **1995,** *67*, 1426-1436.
29. Mann, M.; Ong, S. E.; Gronborg, M.; Steen, H.; Jensen, O. N.; Pandey, A., Analysis of protein phosphorylation using mass spectrometry: deciphering the phosphoproteome. *Trends in Biotechnol.* **2002,** *20*, 261-268.
30. Boersema, P. J.; Mohammed, S.; Heck, A. J. R., Phosphopeptide fragmentation and analysis by mass spectrometry. *J. Mass Spectrom.* **2009,** *44*, 861-878.
31. Aebersold, R.; Goodlett, D. R., Mass spectrometry in proteomics. *Chem. Rev.* **2001,** *101*, 269-295.
32. Smith, S. A.; Kalcic, C. L.; Safran, K. A.; Stemmer, P. M.; Dantus, M.; Reid, G. E., Enhanced Characterization of Singly Protonated Phosphopeptide Ions by Femtosecond Laser-induced Ionization/Dissociation Tandem Mass Spectrometry (fs-LID-MS/MS). *J. Am. Soc. Mass Spectrom.* **2010,** *21*, 2031-2040.
33. Samaraweera, H. Production and characterization of phosphopeptides from egg yolk phosvitin. Ph.D. Dissertation, Iowa State University, Ames, IA, 2011.
34. Ko, K. Y.; Nam, K. C.; Jo, C.; Lee, E. J.; Ahn, D. U., A simple and efficient method for preparing partially purified phosvitin from egg yolk using ethanol and salts. *Poult. Sci.* **2011,** *90*, 1096-1104.
35. Jiang, B.; Mine, Y., Preparation of novel functional oligophosphopeptides from hen egg yolk phosvitin. *J. Agric. Food Chem.* **2000,** *48*, 990-994.

36. Young, D.; Nau, F.; Pasco, M.; Mine, Y., Identification of Hen Egg Yolk-Derived Phosvitin Phosphopeptides and Their Effects on Gene Expression Profiling against Oxidative Stress-Induced Caco-2 Cells. *J. Agric. Food Chem.* **2011,** *59*, 9207-9218.
37. Roepstorff, P.; Fohlman, J., Proposal for a Common Nomenclature for Sequence Ions in Mass Spectra of Peptides. *Biomed. Mass Spectrom.* **1984,** *11*, 601-601.
38. Keil, B., *Specificity of Proteolysis*. Springer-Verlag: New York, NY, 1992.
39. Keil, B., Can a Protein Data Bank Help to Define the Binding Site of Proteolytic Enzymes? *Protein, Nucleic Acid, Enzyme* **1986,** *6*, 11-21.

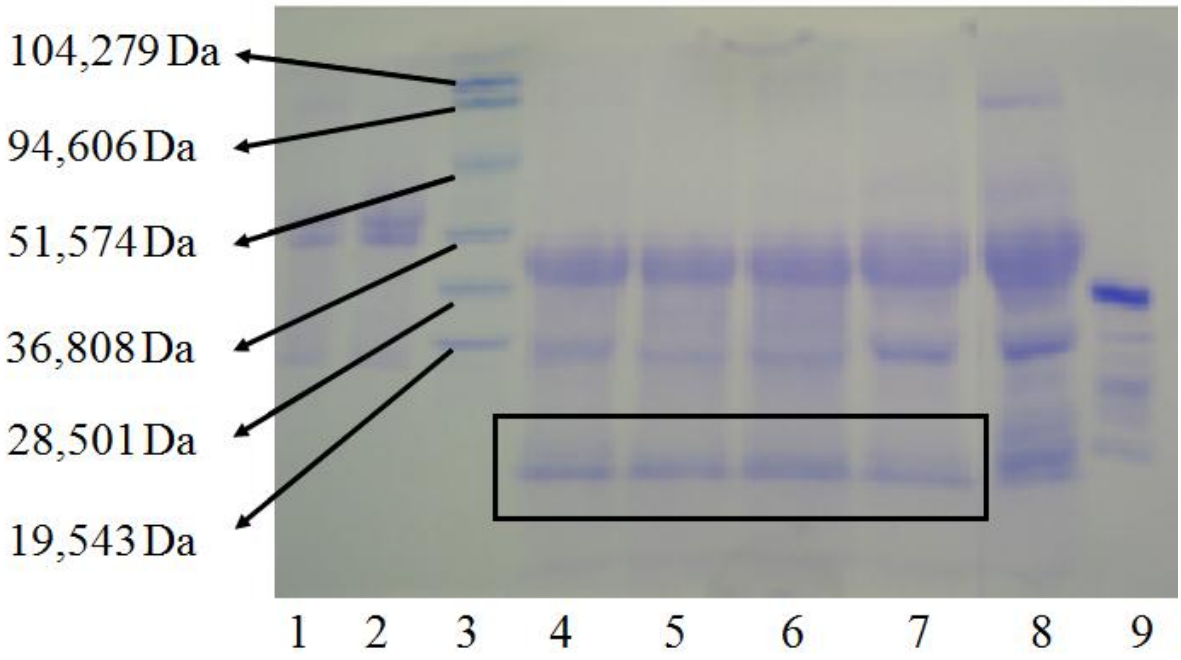

Figure 1. SDS-PAGE of 24 hour trypsin digestion of phosvitin: lane 1 and 2 – native phosvitin; lane 3 – molecular markers; lane 4 to 8 – replicates of trypsin digestion; lane 9 – trypsin. The bands enclosed within the box probably represent the peptides detected during our HPLC-MS/MS analysis.

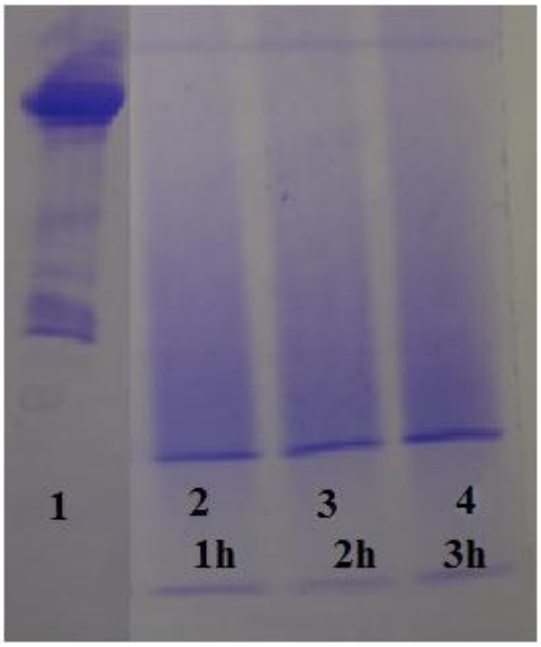

Figure 2. SDS-PAGE pattern of alkaline dephosphorylation of phosvitin with 0.3 M NaOH: lane 1 – native phosvitin; lane 2 – 0.3 M NaOH-treated phosvitin for 1 hour at 37 °C; lane 3 – 0.3 M NaOH-treated phosvitin for 2 hours at 37 °C; lane 3 – 0.3 M NaOH-treated phosvitin for 3 hours at 37 °C.

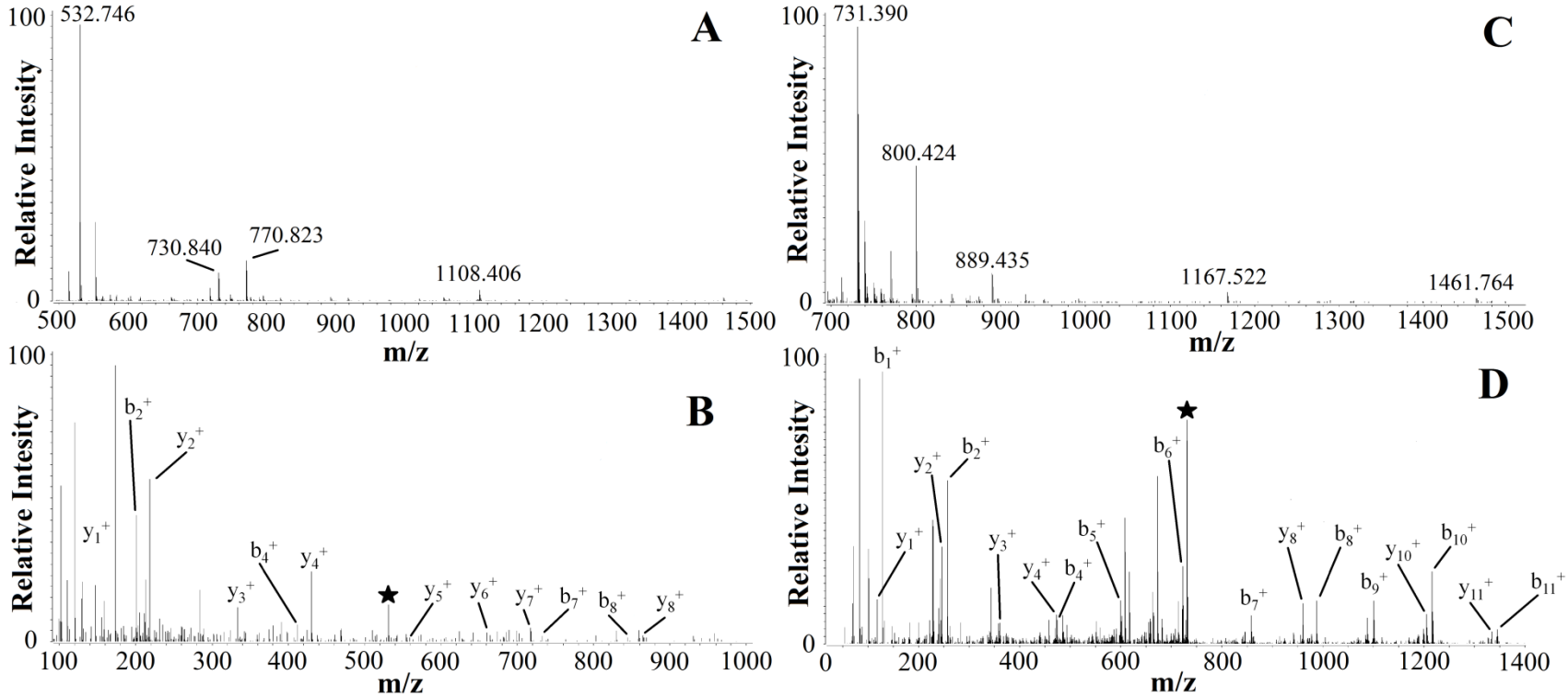

Figure 3. (A) Electrospray ionization mass spectrum of the peptide AEFGTEPDAK (position 1-10) from 24 hour MFP digestion of phosvitin. $[M+2H]^{2+}$ = 532.746. (B) MS/MS spectrum of doubly charged ion, 532.746, with identified b and y fragment ions. The parent ion is marked with a star. (C) Electrospray ionization mass spectrum of the peptide KKPMDEEENDQV (position 36-47) from 24 hour trypsin digestion of phosvitin. $[M+H]^{+}$ = 1461.764 and $[M+2H]^{2+}$ = 731.390. (D) MS/MS spectrum of doubly charged ion, 731.390, with identified b and y fragment ions. The parent ion is marked with a star.

Table 1. Peptides Identified in Trypsin Phosvitin Digestions Using HPLC-ESI-MS/MS

24 hr Trypsin				
Position	**Sequence**	**Obs (m/z)**	**M_r (exp)**	**M_r (calc)**
1-10	AEFGTEPDAK	532.746	1063.478	1063.471
36-47	KKPMDEEENDQV	731.390	1460.765	1460.634
36-48	KKPMDEEENDQVK	795.375	1588.735	1588.729
38-51	PMDEEENDQVKQAR	844.879	1687.743	1687.736
213-217	HEIYQ	689.325	688.318	688.307
24 hr Alkaline Phosphatase + 24 hr Trypsin				
Position	**Sequence**	**Obs (m/z)**	**M_r (exp)**	**M_r (calc)**
5-10	TEPDAK	660.314	659.307	659.302
10-35	TSSSSSSASSTATSSSSSSASSPNR (+1 PO_4)	1187.993	2373.971	2373.963
36-47	KKPMDEEENDQV	731.390	1460.765	1460.634
36-48	KKPMDEEENDQVK	795.375	1588.735	1588.729
52-63	NKDASSSSRSSK (+1 PO_4)	667.289	1332.562	1332.590
81-94	RSSSSSSSSSSSSR (+1 PO_4)	728.304	1454.593	1454.586
82-94	SSSSSSSSSSSSR (+1 PO_4)	650.242	1298.469	1298.485
197-208	SSSSSSSSVLSK (+1 PO_4)	611.779	1221.543	1221.535
3 hr NaOH + 6 hr Trypsin				
Position	**Sequence**	**Obs (m/z)**	**M_r (exp)**	**M_r (calc)**
1-10	AEFGTEPDAK	532.746	1063.478	1063.471
10-35	TSSSSSSASSTATSSSSSSASSPNR (+1 PO_4)	1187.993	2373.971	2373.963
36-48	KKPMDEEENDQVK	795.375	1588.735	1588.729
213-217	HEIYQ	689.325	688.318	688.307

Table 2. Peptides Identified in Chymotrypsin Phosvitin Digestions Using HPLC-ESI-MS/MS

24 hr Chymotrypsin				
Position	**Sequence**	**Obs (m/z)**	**M_r (exp)**	**M_r (calc)**
40-52	DEEENDQVKQARN	787.841	1573.667	1573.686
211-216	GRHEIY	387.701	773.387	773.371
24 hr Alkaline Phosphatase + 24 hr Chymotrypsin				
Position	**Sequence**	**Obs (m/z)**	**M_r (exp)**	**M_r (calc)**
1-10	AEFGTEPDAK	532.746	1063.478	1063.471
35-46	RKKPMDEEENDQ	823.883	1645.751	1645.762
193-206	LEDDSSSSSSSSVL (+1 PO_4)	740.307	1478.599	1478.589
211-216	GRHEIY	387.701	773.387	773.371
3 hr NaOH + 6 hr Chymotrypsin				
Position	**Sequence**	**Obs (m/z)**	**M_r (exp)**	**M_r (calc)**
1-10	AEFGTEPDAK	532.746	1063.478	1063.471
1-35	AEFGTEPDAKTSSSSSSASSTATSSSSSSASSPNR (+9 PO_4)	1015.540	4058.129	4059.434
36-47	KKPMDEEENDQV	731.390	1460.765	1460.634
36-48	KKPMDEEENDQVK	795.375	1588.735	1588.729
193-206	LEDDSSSSSSSSVL (+1 PO_4)	740.307	1478.599	1478.589
213-217	HEIYQ	689.325	688.318	688.307

Table 3. Peptides Identified in Multifect® P-3000 Phosvitin Digestions Using HPLC-ESI-MS/MS

24 hr Multifect® P-3000				
Position	**Sequence**	**Obs (m/z)**	**M_r (exp)**	**M_r (calc)**
1-10	AEFGTEPDAK	532.746	1063.478	1063.471
4-10	GTEPDAK	717.340	716.333	716.323
209-217	IWGRHEIYQ	601.298	1200.581	1200.593
213-217	HEIYQ	689.325	688.318	688.307
24 hr Alkaline Phosphatase + 24 hr Multifect® P-3000				
Position	**Sequence**	**Obs (m/z)**	**M_r (exp)**	**M_r (calc)**
1-10	AEFGTEPDAK	532.746	1063.478	1063.471
1-21	AEFGTEPDAKTSSSSSSASST	1017.429	2032.843	2032.860
4-12	GTEPDAKTS	453.212	904.409	904.403
4-21	GTEPDAKTSSSSSSASST	843.871	1685.727	1685.712
36-47	KKPMDEEENDQV	731.390	1460.765	1460.634
36-48	KKPMDEEENDQVK	795.375	1588.735	1588.729
61-69	*SSKSSNSSK (+1 PO_4)*	496.205	990.394	990.424
72-80	*SSKSSNSSK (+1 PO_4)*	496.205	990.394	990.424
82-94	SSSSSSSSSSSSR (+5 PO_4)	810.350	1618.686	1618.485
95-107	SSSSSSSSSSNSK (+5 PO_4)	809.756	1617.497	1617.489
195-205	DDSSSSSSSSV (+1 PO_4)	562.700	1123.385	1123.378
195-207	DDSSSSSSSSVLS (+1 PO_4)	662.748	1323.481	1323.494
209-217	IWGRHEIYQ	601.298	1200.581	1200.593
3 hr NaOH + 6 hr Multifect® P-3000				
Position	**Sequence**	**Obs (m/z)**	**M_r (exp)**	**M_r (calc)**
1-10	AEFGTEPDAK	532.746	1063.478	1063.471
36-47	KKPMDEEENDQV	731.390	1460.765	1460.634
36-48	KKPMDEEENDQVK	795.375	1588.735	1588.729
61-69	*SSKSSNSSK (+1 PO_4)*	496.205	990.394	990.424
72-80	*SSKSSNSSK (+1 PO_4)*	496.205	990.394	990.424
209-217	IWGRHEIYQ	601.298	1200.581	1200.593
213-217	HEIYQ	689.325	688.318	688.307

Supporting Information for

CHARACTERIZATION OF PHOSVITIN PHOSPHOPEPTIDES BY ELECTROSPRAY IONIZATION TANDEM MASS SPECTROMETRY

Derrick L. Morast[a,b], Himali Samaraweera[c], Dong U. Ahn[c], R. S. Houk*[a,b]

[a]Department of Chemistry, Iowa State University, Ames, IA 50011 USA

[b]Ames Laboratory U. S. Department of Energy, Ames, IA 50011 USA

[c]Department of Animal Science, Iowa State University, Ames, IA 50011 USA

*Corresponding Author. Tel (515) 294-9462 Fax-0050 rshouk@iastate.edu

Table S1. List of All Peptides Identified in Phosvitin Digestions Using HPLC-ESI-MS/MS

Position	Sequence	Obs (m/z)	M_r (expt)	M_r (calc)	Treatment[a]
1-10	AEFGTEPDAK	532.746	1063.478	1063.471	A, C, E, F, G, H, I
1-21	AEFGTEPDAKTSSSSSSASST	1017.429	2032.843	2032.860	H
1-35	AEFGTEPDAKTSSSSSSASSTATSSSSSSASSPNR (+9 PO_4)	1015.540	4058.129	4059.434	F
4-10	GTEPDAK	717.340	716.333	716.323	G
4-12	GTEPDAKTS	453.212	904.409	904.403	H
4-21	GTEPDAKTSSSSSSASST	843.871	1685.727	1685.712	H
5-10	TEPDAK	660.314	659.307	659.302	B
10-35	TSSSSSSASSTATSSSSSSASSPNR (+1 PO_4)	1187.993	2373.971	2373.963	B, C
35-46	RKKPMDEEENDQ	823.883	1645.751	1645.762	E
36-47	KKPMDEEENDQV	731.390	1460.765	1460.634	A, B, F, H, I
36-48	KKPMDEEENDQVK	795.375	1588.735	1588.729	A, B, C, F, H, I
38-51	PMDEEENDQVKQAR	844.879	1687.743	1687.736	A
40-52	DEEENDQVKQARN	787.841	1573.667	1573.686	D
52-63	NKDASSSSRSSK (+1 PO_4)	667.289	1332.562	1332.590	B
61-69	*SSKSSNSSK (+1 PO_4)*	496.205	990.394	990.424	H, I
72-80	*SSKSSNSSK (+1 PO_4)*	496.205	990.394	990.424	H, I
81-94	RSSSSSSSSSSSSR (+1 PO_4)	728.304	1454.593	1454.586	B
82-94	SSSSSSSSSSSSR (+1 PO_4)	650.242	1298.469	1298.485	B
82-94	SSSSSSSSSSSSR (+5 PO_4)	810.350	1618.686	1618.485	H
95-107	SSSSSSSSSSNSK (+5 PO_4)	809.756	1617.497	1617.489	H
193-206	LEDDSSSSSSSSVL (+1 PO_4)	740.307	1478.599	1478.589	E, F
193-210	LEDDSSSSSSSSVLSKIW (+1 PO_4)	997.441	1992.867	1992.879	E
195-205	DDSSSSSSSSV (+1 PO_4)	562.700	1123.385	1123.378	H
195-207	DDSSSSSSSSVLS (+1 PO_4)	662.748	1323.481	1323.494	H
197-208	SSSSSSSSVLSK (+1 PO_4)	611.779	1221.543	1221.535	B

Table S1. (continued)

209-217	IWGRHEIYQ	601.298	1200.581	1200.593	G, H, I
211-216	GRHEIY	387.701	773.387	773.371	D, E
213-217	HEIYQ	689.325	688.318	688.307	A,C, F,G, I

a Treatment legend – A: 24 hr Trypsin, B: 24 hr alkaline phosphatase + 24 hr Trypsin, C: 3 hr NaOH + 6 hr Trypsin, D: 24 hr chymotrypsin, E: 24 hr alkaline phosphatase + 24 hr chymotrypsin, F: 3 hr NaOH + 6 hr chymotrypsin, G: 24 hr MFP, H: 24 hr alkaline phosphatase + 24 hr MFP, I: 3 hr NaOH + 6 hr MFP.

CHAPTER 5

ULTRAVIOLET LASER DESORPTION ATMOSPHERIC PRESSURE PHOTOIONIZATION MASS SPECTROMETRY

Derrick L. Morast, Timothy J. Anderson, Andrew R. Korte, Young Jin Lee, R. S. Houk*

Ames Laboratory U. S. Department of Energy, Ames, IA 50011 USA

*Corresponding Author. Tel (515) 294-9462 Fax-0050 rshouk@iastate.edu

A manuscript for submission to Rapid Communications in Mass Spectrometry

ABSTRACT

This paper introduces a novel atmospheric pressure ion source, laser desorption atmospheric pressure photoionization (LD APPI) with a UV laser (355 nm). Analytes are desorbed from the sample surface and are ionized with a 10 eV krypton discharge vacuum ultraviolet (VUV) lamp. UV absorbing analytes can be desorbed and analyzed without added matrix. For other compounds, i.e. alkanes and fatty acids, colloidal silver is employed as a UV absorbing matrix. Analytes were detected as singly charged protonated and/or oxygenated species. The analysis of polar, nonpolar, and aromatic compounds by LD APPI is described.

KEYWORDS

Laser desorption, atmospheric pressure photoionization, mass spectrometry, colloidal silver

INTRODUCTION

In recent years, mass spectrometric imaging (MSI) has shown great promise for profiling the molecular distribution of analytes on biological surfaces (*1-6*). The most widely used ionization techniques have been matrix-assisted laser desorption/ionization (MALDI) and desorption electrospray ionization (DESI) (*7, 8*). In MALDI, analytes are co-crystalized with an organic acid matrix. An ultraviolet laser is generally used for desorption and ionization of the analyte from the sample surface. MSI utilizing MALDI typically occurs in the vacuum chamber (vMALDI) of the mass spectrometer, although ambient pressure MADLI (AP MALDI) has also been described (*9, 10*). For the reduced pressure MALDI system, two complications arise: 1) analyte turnover during sample preparation and/or vacuum dehydration, and 2) loss or reduction of volatile analytes prior to sample analysis. AP MALDI reduces these issues, particularly the loss of volatile analytes; however its effectiveness for MSI applications is often limited by poorer sensitivity than vMALDI. Specifically, the efficiency of ion extraction into the MS inlet for AP MALDI is low compared to collection of ions from a source in vacuum. Small molecule analysis by MALDI also suffers from matrix interferences, e.g., abundant ions from the matrix at low m/z values.

Desorption electrospray ionization (DESI), a matrix-free ambient pressure ionization technique, is routinely used for imaging small molecules (*11-13*). The ionization process in DESI is similar to conventional ESI, whereby charged solvent droplets ionize surface analytes. MALDI and DESI also have low ionization efficiencies for nonpolar compounds and are therefore better suited for the analysis of ionic and polar compounds.

Three matrix-free ionization techniques, electrospray-assisted laser desorption/ionization (ELDI) (*14*), laser ablation electrospray ionization (LAESI) (*15*), and infrared laser ablation atmospheric pressure photoionization (IR-LA APPI) (*16*), have been developed to improve sensitivity in ambient pressure laser desorption. Matrix-assisted laser desorption electrospray ionization (MALDESI) also addresses this issue (*17*); however, due to the use of conventional MALDI matrices it is better suited for larger molecular weight analytes. ELDI and LAESI rely on electrospray-assisted post-ionization. As such, the analysis of nonpolar compounds by these techniques remains a challenge.

Vertes et al. describe IR-LA APPI experiments that combine infrared laser ablation with photoionization with high ionization efficiencies for both polar and nonpolar analytes (*16*). In the present work, we describe initial experiments that combine ultraviolet (UV) laser ablation/desorption with photoionization. Two potential advantages of using a UV laser instead of an IR laser are a) smaller diffraction limited spot size and b) the ability to image a wider range of sample media since the UV laser does not rely on energy transfer through water molecules. The supplemental photoionization step also facilitates use of colloidal Ag matrix. This material has physical characteristics conducive to good spatial resolution and is a good UV absorber but does not yield Ag^+-analyte adduct ions at atmospheric pressure, in our experience.

MATERIALS AND METHODS

Chemicals - Colloidal silver (99.99% pure silver, 0.65 nm, 20 ppm in water) was purchased from Purest Colloids, Inc. (Westhampton, NJ, USA). Standard compounds 2′-hydroxy-4,4′,6′-trimethoxychalcone, 2′-methoxyacetophenone, *n*-hexadecane, and stearic

acid were purchased from Sigma-Aldrich (St. Louis, MO, USA). Methanol (MeOH) and 2-propanol (IPA) were purchased from Fisher Scientific (Fairlawn, NJ, USA).

Sample Preparation for LD APPI Experiments - For the analysis of each sample, 2 to 5 µL of standard solution (in MeOH) was pipetted onto a stainless steel MALDI plate and allowed to air dry. Total sample loadings were between 10 and 20 nmol with ~ 400 pmol of sample removed during ablation. If no matrix was used for the analysis, samples were analyzed once dry. If colloidal silver was utilized as the matrix, the following procedure was used. The aqueous colloidal silver suspension was mixed 1:1 (v/v) with IPA. A modified commercial airbrush (Aztek A470, Rockford, IL, USA) was used as an oscillating spray device (*18*) to coat the sample with matrix. The inner spraying tip of the airbrush was replaced with a fused silica capillary (100 µm i.d., 360 µm o.d., Polymicro Technology, Phoenix, AZ, USA), which improved the homogeneity of the applied matrix layer. The colloidal silver matrix was pumped into the airbrush at a flow rate of 50 µL min^{-1} with a spray volume of 0.3 mL and nebulized with N_2 gas at 40 psi onto the spotted, dry standard sample. The distance between the stainless steel plate and the capillary tip was 9 cm. The flow was halted every ~30 s to allow for vaporization of the solvent.

Mass Spectrometer and Laser - A LTQ-Orbitrap Discovery (Thermo Fisher Scientific, Waltham, MA, USA) operated in electrospray ionization configuration was used to collect all mass spectra. The mass spectrometer can collect low resolution data via the linear ion trap and two electron multiplier detectors located orthogonal to the linear ion trap. High resolution data can be obtained via the orbitrap Fourier transform (FTMS) detector. Spectra were collected from the low resolution ion trap detectors as well as the high

resolution orbitrap detector. Conditions for each spectrum are specified in the Results and Discussion section.

A frequency tripled Nd:YAG laser (355 nm, Big Sky Laser Ultra 20, now Quantel USA, Bozeman, MT, USA) was used for desorption. The laser beam was transferred through mirrors and focused onto the sample surface through a 30 mm focal length lens (ThorLabs, Newton, NJ, USA) with an incident angle of 90° (Fig. 1). The repetition rate of the laser was 15 to 50 Hz and pulse energy was between 120 and 180 µJ per pulse. The spot size at the sample was approximately 200 µm. These settings are discussed further in the Results and Discussion section below.

LD APPI Ion Source - Figure 1 shows a schematic diagram of the LD APPI ion source. The MS inlet was an extended metal transfer tube constructed using stainless steel tubing (add in dimensions here). A stage was placed below the extended ion transfer tube such that the MALDI plate was 5 mm (z in Figure 1) below the center of the MS inlet. A radio frequency krypton discharge vacuum ultraviolet (VUV) photoionization lamp (PhotoMate APPI, Syagen Technologies, Tustin, CA, USA) was placed with outer surface of the exit window 4 mm (x + y in Figure 1) on axis from the MS inlet. The VUV lamp produced 10.0 and 10.6 eV photons, which ionized the sample plume. The laser focal point was centered between the VUV lamp and the MS inlet (y in Figure 1).

RESULTS AND DISCUSSION

LD APPI Ion Source Configuration - In order to minimize the amount of VUV light absorbed by the ambient air, the VUV lamp was mounted closes to (4 mm) the MS

inlet. This distance was large enough to allow space for the sample stage, laser, and sample plume, yet close enough for effective post-ionization and ion collection. The VUV lamp could also be mounted orthogonal to the MS inlet, as in a recent LA APPI article by Vertes et al. (*16*). However, space constraints and the lack of an APPI dopant spray led to the chosen configuration. The sample stage was placed 5 mm below the MS inlet. This distance can be changed by several mm up or down without major changes in sensitivity. However, previous AP LDI work in our group and by others have shown sensitivity advantages if the sample plate is relatively close (less than ~7 mm) to the MS inlet (*19, 20*).

The pathway of the laser beam was about halfway between the MS inlet and the VUV lamp (~ 2 mm). This location could be adjusted ±1 mm as needed without changing sensitivity significantly.

A variety of standards, with or without matrix, were chosen to test the effectiveness of the UV-LD APPI ion source. It is important to note that the data acquisition cycles of the mass spectrometer were not synchronized to the laser pulse. In typical vMALDI experiments, the firing of the laser is synced to the dwell time of the ion trap so that the mass spectrometer begins trapping ions at a desired time after the laser has fired. These events were independent in the present experiments. As such, the dwell time in the ion trap was increased to 300 ms in an effort to "capture" ions from as many laser shots per spectra as possible. The spectra shown below represent the average maximum counts obtained during analysis for periods of ~ 5 minutes.

Matrix-Free Desorption and Ionization of Chalcone - Figure 2 shows the mass spectra from 2′-hydroxy-4,4′,6′-trimethoxychalcone (MW = 314.2 Da). This compound

absorbs the UV laser and was therefore analyzed without matrix. Data were collected over 1.5 min. During this time, the laser was operating continually while the VUV lamp was turned on and off in 15 sec intervals. Figure 2A displays a spectrum obtained with the laser operating at 25 Hz and the VUV lamp off. The $[M + H]^+$ peak is 315.13 Da, with intensity about 30,000 counts. Figure 2B shows a spectrum obtained while the VUV lamp was on. The intensity is about 260,000 counts, which represents a 9x signal enhancement. This was the best signal enhancement factor seen for the various compounds studied, all of which yielded higher signals with the VUV lamp on.

Desorption and Ionization of an Alkane - Photoionization has the ability to ionize analytes which are not readily observed by ESI or MALDI, specifically nonpolar molecules. Alkanes are of interest in plant metabolomics pathways (*21*); they do not absorb the laser efficiently. To demonstrate this, *n*-hexadecane (MW = 226.4 Da) was analyzed (Figure 3). The standard sample of *n*-hexadecane was coated with colloidal silver following the procedure described above. Colloidal silver is a good matrix to transfer the UV laser energy to the sample. Reduced pressure ionization using colloidal silver matrix yields mass spectra with low background noise and few interferences. Yeung et al. have previously shown results for vacuum LDI analysis with colloidal silver (*22, 23*). In those experiments, analyte ions were predominantly measured as silver adducts. However, our results at ambient pressure show little evidence of Ag^+ adducts for n-hexadecane or other compounds of various types. Instead, analyte ions were detected as oxygenated species when APPI was used. Similar oxygenated alkane ions from APPI have been reported previously (*24*). Figure 3 shows the three most abundant peaks from *n*-hexadecane with colloidal silver matrix. The

spectra shown were obtained via the orbitrap FTMS detector. The most abundant peak with the low resolution ion trap detectors was m/z = 257.25 (data not shown). For FTMS collection, m/z = 239.24 and m/z = 255.24 had similar intensities (~ 320,000 counts). The m/z = 257.25 peak corresponds to singly-charged *n*-hexadecane minus one hydrogen plus two oxygen atoms. The assignment for m/z = 239.24 and m/z = 255.24 can be seen in Figure 3A and 3B, respectively.

The mechanism for ionization of these two species is unclear. One possible pathway which accounts for the loss of three hydrogen atoms is cyclization through a $M^{+\bullet}$ radical intermediate. A second possibility is the formation of a double bond through a similar intermediate radical.

Desorption and Ionization of Fatty Acids - Fatty acids represent another class of compounds which are not easily identified using vMALDI. The high volatility of the short- and medium-chain (aliphatic tails less than 12 carbons) fatty acids result in substantial loss of analyte once the MALDI plate has entered the intermediate vacuum region of the mass spectrometer. Long chain fatty acids (aliphatic tails between 12 and 22 carbons) are not as volatile; however, analysis of bio-oil samples for these fatty acids using vLDI still had volatility concerns (*25*).

One possible way to address the volatility issue is to analyze the fatty acid samples under atmospheric conditions. Figure 4 shows an orbitrap FTMS spectrum of stearic acid ($C_{16}H_{35}COOH$, MW = 284.48 Da). A number of peaks are observed including $[M + H]^+$ and $[M + O – H]^+$.

CONCLUSION

We have described a novel ionization source for the analysis of a variety of compounds. The LD APPI source can be used to analyze samples with and without matrix. Analytes were observed as singly charged protonated and/or oxygenated ions. The exact mechanism/pathway for formation of oxygenated ions, especially of *n*-hexadecane, needs to be investigated further. LD APPI should prove to be a useful ionization method alone or in tandem with other atmospheric ionization techniques. Improvements in the analyte signal stability could be made if the laser and mass spectrometer were operated in tandem with each other. These issues are being addressed in subsequent work.

ACKNOWLEDGEMENTS

This research is supported by the U.S. Department of Energy, Office of Basic Energy Sciences, Division of Chemical Sciences, Geosciences, and Biosciences through the Ames Laboratory. The Ames Laboratory is operated for the U.S. Department of Energy by Iowa State University under Contract No. DE-AC02-07CH11358.

REFERENCES

1. Greer, T.; Sturm, R.; Li, L., Mass spectrometry imaging for drugs and metabolites. *J. Proteomics* **2011,** *74*, 2617-2631.
2. Kaspar, S.; Peukert, M.; Svatos, A.; Matros, A.; Mock, H.-P., MALDI-imaging mass spectrometry - An emerging technique in plant biology. *Proteomics* **2011,** *11*, 1840-1850.
3. Lee, Y. J.; Perdian, D. C.; Song, Z.; Yeung, E. S.; Nikolau, B. J., Use of mass spectrometry for imaging metabolites in plants. *Plant Journal* **2012,** *70*, 81-95.
4. Svatos, A., Mass spectrometric imaging of small molecules. *Trends Biotechnol.* **2010,** *28*, 425-434.
5. van Hove, E. R. A.; Smith, D. F.; Heeren, R. M. A., A concise review of mass spectrometry imaging. *J. Chromatogr. A* **2010,** *1217*, 3946-3954.
6. Zaima, N.; Hayasaka, T.; Goto-Inoue, N.; Setou, M., Matrix-Assisted Laser Desorption/Ionization Imaging Mass Spectrometry. *Int. J. Mol. Sci.* **2010,** *11*, 5041-5056.
7. Takats, Z.; Wiseman, J. M.; Cooks, R. G., Ambient mass spectrometry using desorption electrospray ionization (DESI): instrumentation, mechanisms and applications in forensics, chemistry, and biology. *J. Mass Spectrom.* **2005,** *40*, 1261-1275.
8. Tanaka, K.; Waki, H.; Ido, Y.; Akita, S.; Yoshida, Y.; Yohida, T., Protein and Polymer Analyses up to m/z 100,000 by Laser Ionization Time-of-Flight Mass Spectrometry. *Rapid Commun. Mass Spectrom.* **1988,** *2*, 151-153.
9. Laiko, V. V.; Baldwin, M. A.; Burlingame, A. L., Atmospheric pressure matrix assisted laser desorption/ionization mass spectrometry. *Anal. Chem.* **2000,** *72*, 652-657.
10. Li, Y.; Shrestha, B.; Vertes, A., Atmospheric pressure molecular imaging by infrared MALDI mass spectrometry. *Anal. Chem.* **2007,** *79*, 523-532.
11. Wiseman, J. M.; Ifa, D. R.; Zhu, Y.; Kissinger, C. B.; Manicke, N. E.; Kissinger, P. T.; Cooks, R. G., Desorption electrospray ionization mass spectrometry: Imaging drugs and metabolites in tissues. *Proc. Natl. Acad. Sci. U. S. A.* **2008,** *105*, 18120-18125.
12. Ifa, D. R.; Wiseman, J. M.; Song, Q.; Cooks, R. G., Development of capabilities for imaging mass spectrometry under ambient conditions with desorption electrospray ionization (DESI). *Int. J. Mass Spectrom.* **2007,** *259*, 8-15.
13. Wiseman, J. M.; Ifa, D. R.; Song, Q.; Cooks, R. G., Tissue imaging at atmospheric pressure using desorption electrospray ionization (DESI) mass spectrometry. *Angew. Chem. Int. Edit.* **2006,** *45*, 7188-7192.
14. Shiea, J.; Huang, M. Z.; Hsu, H. J.; Lee, C. Y.; Yuan, C. H.; Beech, I.; Sunner, J., Electrospray-assisted laser desorption/ionization mass spectrometry for direct ambient analysis of solids. *Rapid Commun. Mass Spectrom.* **2005,** *19*, 3701-3704.
15. Nemes, P.; Vertes, A., Laser ablation electrospray ionization for atmospheric pressure, in vivo, and imaging mass spectrometry. *Anal. Chem.* **2007,** *79*, 8098-8106.
16. Vaikkinen, A.; Shrestha, B.; Kauppila, T. J.; Vertes, A.; Kostiainen, R., Infrared Laser Ablation Atmospheric Pressure Photoionization Mass Spectrometry. *Anal. Chem.* **2012,** *84*, 1630-1636.
17. Sampson, J. S.; Hawkridge, A. M.; Muddiman, D. C., Generation and detection of multiply-charged peptides and proteins by matrix-assisted laser desorption electrospray

ionization (MALDESI) Fourier transform ion cyclotron resonance mass spectrometry. *J. Am. Soc. Mass Spectrom.* **2006,** *17*, 1712-1716.
18. Chen, Y.; Allegood, J.; Liu, Y.; Wang, E.; Cachon-Gonzalez, B.; Cox, T. M.; Merrill, A. H., Jr.; Sullards, M. C., Imaging MALDI mass spectrometry using an oscillating capillary nebulizer matrix coating system and its application to analysis of lipids in brain from a mouse model of Tay-Sachs/Sandhoff disease. *Anal. Chem.* **2008,** *80*, 2780-2788.
19. Perdian, D. C.; Schieffer, G. M.; Houk, R. S., Atmospheric pressure laser desorption/ionization of plant metabolites and plant tissue using colloidal graphite. *Rapid Commun. Mass Spectrom.* **2010,** *24*, 397-402.
20. Shrestha, B.; Nemes, P.; Nazarian, J.; Hathout, Y.; Hoffman, E. P.; Vertes, A., Direct analysis of lipids and small metabolites in mouse brain tissue by AP IR-MALDI and reactive LAESI mass spectrometry. *Analyst* **2010,** *135*, 751-758.
21. Samuels, L.; Kunst, L.; Jetter, R., Sealing plant surfaces: Cuticular wax formation by epidermal cells. *Annu. Rev. Plant Biol.* **2008,** *59*, 683-707.
22. Perdian, D. C.; Cha, S.; Oh, J.; Sakaguchi, D. S.; Yeung, E. S.; Lee, Y. J., In situ probing of cholesterol in astrocytes at the single-cell level using laser desorption ionization mass spectrometric imaging with colloidal silver. *Rapid Commun. Mass Spectrom.* **2010,** *24*, 1147-1154.
23. Jun, J. H.; Song, Z.; Liu, Z.; Nikolau, B. J.; Yeung, E. S.; Lee, Y. J., High-Spatial and High-Mass Resolution Imaging of Surface Metabolites of Arabidopsis thaliana by Laser Desorption-Ionization Mass Spectrometry Using Colloidal Silver. *Anal. Chem.* **2010,** *82*, 3255-3265.
24. Cody, R. B. Atmospheric Pressure Charge-Exchange Analyte Ionization. U.S. Patent application 20,120,112,051, June 1, 2007.
25. Smith, E. A.; Lee, Y. J., Petroleomic Analysis of Bio-oils from the Fast Pyrolysis of Biomass: Laser Desorption Ionization-Linear Ion Trap-Orbitrap Mass Spectrometry Approach. *Energy Fuels* **2010,** *24*, 5190-5198.

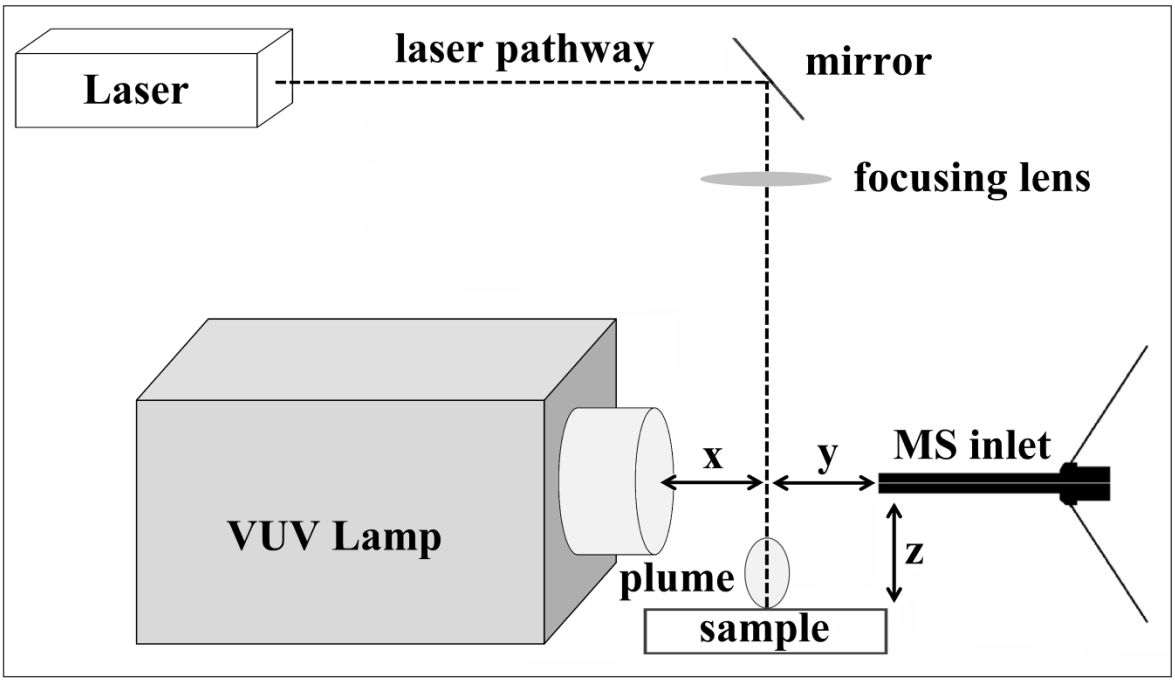

Figure 1. A schematic of the LD APPI ion source. The laser was a tripled Nd:YAG operating at 355 nm. The distance of the VUV lamp from the MS inlet (x + y) was 4 mm. The distance of the sample plate from the MS inlet (z) was 5 mm.

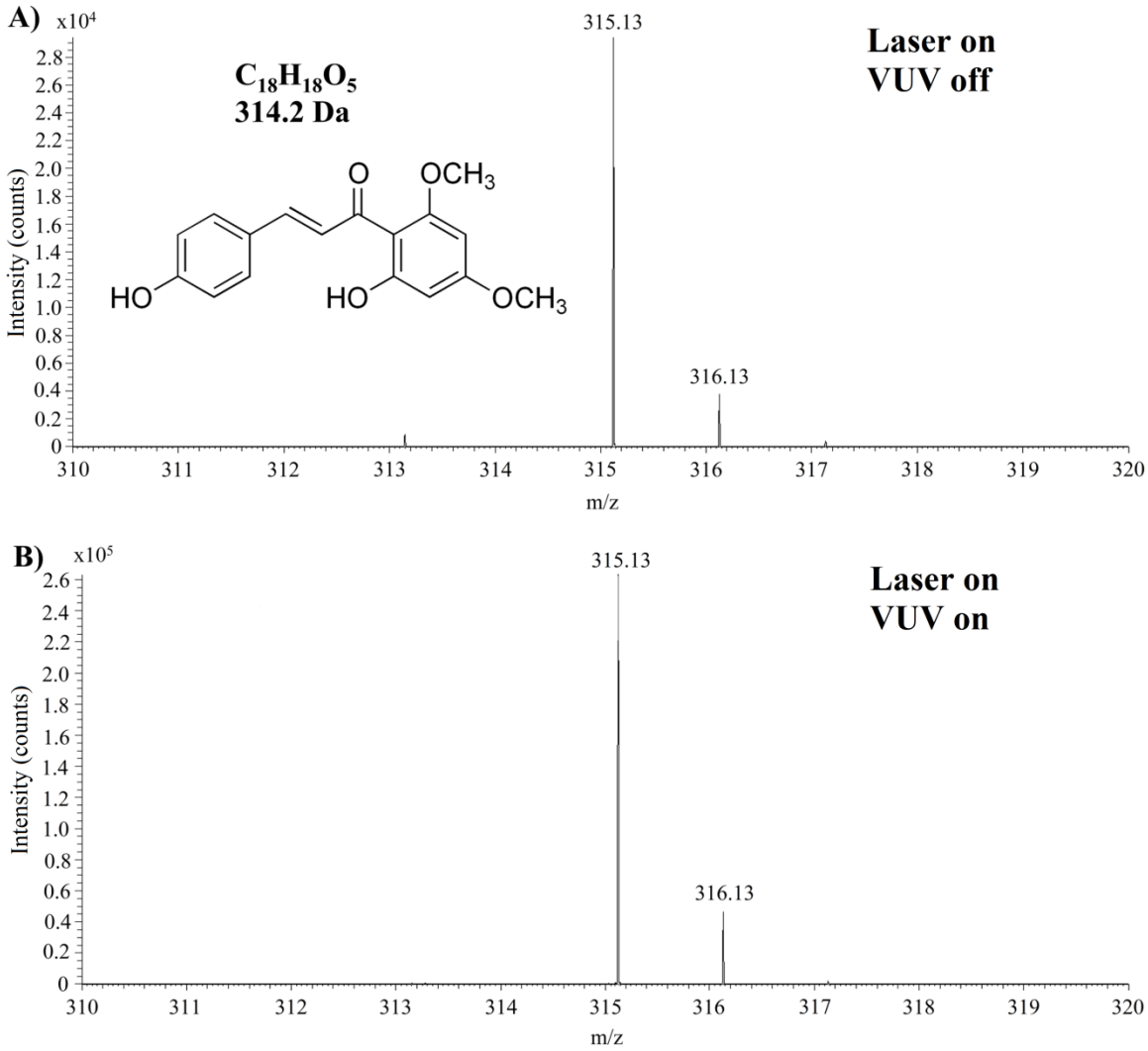

Figure 2. LD APPI spectra of 2′-hydroxy-4,4′,6′-trimethoxychalcone without matrix. The chemical formula, molecular mass, and structure are shown above. Panel A is a mass spectrum obtained while the laser was operating but the VUV lamp was off. Total counts are around 30,000. Panel B is a mass spectrum obtained while both the laser and the VUV lamp were on. Full scale is approximately 260,000 counts.

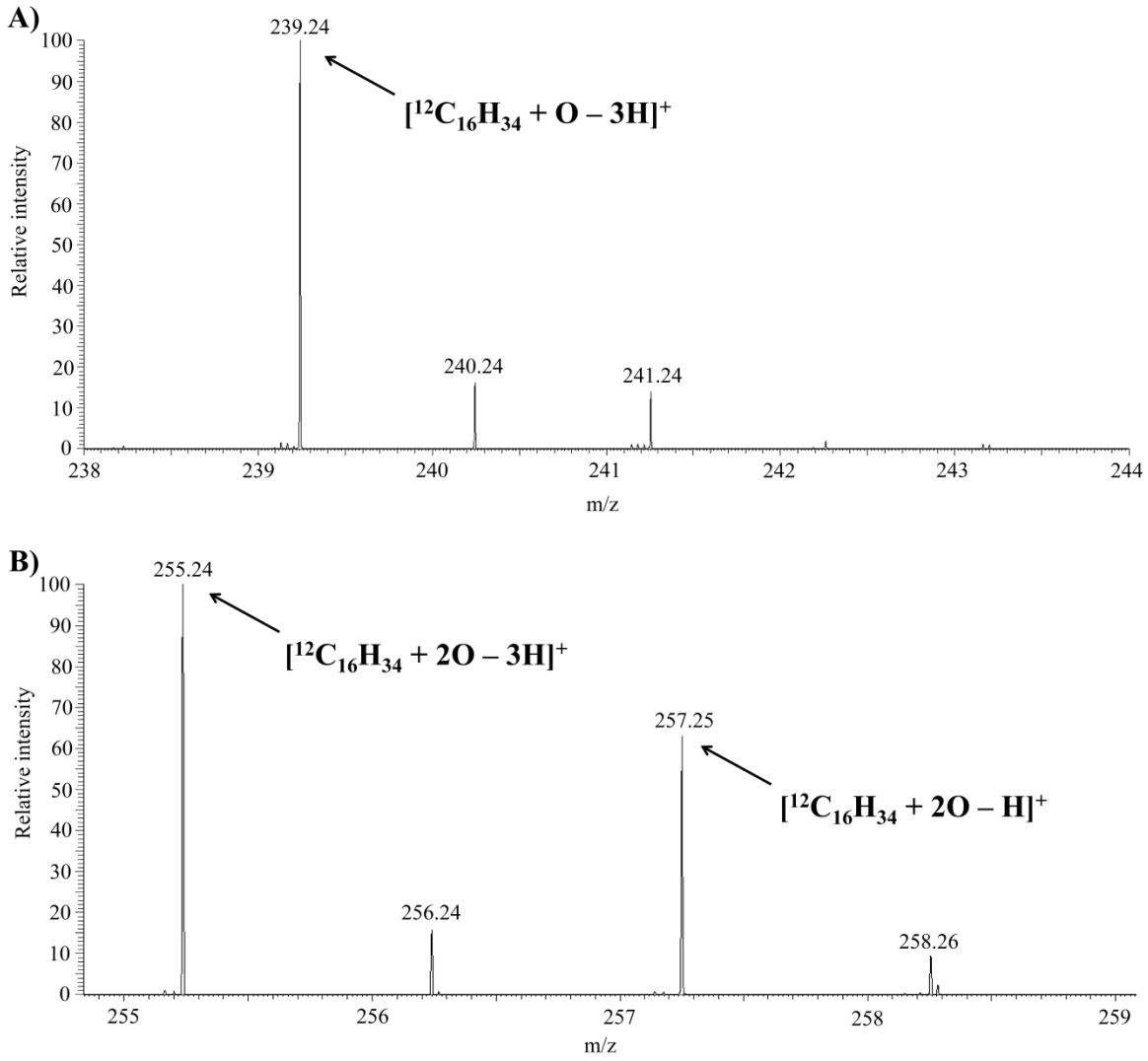

Figure 3. LD APPI orbitrap FTMS spectra of *n*-hexadecane (MW = 226.4 Da) with colloidal silver matrix. Panel A shows the singly charged ion of *n*-hexadecane with the addition of one oxygen and loss of three hydrogen atoms. Panel B shows the singly charged ions of *n*-hexadecane with the addition of two oxygen atoms and loss of one or three hydrogen atoms (m/z = 257.25 and 255.24, respectively). Full scale for each spectrum is ~ 320,000 counts.

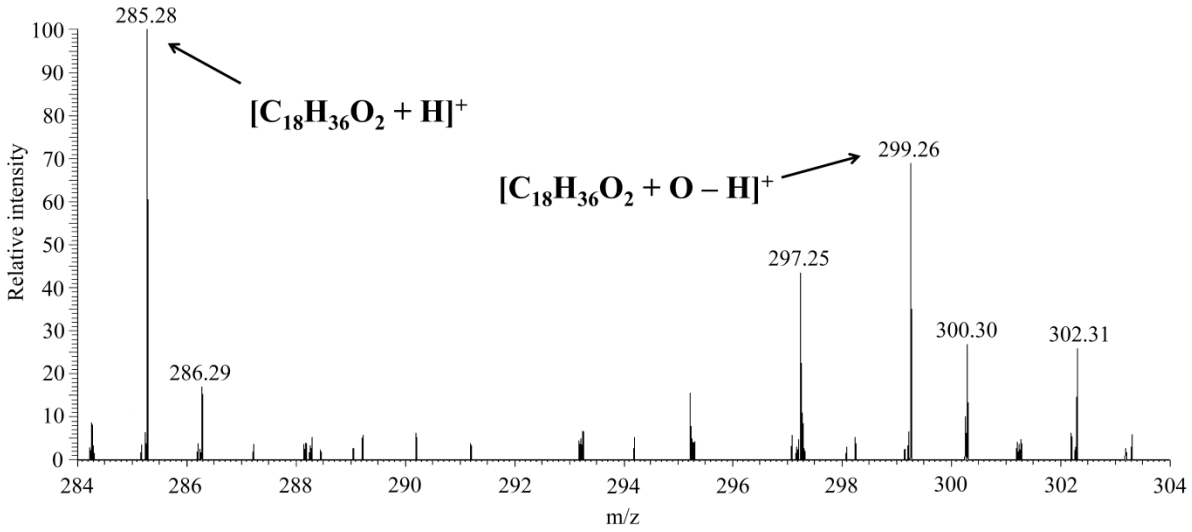

Figure 4. LD APPI orbitrap FTMS spectra of stearic acid (MW = 284.48 Da) with colloidal silver matrix. Two singly charged ions are prominent; m/z = 285.28 is the protonated ion of stearic acid while m/z = 299.26 is stearic acid plus the addition of one oxygen atom and loss of one hydrogen atom.

CHAPTER 6

GENERAL CONCLUSIONS AND OVERVIEW OF FUTURE DIRECTIONS

The focus of this dissertation was the analysis of biological compounds using hyphenated mass spectrometry methods. Chapter 2 combined ion mobility and mass spectrometry to measure highly folded gas-phase conformations of protein cations from alkaline solutions. Cations from alkaline solutions of ubiquitin, cytochrome *c*, lysozyme, and α-lactalbumin were found to be 14% to 36% more folded than cations generated via proton-transfer reactions.

Further experiments could be performed in order to advance our understanding of these results. First, it would be beneficial to perform proton transfer reactions on the alkaline cations. Specifically, the 6+ ion of α-lactalbumin has a similar gas-phase conformation from the pH 8.0 solution and from proton transfer reactions of the native solution. However, the 4+ and 5+ ions from the alkaline solution are more highly folded than the 4+ and 5+ ions from proton transfer. Although sensitivity may be an issue, it is possible to isolate the 6+ ion in the ion trap and perform charge reduction. The resulting 4+ and 5+ ions should have gas-phase conformations similar to either the alkaline solution ions or the native solution ions. Second, analysis of more proteins would be beneficial, including proteins known to be stable at pH 8.0 such as alkaline phosphatases.

Chapter 3 described a comprehensive analysis of α-zein proteins by combining HPLC and an accurate-mass TOF MS. Overall, 95 α-zein proteins were identified with the aid of deconvolution software. These results included 48 α-zein proteins which were previously

identified and reported in literature and 47 α-zein proteins being reported for the first time. The sequence homology of these proteins complicates the HPLC separation. Therefore it is necessary to analyze them using a high-resolution mass spectrometer. Further sequence verification and identification would be possible with the use of a Fourier transform ion cyclotron resonance (FT-ICR) MS; top-down proteomics could also be performed via electron capture dissociation. This route would be much easier than isolating and hydrolyzing each α-zein protein.

Chapter 4 utilized HPLC and tandem mass spectrometry to analyze the amino acid sequence of peptides from phosvitin hydrolysis. Two of the goals of the experiments were to improve the enzyme digestibility of phosvitin and identify phosphopeptides. It was found that partial dephosphorylation prior to enzyme digestion improved sequence coverage and increased the number of phosphopeptides measured by ESI-MS/MS. Identification of phosphopeptides could be improved by a 2D HPLC system utilizing a titania column for phosphopeptide enrichment.

Chapter 5 introduced a novel ionization source which combined UV laser desorption and APPI on an Orbitrap mass spectrometer. This ionization source showed promising results for the analysis of nonpolar and volatile compounds. The use of a UV laser also allowed for samples to be analyzed with or without matrix. Further experiments and improvements to the source design are required to fully characterize the effectiveness of this technique. First and foremost, it is essential to combine the laser firing event with the mass spectrometer scan sequence as it is done during vMALDI experiments. This will ensure that ions generated from each laser shot will be captured in the ion trap. Once this is complete it will be possible to perform more robust fundamental experiments to optimize the source

geometry and laser power. Also, the improved sensitivity will allow for a smaller laser spot size and a lower limit of detection.

There continues to be much interest in the analysis of biological compounds. Over the last few decades we have seen a dramatic increase in the applications of mass spectrometry through hyphenated techniques. This versatility will ensure that mass spectrometry remains one of the most utilized analytical instruments for years to come.

ACKNOWLEDGEMENTS

Funding for part of this research was supported by the U.S. Department of Energy, Office of Basic Energy Sciences, Division of Chemical Sciences, Geosciences, and Biosciences through the Ames Laboratory. The Ames Laboratory is operated for the U.S. Department of Energy by Iowa State University under Contract No. DE-AC02-07CH11358. Other funding was provided by the Velmer A. and Mary K. Fassel Fellowship and the GAANN Fellowship.

First, I would like to thank Dr. Houk for his expertise and guidance throughout my graduate school career. I chose to attend Iowa State University specifically to do research in his group and I am grateful he gave me that opportunity. I would also like to thank Gregg Schieffer. He very graciously passed along his knowledge of the ion-trap – ion mobility – TOF MS instrument to me. I learned more during the two and a half years we worked in the lab together than at any other point. I thank Tim Anderson and Himali Samaraweera for their expertise in our collaborative projects. I also thank past and present Houk group members, specifically DC Perdian, Chris Ebert, Travis Witte, Megan Mekoli, and Sally McIntyre for helpful discussions about my research and their friendship throughout our time working together. I would also like to thank the other graduate committee members, Dr. Young Jin Lee, Dr. Joseph Burnett, Dr. Jesudoss Kingston, and Dr. Emily Smith for their time spent on my research work. I would like to personally thank Dr. Lee for his expertise with the laser desorption work.

There are several other people who have been instrumental in supporting me throughout this process. I wouldn't be who I am today without the love and support from my parents. From a young age they instilled in me the value of education and ensured that I

could accomplish everything I put my mind to. I couldn't have been blessed with better role models and I owe them more than they will ever know. I would also like to thank my sister and grandparents for their support along the way. And finally to my wife Alysen. You have been through this entire process with me and supported me through all of the highs and lows. You are my best friend and I am truly grateful to have you in my life.

APPENDIX I

TIME-RESOLVED HEATING AND UNFOLDING OF PROTEIN IONS DUE TO ION INJECTION CONDITIONS IN AN ION TRAP – ION MOBILITY – TIME-OF-FLIGHT MASS SPECTROMETER

Gregg M. Schieffer, Derrick L. Morast, Qin Zhao, Ethan R. Badman[b], and R. S. Houk*

Ames Laboratory U. S. Department of Energy
Department of Chemistry
Iowa State University, Ames, IA 50011 USA
*Corresponding Author. Tel (515) 294-9462 Fax-0050 rshouk@iastate.edu

[b]Hoffman-La Roche Inc., Non-Clinical Safety, Nutley, NJ 07110 USA

Submit to: International Journal of Mass Spectrometry

ABSTRACT

Heating and unfolding of protein ions as they are extracted from a 3D quadrupole ion trap and injected into an ion mobility drift tube are studied. The square wave extraction pulse on the ion trap exit induces extensive unfolding for ions in certain charge states with a range of conformations available. The extent of unfolding differs for even 1 μs differences in extraction pulse duration. This negative square wave on the ion trap exit induces as much unfolding as some 500 volts DC applied to the front of the drift tube. Various proteins unfold to a maximum extent at a common spatial position about 0.9 cm in front of the entrance to the drift tube.

INTRODUCTION

Ion mobility spectrometry (IMS) coupled to mass spectrometry, can quickly provide low resolution structural information on gas-phase ions. Low electric field IMS separates ions by shape-to-charge measurement, based on the time they take to drift through an inert gas under a weak electric field in a mobility cell [1]. The drift times from the low-field IMS measurements are readily converted to the collision cross section. The IMS measurement is orthogonal to MS, which measures the mass-to-charge ratio (m/z or Th). The cross-section provides coarse shape and structure information [1, 2], particularly if it is combined with simulations or other experimental data like H/D exchange.

In 2009 we published a paper describing a home-built ion trap – ion mobility – time-of-flight mass spectrometer (IT – IM – TOF MS) with the capability for ion / ion reactions [3]. During experiments to characterize and understand this instrument, we came across the unexpected result that the magnitude of the voltage and duration of the square wave applied

to the ion trap exit endcap can greatly affect the measured cross-section values and the relative abundances of different protein conformers, particularly for protein ions in charge states that have several accessible conformations with substantially different cross sections. This effect, in addition to the injection voltage on the front of the mobility cell, was shown (Figure 5 in [3]) using the ubiquitin 7+ ion (Ubq). A few μs difference in the duration of the extraction pulse changed the Ubq 7+ ion conformation from compact to elongated. The explanation offered in that paper suggested that ions closer to the entrance of the drift tube experienced more heating from collisions in the gas plume leaving the drift tube entrance when the extraction voltage returned to zero than ions just exiting the trap. As the extraction voltage returned to zero, collisions with the background buffer gas are more energetic. Thus the collisions experienced by the ion packet converted some of the kinetic energy into heat and unfolded the protein ions. Similar effects were reported for cytochrome c.[4, 5]

All ion mobility instruments use an attractive, DC voltage on the entrance of the mobility cell called the injection voltage to send ions into the cell. The injection voltage and the ion charge state determine the kinetic energy of the collisions that the ion experiences with the buffer cell gas (usually helium or another inert gas). Ions entering the drift tube rapidly heat as their kinetic energies are thermalized by collisions with the buffer gas [6]. Further collisions cool the ion to the buffer gas temperature; it is estimated that protein ions undergo 105 collisions per centimeter inside the mobility cell for a helium buffer gas at 1 mbar. The rapid heating and cooling anneal the ions into more stable conformations [7]. Ions can unfold [3, 6-12], dissociate [13-18], and have protons stripped by the (helium) buffer gas [8, 15, 19] by manipulating the injection energy.

Our instrument design follows the IM – TOF MS built in Clemmer's group

[8, 15, 16, 20], but to our knowledge other groups did not see the effect concerning the extraction duration and voltage magnitude. A paper discussing an early design of the IT – IM – MS instrument in Clemmer's group states that varying the extraction pulse duration between 0.2 and 4 μs [13] did not change the quality of the ion signal. The motivation behind lengthening the duration pulse on our instrument to more than 4 μs and using an extraction voltage more negative than the entrance of the drift tube was the need to increase signal for protein ions in low charge states (1+ and 2+) made by proton transfer ion/ion reaction from more highly charged precursors.

Further discussion of this injection heating effect, as well as other examples of intermediate protein charge states prone to this effect, follow in this paper. The unfolding phenomena shown below may have interest in their own right, as protein unfolding sometimes provides clues to protein folding.[21, 22] Furthermore, rapid unfolding events are believed to occur as electrosprayed protein ions are desolvated and extracted into a mass spectrometer.[23, 24] These phenomena are of great interest in the projected use of ESI mass spectrometry to study the three-dimensional structures of biomolecules.

EXPERIMENTAL

Protein Samples - The protein samples used are bovine heart cytochrome c (Sigma C3131), porcine trypsin (Sigma T0303), bovine ubiquitin (Sigma U6253), lysozyme (Sigma L7651), carbonic anhydrase (Sigma C7025), bovine insulin (Sigma I5500), and bovine trypsin inhibitor (BPTI, Sigma T0256). The YbhB protein is described here.[25] Each protein was electrosprayed from a 30 μM 1% aqueous acetic acid solution using

nanoelectrospray tips (~ 20 μm i.d.). The nanoelectrospray tips were made from capillary tubes (1.5 mm o.d., 0.86 mm i.d.)
via a tip puller (P97; Sutter Instruments, Novato, CA).

Instrumentation - The design and general instrument details for the home built three ion source - ion trap - ion mobility - qTOF mass spectrometer are reported here [3]. Briefly we electrosprayed the protein solution, collected ions in the trap for 20 ms, and cooled them for another 30 ms. Ions were extracted from the trap with an attractive, square wave voltage using a pulse generator (PVX-4150; Directed Energy Corp.; Fort Collins, CO, USA, applied to the exit endcap) and injected into the drift tube mobility cell (Figure 1). The electric field across the drift tube was 11.2 V/cm, which should be in the low-field regime. The TOF mass range was as short as possible (≳70 μs) to measure the maximum points across the ion mobility peaks. The ion trap extraction voltage (Vext), extraction voltage pulse duration, and drift cell injection voltage (Vinj) were varied to understand this heating effect.
Figure 1 shows a schematic diagram of the ion trap and drift tube entrance. The distance from the trap center to the trap exit (z0) is 0.707 cm, and the distance from the trap exit to the drift tube entrance (z1) is 1.30 cm, as indicated. Ions are extracted from the trap
with a negative voltage pulse of amplitude Vext on the exit end cap. The duration
of this pulse varies from 1 μs to as long as 15 μs. The fall and rise times depend on the pulse amplitudes but are less than 40 and 60 ns, respectively, so they do not distort the square wave extraction pulse appreciably. The DC voltage on the drift tube entrance is Vinj and is varied from zero to –100 volts; -50 to -100 are typical values.

The drift tube contains He gas at 1.5 to 2.0 mbar. Figure 1 also shows a depiction of a small gas plume flowing out of the drift tube entrance orifice (0.50 mm diam.). Ions

from the trap must travel through this plume to get into the drift tube. The dimensions of and conditions in the He plume are not known precisely; the pressure and number density of He are assumed to be intermediate between that in the drift tube (1.5 to 2.0 mbar) and that in the external vacuum chamber (~1 µbar).

The collision cross sections of the protein ions were calculated using Equation 1:

$$\Omega = \frac{3}{16}\sqrt{\frac{2\pi}{\mu k_B T}}\frac{Q}{n}\frac{t_d U}{L^2} \qquad (1)$$

where Ω = rotationally averaged cross section of the ion of interest, µ = reduced mass, k_B = Boltzmann constant, T = temperature, Q = ion charge, n = number density of buffer gas, calculated using the pressure and temperature in the drift cell. Other parameters are nested drift time, t_d, voltage across the drift cell, U, and drift cell length, L. The t_d is corrected for time spent between the drift tube exit and TOF source region, as described.[3]

Ion Flight Times During Extraction from IT and Injection into Drift Tube - Examination of the mobility spectra indicates that the time and amplitude of the extraction voltage pulse (V_{ext}, Figure 1) can have a strong effect on the conformer(s) observed and their relative abundances. Analysis of these observations shows that the position of the ion when the negative extraction voltage returns to zero is important.

This position is estimated as described below.

Figure 1 shows a schematic diagram of the ion trap and injection region just before the drift tube. Upper case Z is used for position to avoid confusion with ion charge z. Consider an ion at rest in the center of the trap. The potential in the center is ground.

A negative voltage (say V_{ext} = -50 volts) is applied to the right endcap electrode to extract the ion. While this voltage is on, the ion travels the distance Z_0 = 0.707 cm in a time t_0. Here the ion is accelerated through a field gradient region with potential from zero to V_{ext}. The time required is t_0 (Eqn. 2):

$$t_o^2 = \frac{2mZ_0^2}{Q\,\Delta V} = \frac{2mZ_0^2}{Q\,V_{ext}} \qquad (2)$$

To get into the drift tube, the ion must next travel the distance Z_1 = 1.30 cm. Suppose $V_{inj} = V_{ext}$ = -50 volts. In this simple case, the second region is field-free, so the time t_1 is given by the familiar time-of-flight equation (3):

$$t_1^2 = \frac{mZ_1^2}{2QV_{ext}} \qquad (3)$$

For ubiquitin 7+, m = 1.42x10-20 g, t_0 = 5.0 μs , t_1 = 4.7 μs

and the total time $t = t_0 + t_1$ = 9.7 μs.

Next consider the more common case when Vext is more negative than V_{inj}. Typical values used in this study would be V_{ext} = -100 volts and V_{inj} = -50 volts. The time to the trap exit is still given by Equation 2; in this case t_0 = 3.6 μs for ubiquitin 7+. The ion is then decelerated as it continues toward the drift tube. The considerations below are derived from those used to calculate flight times and velocities in a reflectron.[26, 27]

Let $v_{it\ exit}$ and $v_{dt\ ent}$ be the ion velocities at the ion trap exit and drift tube entrance. These values are given by the following equations (4):

$$v_{it\ exit}^2 = \frac{2QV_{ext}}{m} \qquad v_{dt\ entrance}^2 = \frac{2QV_{inj}}{m} \qquad (4)$$

The average velocity v_{avg} in this region is just the mean of these two values, shown with this relationship (5):

$$v_{avg} = \frac{v_{it\ exit} + v_{dt\ entrance}}{2} \qquad (5)$$

The distance Z_1 is then merely:

$Z_1 = (v_{avg})$ x (time between trap and drift tube) = $v_{avg}\,(t - t_0)$ (6)

Thus, if the total time duration of the ion trap extraction pulse ($t = t_0 + t_1$) is known, the approximate position Z_1 of the ion when the pulse returns to zero can be estimated from Equation 6. For the example under consideration (ubiquitin 7+, V_{ext} = -100 volts, V_{inj} = -50 volts), t_1 = 3.8 μs and t = 7.4 μs. Thus, ubiquitin 7+ is just leaving the ion trap for an extraction pulse 4 μs long; for a pulse longer than about 8 μs, the ubiquitin 7+ ions are already inside the drift tube when the ion trap extraction voltage returns to zero.

These estimates neglect several factors: a) the ions are not at rest in the trap, b) the ions lose kinetic energy due to collisions (described below), and c) the outside surface of the endcap electrode is curved, which makes the potential not quite linear over the entire distance between the exit and the drift tube entrance. For the present purposes, approximate values of ion velocity and position are adequate.

RESULTS AND DISCUSSION

Effect of Extraction Pulse Time - The basic result has been shown for ubiquitin ions in a previous paper [3] and for cytochrome *c* ions in a dissertation.[5] The initial observations are summarized as follows. Ions in high charge states remain unfolded, and ions in low charge states remain folded, regardless of extraction and injection conditions,

unless extreme values are employed. For charge states that have a range of accessible conformers of widely different cross sections, e.g., ubiquitin 7+ and cytochrome *c* 8+, the mobility spectra vary substantially

with the duration of V_{ext}, especially if V_{ext} is more negative than V_{inj} (see Figure 1).

Most other proteins studied here show similar behavior; such charge states are listed in Table 1. A detailed example is shown for carbonic anhydrase 21+ in Figure 2. With the shortest pulse (3 μs) the ions are mostly in compact conformation(s), with some partially unfolded conformers. With the longest pulse (11 μs) the ions are almost all compact. Between these extremes, intermediate behavior is observed. The ions are mostly unfolded if the extraction pulse lasts for 7 μs. Changing the extraction pulse length by only 1 μs yields a substantially different distribution of conformers in the time regime shown, which indicates that the unfolding events occur on or faster than this time scale.

Extraction conditions used for these and other figures are given for various proteins in Table 2. Note that a variety of conditions were employed. In some experiments, the intent was to reproduce the spatial position of different protein ions, so the extraction and injection conditions were varied as appropriate, based on their mass and charge.

Consider the cross-section distribution shown in Figure 2 for carbonic anhydrase 21+ at extraction time of 6 μs. These ions are mostly unfolded. Use of slightly longer extraction times does not generate much more elongated conformers. The various proteins studied show a similar effect; there is an extraction time value when the extent of unfolding is at or near the maximum. Table 3 lists these experimentally-observed time values. Table 3 also lists the actual distance Z travelled by the protein ions in these extraction times. Although the times vary from protein to protein, the total distances are similar; all are about 1 to 1.2 cm

from the ion trap center, or about 0.9 cm in front of the drift tube entrance. This observation shows that this unfolding phenomenon has reached a maximum at a common spatial position for a variety of proteins. It is related to some change that occurs when the ions are between the trap exit and drift tube entrance. Note also that these unfolding effects occur at less negative values of V_{inj} than those described by Jarrold and Clemmer, et al.[6-12, 28]

Initial Explanation of Unfolding - The effect shown in Figure 2 and Table 3 is explained with the diagram in Figure 3. The figure assumes the ions are folded and start at rest in the center of the trap. With a short extraction pulse (Figure 3a), the ions are barely outside the trap when the voltage on the exit electrode returns to zero. Unfolding occurs to only a small extent in this case. With a long extraction time (Figure 3c), the ions are already inside the drift tube when the ion trap exit electrode voltage returns to zero. Obviously, the change in V_{ext} can no longer affect these ions. Thus, long extraction times yield spectra with the highest abundances of compact conformers.

The most extensive unfolding is observed when the extraction time is selected such that the ions are between the trap exit and drift tube entrance when V_{ext} returns to zero. Such a condition exacerbates the amount of unfolding observed. This is illustrated in Figure 3b; the ion has unfolded partially, and then unfolds more extensively in the second part of its travel. Ions that unfold here are then stabilized in open conformations by the many cooling collisions that occur in the higher pressure region just inside the entrance to the drift tube.[6, 28]

Suppose a relatively low value of V_{inj} is used, -50 V. If the ions are between the trap exit (ground) and the drift tube entrance when the extraction pulse returns to zero, the electric field is roughly 50 V/1.3 cm = 30 V/cm. Such a value is well outside the low-field regime

for IMS and heating is expected. The time frame of such heating and unfolding events is a few μs, also comparable to the time frame of such processes in high-field asymmetric ion mobility spectrometry (FAIMS).[29, 30]

The time-resolved protein ion heating has no dependence on the shutting down of the RF voltage on the center ring electrode on the ion trap. The IT_{RF} voltage at full amplitude ($V_{0\text{-}p}$ = 5000) shuts off in 15 μs. Ubiquitin 6+ and 7+ ions unfolded under the injection conditions described in this paper 60 μs after turning off the IT_{RF} voltage (data not shown).

Heating and Unfolding Observations with Ubiquitin 7+ - To further test the above explanation, instrument parameters were varied with ubiquitin as the test protein. Figure 4 shows data for three charge states of ubiquitin measured with the same extraction voltage (-80 volts) and injection energy (260 eV = zV_{inj}). The extraction time is varied and selected to put the ions at about the same position when the polarity of V_{ext} changes. We call this position Z in the following discussion.

For Z > 2 cm, the ions are inside the drift tube when the extraction voltage changes, and these ions are mostly folded for all three charge states. Some partially elongated ions are seen from ubiquitin 8+, as expected for a more highly charged species with greater electrostatic repulsion between charged groups.

For short extraction times, Z = 0.5 cm, a distribution of compact, partially elongated and unfolded conformers is seen. Again, the 8+ ion has the highest abundance of unfolded conformers. For intermediate extraction times, selected so that Z = 1.8 cm in each case, all three charge states yield mostly unfolded conformers. In the latter case, the ions are heated enough to entirely remove even the compact forms.

In another experiment, the unfolding and energy transfer caused by the change in extraction voltage are compared to that observed in more conventional experiments, where unfolding is induced by use of a large negative DC voltage on the drift tube entrance.[6-12, 28] Here one set of experiments are done with an extraction pulse duration timed to change when the ions are in the position shown in Figure 3b; these results are termed "heated" conditions. Then "gentle" conditions, (i.e., conditions selected so that the ions are inside the drift tube when the extraction voltage changes, Figure 3c) are used. V_{inj} is then made more negative to match the extent of unfolding seen under "heated" conditions. In a sense, the mobility spectra observed under "gentle" conditions are titrated to the same values as those seen under "heated" conditions, with the DC injection voltage being the titration variable.

The results are shown for ubiquitin 7+ in Figure 5. Part a shows that the drift tube injection energy has to be as high as 518 eV to match the unfolding induced by the extraction pulse with the drift tube entrance at ground. In Frames b and c, the DC value of the injection energy needed to produce similar unfolding as the extraction pulse are again some 550 eV higher than the trap exit voltage under "gentle" conditions. Something happens to impart a lot of energy to the ions when the injection voltage changes under the "heated" conditions.

Another indication of the energy imparted to the ions by the extraction pulse is depicted in Figure 6. Here the drift tube entrance is kept grounded and a short (1 μs), very negative (-500 V) extraction pulse is used. Ubiquitin 6+ is seen in a range of conformers; ubiquitin7+ and 8+ are unfolded, even though the gentlest injection voltage is used. Comparison with Figure 5 shows that an injection energy of 500 eV or more are need to unfold the ions like this if the effect of the extraction pulse is not used.

Observations on Trypsin and BPTI - The importance of the ion's position when the extraction voltage changes was observed for other proteins as well. The relative values of extraction voltage and injection voltage are also important. For example, cross-sections for trypsin 11+ are shown in Figure 7 when the ion extraction voltage and time and injection voltage are selected to reproduce the ion position. In Figure 7a, the ions are at Z = 0.5 cm for all three sets of extraction conditions; the mobility spectra are similar and show all or mostly compact conformers.

In Figure 7c, the ions are inside the drift tube, and all are compact. In Figure 7b, the conditions are such that the ions are at Z = 1.2 cm, a condition where unfolding is expected. For the solid line, the extraction voltage equals the injection voltage, and the ions remain compact. There is less ion heating when there is no voltage gradient between the trap exit electrode and the drift tube entrance during the extraction pulse. In the remaining two plots in Figure 7b, injection voltage is made more negative, to - 75 and -150 volts. This heats the ions and unfolds them more extensively as the extraction voltage is made more negative.

Bovine pancreas trypsin inhibitor (BPTI) is a small, 58 amino acid, protein that is highly constrained by three disulfide bonds. Cross-section results are shown for BPTI in Figure 8 under both gentle and heated injection conditions. Three charge states (4+, 5+, and 6+) are observed. Under gentle conditions, BPTI 4+ is mostly compact conformer(s) with cross-section ~ 620 $Å^2$. Under heated conditions, this ion expands to ~ 800 $Å^2$. BPTI 5+ is almost all in an open conformation, whereas BPTI 6+ has two conformers. The cross sections for the open conformers shown in Figure 8 agree well

with those reported by Shelimov with fairly energetic injection conditions.[12] It is likely that the cross sections reported by Shelimov et al. were for ions that were all in the more open state.

Estimates of Collisions and Kinetic Energy Losses between Ion Trap Exit and Drift Tube Entrance - Figures 1 and 3 show a plume of helium gas flowing from the drift tube entrance toward the ion trap exit. Presumably, the collisions that excite the ions and unfold them occur in this plume. These collisions will also cause the ions to lose some of their kinetic energy, which could play a role in their unfolding behavior. Thus, an estimate of the number of collisions and the corresponding kinetic energy losses is of interest.

The discussion below is derived from Douglas' paper on kinetic energy losses in a quadrupole collision cell.[31, 32] The entrance aperture diameter is 0.50 mm. Conditions in the He plume are not known exactly; for the present discussion it is assumed to have length L, temperature T = 300 K, average pressure p_{avg}, and average number density n_{avg}. The drift tube is 1.3 mbar, the vacuum chamber is 1.3×10^{-4} mbar, so p_{avg} is $(1.3 + 1 \times 10^{-4})/2 \sim 0.65$ mbar and n_{avg} is $\sim 1.6 \times 10^{16}$ cm^{-3}. The subsequent mobility separation measures the cross section Ω of the protein ion. It is the compact conformers that unfold the most. Ubiquitin ($\Omega \approx 900$ Å^2 = 9×10^{-14} cm^2) is taken as the protein of interest. These ions have a mean free path λ given by equation (7).

$$\lambda = {}^{1}/_{n\Omega} \qquad (7)$$

For compact conformers of ubiquitin, $\lambda \sim 7 \times 10^{-4}$ cm. The number of collisions N is just L/λ. If the plume persists back for a distance 10 times the orifice diameter, then L = 0.5 cm and N

= $0.5/7x10^{-4}$ = 700 collisions. Thus, hundreds of collisions are expected before the protein ions enter the drift tube. Compact conformers of other protein ions have cross sections of ≈ 1000 $Å^2$, not much larger than that of ubiquitin.

If the ions have initial kinetic energy E_0, their energy after one collision is E_1:

$$\alpha = \frac{E_1}{E_0} = \frac{m_{protein}^2 + m_{He}^2}{M^2} \qquad (8)$$

where $m_{protein}$ = 8600 Da = $1.43x10^{-20}$ g for ubiquitin, m_{He} = 4 Da = $6.67x10^{-24}$ g, and M = $m_{protein}$ + m_{He}.[31] The value of α is 0.9990706 in this case.

After N collisions the kinetic energy remaining is approximately α^N. For N = 700 collisions, α^N is roughly 0.52. Thus, protein ions in compact conformations are likely to lose roughly half of their initial kinetic energy due to collisions before they enter the drift tube.

This large loss of kinetic energy has several implications. First, much of this initial kinetic energy is converted into internal energy, hence the heating and unfolding. Second, the ions will actually move through the plume more slowly than indicated by the time values discussed above, which do not account for kinetic energy losses. Third, assume V_{ext} is kept more negative than V_{inj} while the ions undergo collisions in the plume, which is the condition that maximizes unfolding. In this case, the positively-charged protein ions will actually see a net electrostatic force back toward the ion trap as they are being slowed down by the collisions, which is an additional effect that would slow them further still. When V_{ext} then changes back to zero, the ions are accelerated into the drift tube, the electric field between trap exit and drift tube entrance is now in the high-field regime (as noted above), and perhaps these "slow" ions are now highly prone to heating and unfolding.

CONCLUSION

The magnitude and duration of the extraction pulse on the ion trap exit endcap can induce extensive protein ion heating and unfolding for intermediate protein charge states with a wide range of accessible conformations, especially when the extraction voltage is more negative than the voltage on the entrance of the drift tube. Experimental confirm simple time-of-flight equations (Eqns. 2 through 5) estimate the time and position of the ion packet when the ion trap exit electrode returns to ground. Protein ions unfold to the maximum extent 0.9 cm in front of the drift tube entrance. BPTI, a protein about the size of ubiquitin, is constrained by three disulfide bonds and does not unfold as extensively as ubiquitin during "heated" injection conditions.

The protein ion heating may be due to the high field-regime formed by the voltage on the entrance to the drift tube when the extraction voltage returns to ground. About half of the ion kinetic energy lost between the ion trap exit endcap and the drift tube entrance is lost due to collisions in the He buffer gas plume. As kinetic energy is lost, the ion's velocity decreases. These slow ions are caught in a high-field regime and unfold, similar to FAIMS experiments. Protein ions already inside the drift tube are not perturbed by the extraction voltage returning to ground. These ion conformers remain the most compact and only the voltage on the drift tube entrance dictates the extent of heating and unfolding.

ACKNOWLEDGEMENTS

GMS acknowledges funding from the Graduate Assistance in Areas of National Need (GAANN) for the 2008 and 2009 school years.

REFERENCES (Set to the International Journal of Mass Spectrometry format)

[1] B.C. Bohrer, S.I. Merenbloom, S.L. Koeniger, A.E. Hilderbrand, D.E. Clemmer, Biomolecule Analysis by Ion Mobility Spectrometry, Annu. Rev. Anal. Chem., 1 (2008) 293-327.
[2] J.A. McLean, The Mass-Mobility Correlation Redux: The Conformational Landscape of Anhydrous Biomolecules, J. Am. Soc. Mass Spectrom., 20 (2009) 1775-1781.
[3] Q. Zhao, M.W. Soyk, G.M. Schieffer, K. Fuhrer, M.M. Gonin, R.S. Houk, E.R. Badman, An Ion Trap-Ion Mobility-Time of Flight Mass Spectrometer with Three Ion Sources for Ion/Ion Reactions, J. Am. Soc. Mass Spectrom., 20 (2009) 1549-1561.
[4] Q. Zhao, G.M. Schieffer, M.W. Soyk, T.J. Anderson, R.S. Houk, E.R. Badman, Effects of Ion/Ion Proton Transfer Reactions on Conformation of Gas-Phase Cytochrome *c* Ions, J. Am. Soc. Mass Spectrom., (2010) *in press*.
[5] Q. Zhao, Development of Ion Mobility Mass Spectrometry Coupled with Ion/Ion Reactions: Instrumentation and Applications for Protein Analysis, in: Chemistry, Iowa State University, Ames, IA, 2008, pp. 80-113.
[6] Y.S. Liu, S.J. Valentine, A.E. Counterman, C.S. Hoaglund, D.E. Clemmer, Injected-ion mobility analysis of biomolecules, Anal. Chem., 69 (1997) A728-A735.
[7] K.B. Shelimov, M.F. Jarrold, Conformations, unfolding, and refolding of apomyoglobin in vacuum: An activation barrier for gas-phase protein folding, J. Am. Chem. Soc., 119 (1997) 2987-2994.
[8] C.S. Hoaglund, S.J. Valentine, C.R. Sporleder, J.P. Reilly, D.E. Clemmer, Three-dimensional ion mobility TOFMS analysis of electrosprayed biomolecules, Anal. Chem., 70 (1998) 2236-2242.
[9] S.J. Valentine, J.G. Anderson, A.D. Ellington, D.E. Clemmer, Disulfide-intact and -reduced lysozyme in the gas phase: Conformations and pathways of folding and unfolding, J. Phys. Chem. B, 101 (1997) 3891-3900.
[10] S.J. Valentine, D.E. Clemmer, H/D exchange levels of shape-resolved cytochrome c conformers in the gas phase, J. Am. Chem. Soc., 119 (1997) 3558-3566.
[11] S.J. Valentine, A.E. Counterman, D.E. Clemmer, Conformer-dependent proton-transfer reactions of ubiquitin ions, J. Am. Soc. Mass Spectrom., 8 (1997) 954-961.
[12] K.B. Shelimov, D.E. Clemmer, R.R. Hudgins, M.F. Jarrold, Protein structure in vacuo: Gas-phase confirmations of BPTI and cytochrome c, J. Am. Chem. Soc., 119 (1997) 2240-2248.
[13] C.S. Hoaglund, S.J. Valentine, D.E. Clemmer, An ion trap interface for ESI-ion mobility experiments, Anal. Chem., 69 (1997) 4156-4161.
[14] Y.S. Liu, D.E. Clemmer, Characterizing oligosaccharides using injected-ion mobility mass spectrometry, Anal. Chem., 69 (1997) 2504-2509.
[15] S.C. Henderson, S.J. Valentine, A.E. Counterman, D.E. Clemmer, ESI/ion trap/ion mobility/time-of-flight mass spectrometry for rapid and sensitive analysis of biomolecular mixtures, Anal. Chem., 71 (1999) 291-301.
[16] C.S. Hoaglund-Hyzer, D.E. Clemmer, Ion trap/ion mobility/quadrupole/time of flight mass spectrometry for peptide mixture analysis, Anal. Chem., 73 (2001) 177-184.
[17] C.S. Hoadlund-Hyzer, J.W. Li, D.E. Clemmer, Mobility labeling for parallel CID of ion mixtures, Anal. Chem., 72 (2000) 2737-2740.

[18] C.S. Hoaglund-Hyzer, Y.J. Lee, A.E. Counterman, D.E. Clemmer, Coupling ion mobility separations, collisional activation techniques, and multiple stages of MS for analysis of complex peptide mixtures, Anal. Chem., 74 (2002) 992-1006.
[19] S.G. Lias, J.F. Liebman, R.D. Levin, Evaluated Gas-Phase Basicities and Proton Affinities of Molecules - Heats of Formation of Protonated Molecules, J. Phys. Chem. Ref. Data, 13 (1984) 695-808.
[20] E.R. Badman, S. Myung, D.E. Clemmer, Gas-phase separations of protein and peptide ion fragments generated by collision-induced dissociation in an ion trap, Anal. Chem., 74 (2002) 4889-4894.
[21] A.V. Finkelstein, Can protein unfolding simulate protein folding?, Protein Eng., 10 (1997) 843-845.
[22] A.V. Finkelstein, O.V. Galzitskaya, Physics of protein folding, Phys. Life Rev., 1 (2004) 23-56.
[23] K. Breuker, F.W. McLafferty, Stepwise evolution of protein native structure with electrospray into the gas phase, 10(-12) to 10(2) S, Proc. Natl. Acad. Sci. U. S. A., 105 (2008) 18145-18152.
[24] E. Segev, T. Wyttenbach, M.T. Bowers, R.B. Gerber, Conformational evolution of ubiquitin ions in electrospray mass spectrometry: molecular dynamics simulations at gradually increasing temperatures, Physical Chemistry Chemical Physics, 10 (2008) 3077-3082.
[25] G.M. Schieffer, L. Brachova, B.J. Nikolau, E.R. Badman, R.S. Houk, The YbhB Protein from *Escherichia coli* and *Arabidopsis thaliana* homolog of YbhB Characterized by Mass Spectrometry and Ion Mobility Mass Spectrometry, in preparation, (2010).
[26] R.J. Cotter, Time-of-Flight Mass Spectrometry: Instrumentation and Applications in Biological Research, American Chemical Society, Washington, DC, 1997.
[27] E. deHoffmann, V. Stroobant, Mass Spectrometry: Principles and Applications, Second ed., John Wiley & Sons Ltd, Chichester; New York, 2001.
[28] D.E. Clemmer, M.F. Jarrold, Ion mobility measurements and their applications to clusters and biomolecules, J. Mass Spectrom., 32 (1997) 577-592.
[29] A.A. Shvartsburg, F.M. Li, K.Q. Tang, R.D. Smith, Distortion of ion structures by field asymmetric waveform ion mobility spectrometry, Anal. Chem., 79 (2007) 1523-1528.
[30] S.J. Valentine, S.L. Koeniger, D.E. Clemmer, A split-field drift tube for separation and efficient fragmentation of biomolecular ions, Anal. Chem., 75 (2003) 6202-6208.
[31] T. Covey, D.J. Douglas, Collision Cross-Sections for Protein Ions, J. Am. Soc. Mass Spectrom., 4 (1993) 616-623.
[32] B.A. Collings, D.J. Douglas, Conformation of gas-phase myoglobin ions, J. Am. Chem. Soc., 118 (1996) 4488-4489.

Table 1) The protein ion charge states listed below are prone to the ion heating effect described in this paper and analyzed on the IT-IM-TOF MS instrument. This list is not exhaustive.

Ubiquitin	8+, 7+, 6+, 5+
Trypsin	11+, 10+
Cytochrome *c*	9+, 8+, 7+
Carbonic anhydrase	21+
Lysozyme	10+, 9+
Insulin	3+, 4+
YbhB	10+, 9+
BPTI	6+, 4+

Table 2) Listed are the ion extraction conditions used for various figures. A position ≥ 2.1 cm means the ion packet is fully inside the drift tube when the extraction voltage returns to 0 V.

Figure	Extraction [V]	Extraction time [us]	Injection [V]	KE [eV]	position [cm]
2, CA 21+	-80	3-11	-33	693	variable, 0.5 to 2.6
4a, Ubiquitin 6+	-80	3, 8, 12	-44	260	0.5, 1.8, 2.9
4b, Ubiquitin 7+	-80	3, 8, 12	-37	260	0.5, 1.9, 3.1
4c, Ubiquitin 8+	-80	3, 7, 12	-32	260	0.5, 1.7, 3.1
5a, Ubiquitin 7+	-80	6, 12	0, -74	0, 518	1.1, 3.5
5b, Ubiquitin 7+	-80	6, 12	-7, -85	49, 595	1.2, 3.6
5c, Ubiquitin 7+	-80	6, 12	-19, -97	133, 679	1.2, 3.7
6, Ubq 6, 7, 8+	-500	1	0	0	0.4
7a, Trypsin 11+	-50, -75, -150	5, 4, 3	-49	540	0.5
7b, Trypsin 11+	-50, -75, -150	9, 8, 6	-49	540	1.2 – 1.3
7c, Trypsin 11+	-50, -75, -150	14, 13, 11	-49	540	2.3
8a, BPTI 4+	-80	6, 12	-49	200	1.1, 2.7
8b, BPTI 5+	-80	6, 12	-49	250	1.3, 3.1
8c, BPTI 6+	-80	6, 12	-49	300	1.5, 3.5

Table 3) Axial position of maximum unfolding and corresponding extraction conditions for several proteins.

		Experimental Conditions		
Protein & chg state	Position of max unfolding (Z, cm)	Extraction Time (µs)	V_{ext} (Volts)	V_{inj}
Ubiquitin 7+	1.1	6	-100	-26
Cytochrome c 8+	1.0	6	-100	-26
BPTI 4+	1.1	6	-80	-49
Carbonic anhydrase 21+	1.2	6	-80	-33
Trypsin 11+	1.3	8	-75	-49
Trypsin 11+	1.0	5	-150	-49

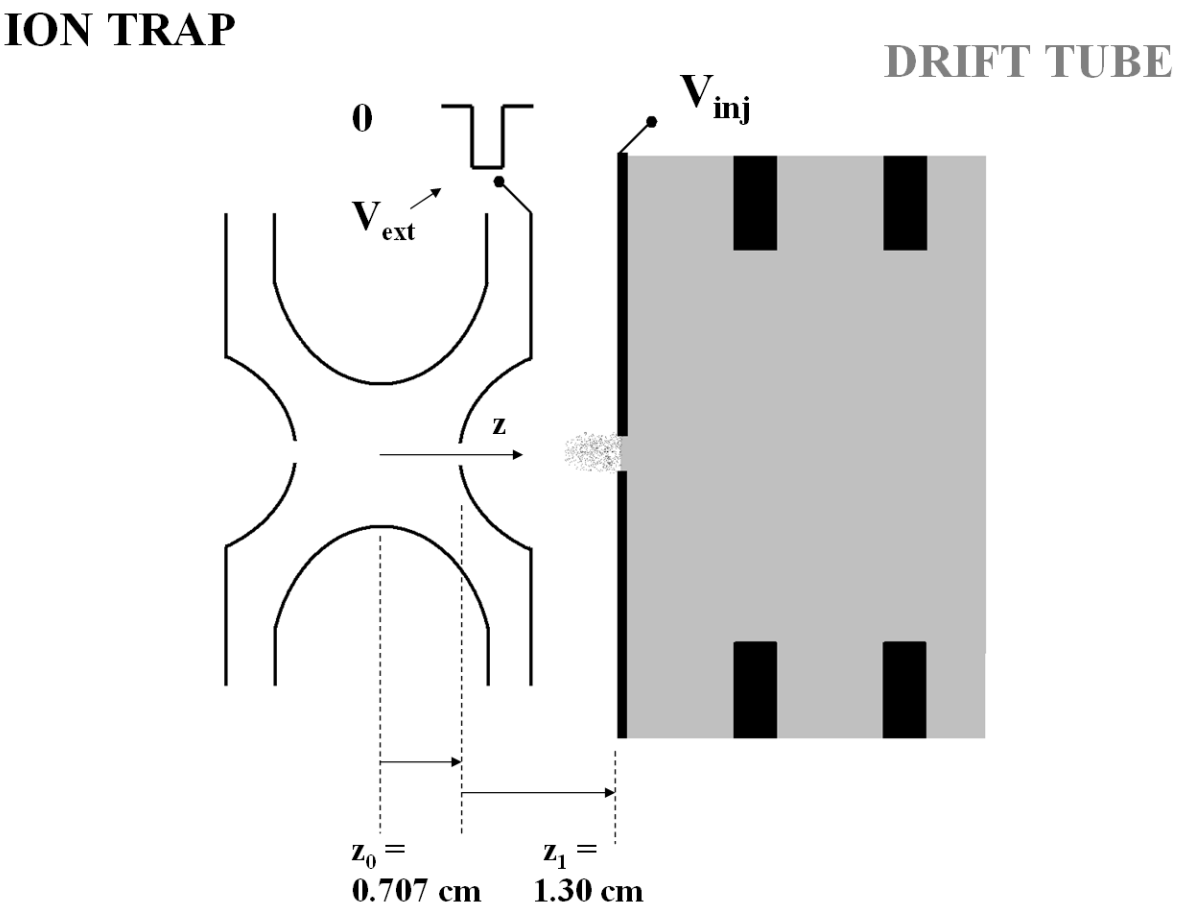

Figure 1) Schematic diagram showing the ion trap, entrance of drift tube, applied voltages, and the distances pertinent to the injection of molecules into the drift tube. The total distance,

$Z = Z_0 + Z_1$ from the center of the ion trap to the entrance of the drift tube is 2.01 cm. A square wave (V_{ext}, typically ~ -100 V) applied to the exit endcap of the ion trap draws ions out of the trap. The voltage on the entrance of the drift tube (V_{inj}, typically -50 V) helps entrain ions into the tube. In the data shown below, unfolding is most extensive when V_{ext} is more negative than V_{inj}.

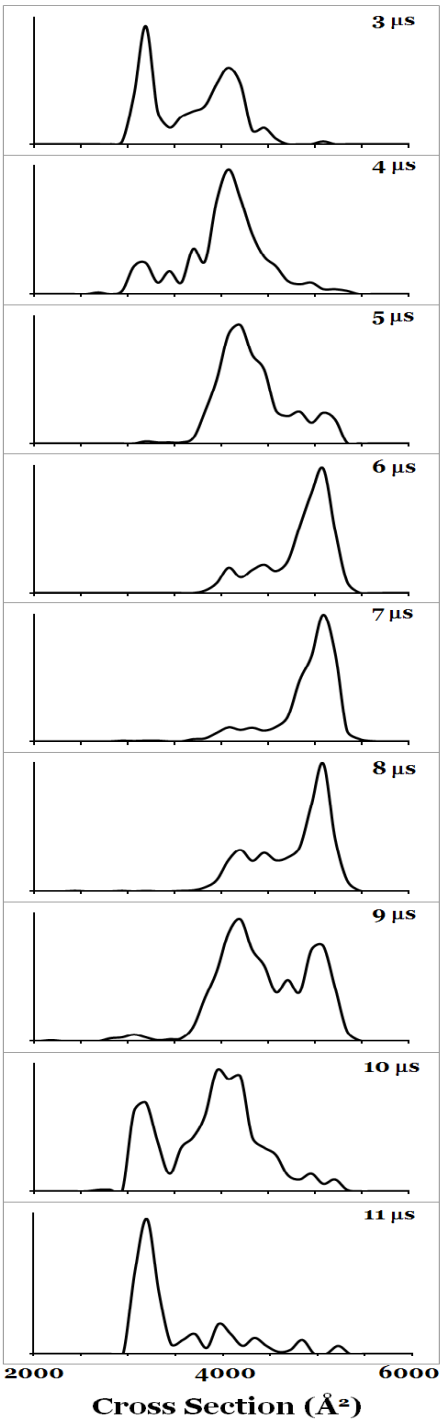

Figure 2) Collision cross-sections for carbonic anhydrase 21+ (m/z 1383) at indicated extraction times. See Table 2 for other experimental details.

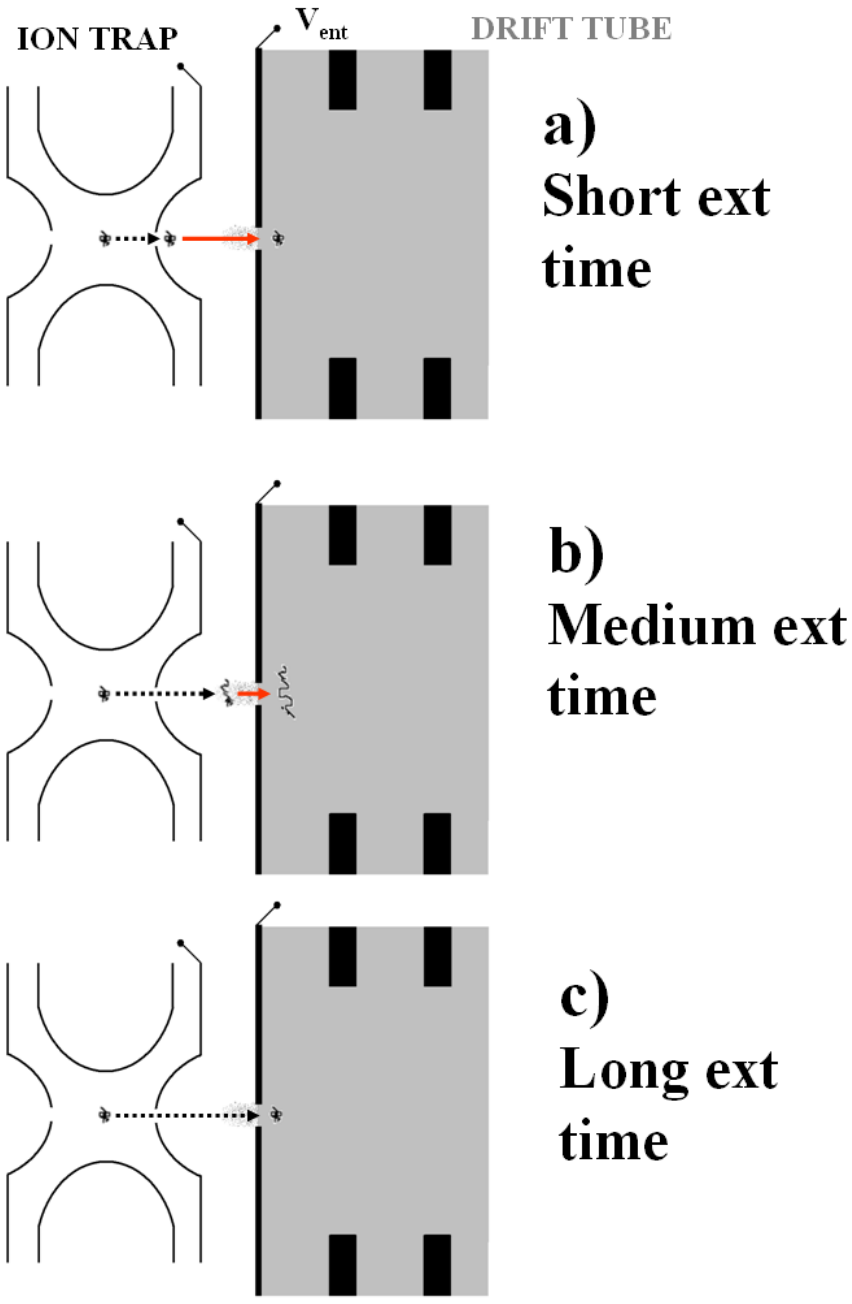

Figure 3) Depiction of mechanism for observed variation of protein unfolding with duration of extraction pulse. See text for discussion.

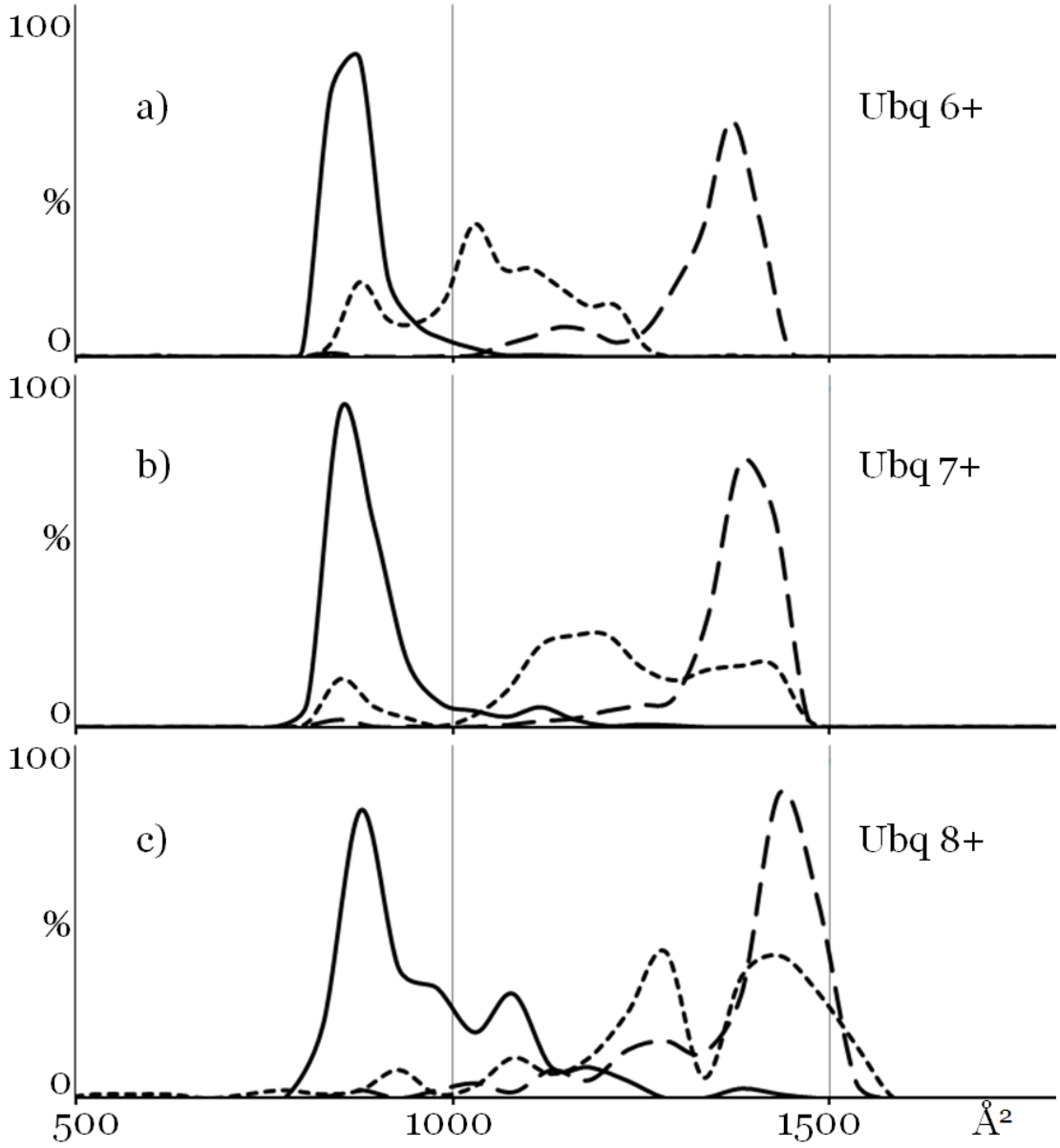

Figure 4) Cross-sections for ubiquitin ions in charge states a) 6+ b) 7+ and c) 8+ at three positions along their path into the DT when the extraction voltage returns to 0 V. The solid line denotes the CCS when the ion packet is fully inside the DT, the short dashed line denotes the CCS when the ion packet is 0.5 cm (inside IT), and the long dashed line denotes the CCS when the ion packet is 1.8 cm (in between the IT and DT) from the center of the ion trap. The ions were injected into the DT at -260 eV. The CCS counts are normalized to each other. Instrument conditions pertinent to this experiment are listed in Table 2.

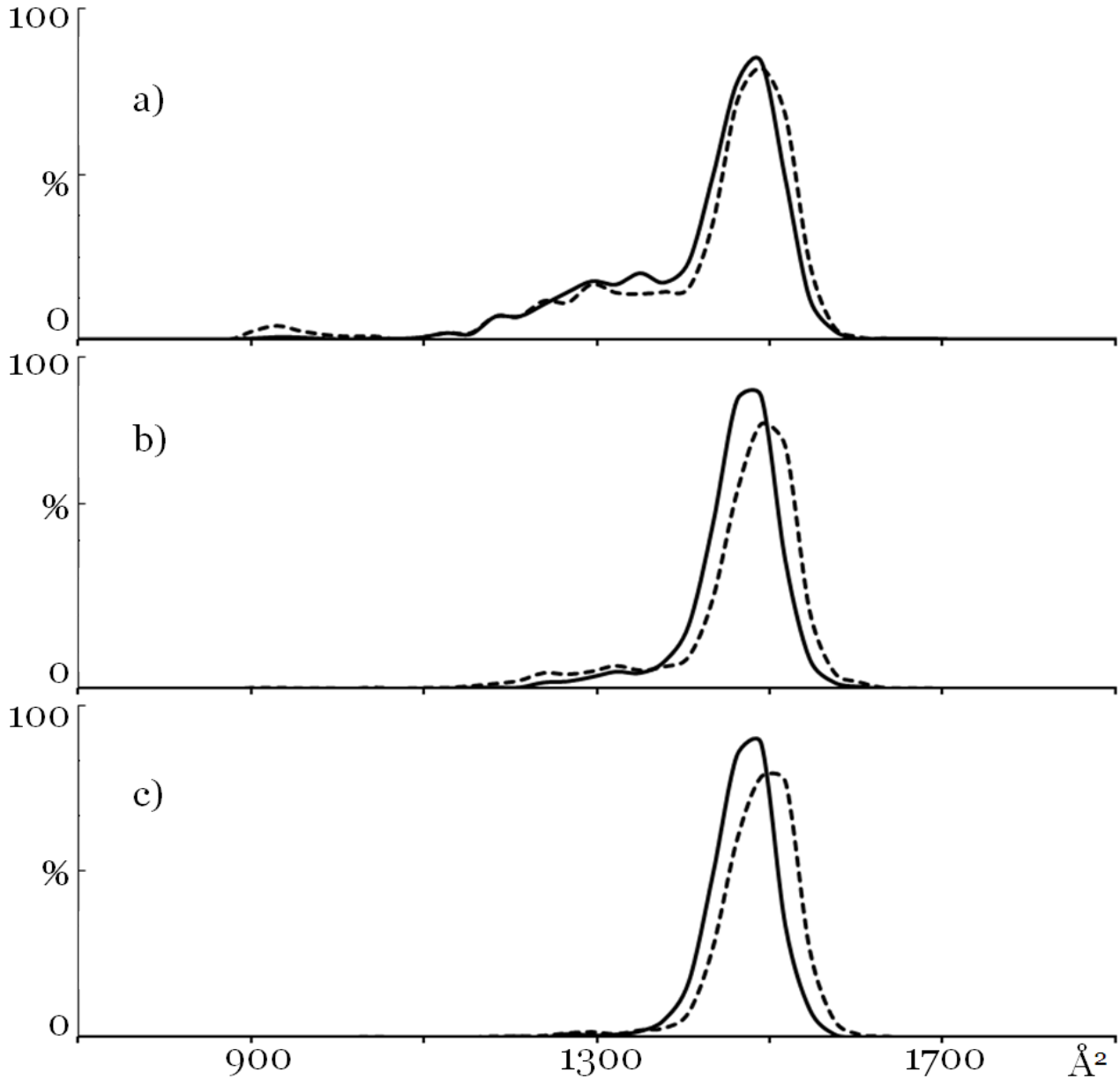

Figure 5) The cross sections for ubiquitin 7+ ion analyzed under gentle (solid line) and heating (dashed line) injection conditions. Similar Ubq 7+ cross sections are compared in a), b), and c). The injection voltage is a) 0 eV, heated; 518 eV, gentle b) 49 eV, heated; 595 eV gentle
and c) 133 eV, heated; 679 eV gentle. The eV difference for a) 518 eV, b) 546 eV, and c) 546 eV is the energy imparted to the Ubq 7+ under the heating injection conditions. Instrument conditions pertinent to this figure are listed in Table 2.

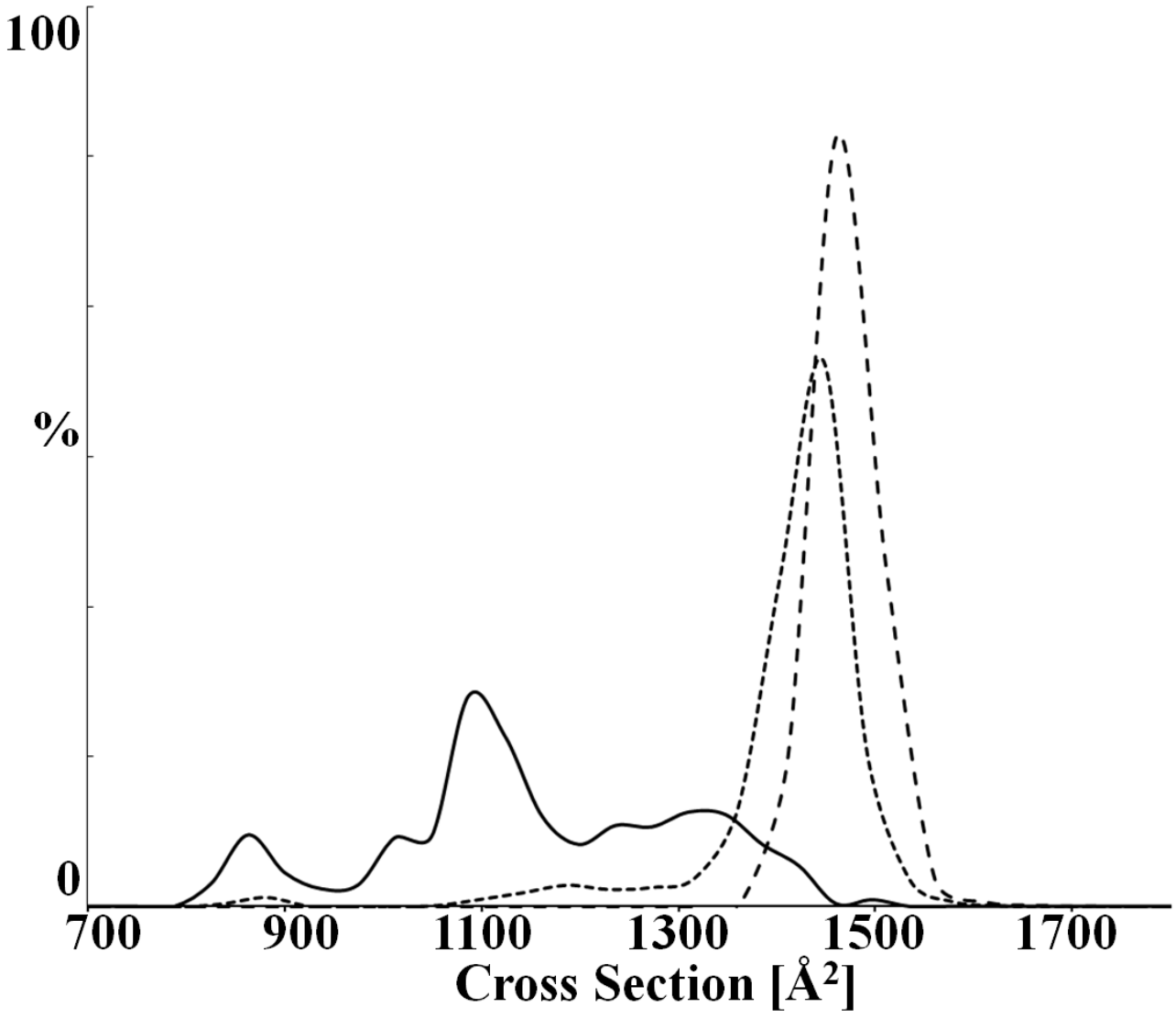

Figure 6) The cross section of ubiquitin ions injected using 0 V (grounded) on the drift tube entrance. The extraction pulse is -500 V for 1 µs. The solid line is Ubq 6+, the short dashed line is Ubq 7+, and the long dashed line is Ubq 8+. Instrument conditions pertinent to this figure are listed in Table 2.

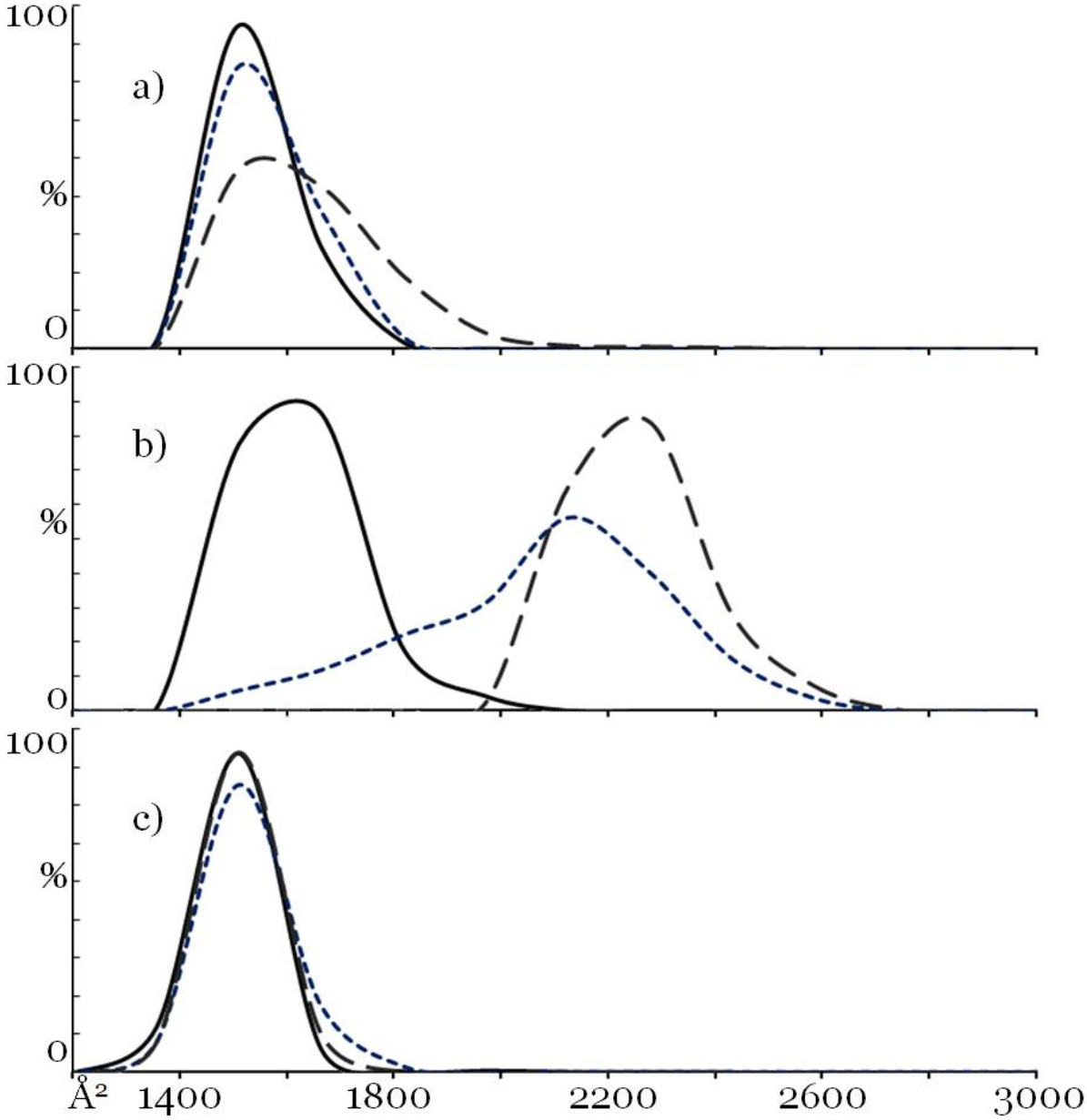

Figure 7) The cross section of trypsin 11+ (m/z 2133) when the ion packet is a) 0.5 cm (inside IT), b) 1.3 cm (between IT and DT), and c) 2.3 cm (inside DT) from the center of the IT when the extraction voltage returns to zero. The solid line used -50 V, the short dashed line used -75 V, and the long dashed line use -150 V as the extraction voltage on the exit endplate of the IT. The CCS counts are normalized to each other. Instrument conditions pertinent to this figure are listed in Table 2.

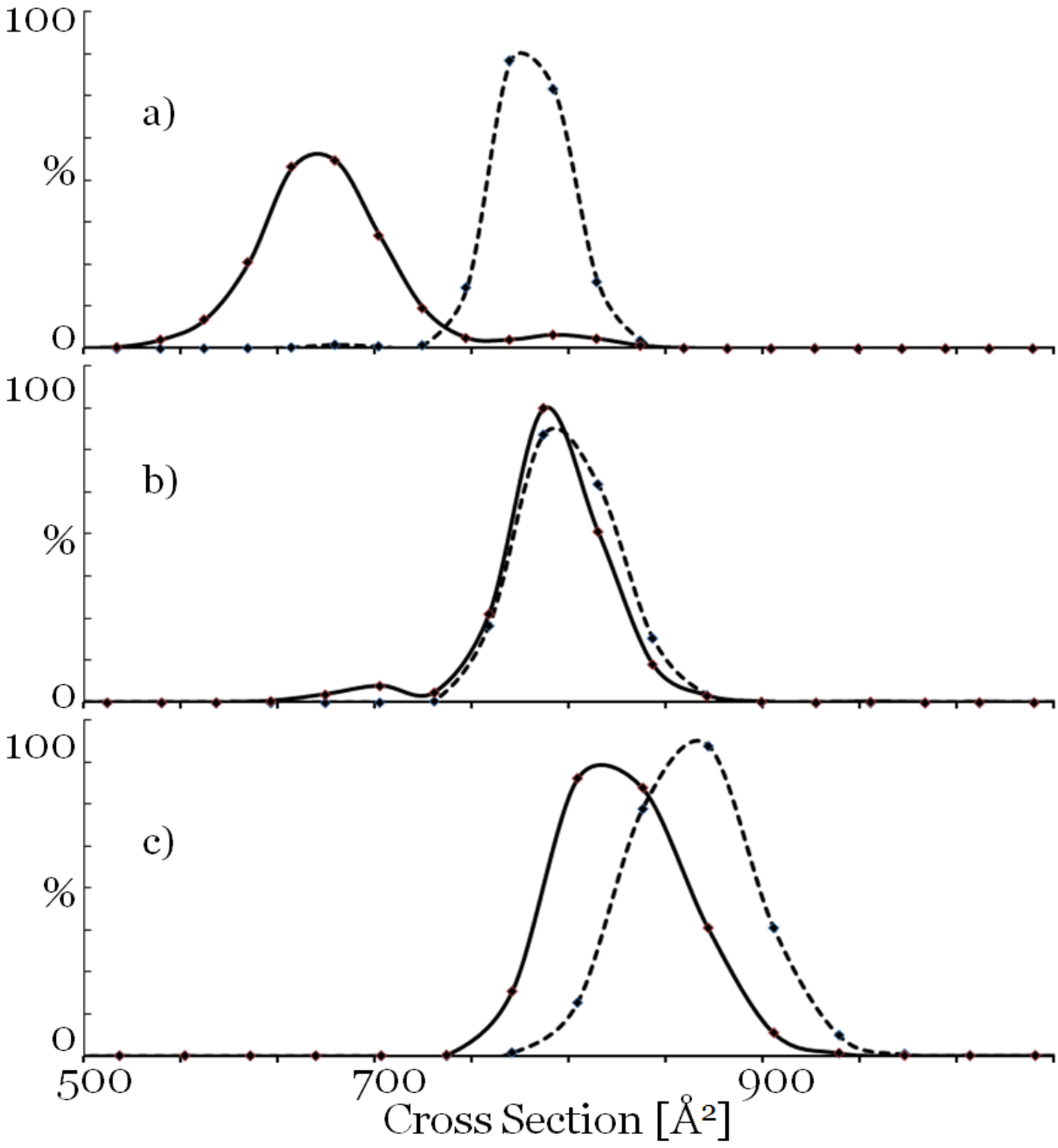

Figure 8) Cross-sections for BPTI a) 4+, b) 5+, and c) 6+ under gentle (solid line) and heated (dashed line) injection conditions. Instrument conditions pertinent to this figure are listed in Table 2.